

LOSS OF TBK1 KINASE FUNCTION IMPROVES DISEASE OUTCOME IN
PANCREATIC CANCER AND METABOLIC SYNDROME

APPROVED BY SUPERVISORY COMMITTEE

Rolf Brekken, Ph.D.

Diego Castrillon, M.D., Ph.D.

Philipp Scherer, Ph.D.

Raymond MacDonald, Ph.D.

Dedication

In Loving Memory of my cousin, Jane Connall (July 7, 1955 - April 5, 2014)

&

My dear friend, Elizabeth Smyth (May 3, 1988 - June 16, 2017)

LOSS OF TBK1 KINASE FUNCTION IMPROVES DISEASE OUTCOME IN
PANCREATIC CANCER AND METABOLIC SYNDROME

By

Victoria Haley Cruz

DISSERTATION

Presented to the Faculty of the Graduate School of Biomedical Sciences

The University of Texas Southwestern Medical Center at Dallas

In Partial Fulfillment of the Requirements

For the Degree of

DOCTOR OF PHILOSOPHY

The University of Texas Southwestern Medical Center at Dallas

Dallas, Texas

August 2018

Copyright

By

Victoria Haley Cruz, 2018

All Rights Reserved

LOSS OF TBK1 KINASE FUNCTION IMPROVES DISEASE OUTCOME IN
PANCREATIC CANCER AND METABOLIC SYNDROME

Victoria Haley Cruz, Ph.D.

The University of Texas Southwestern Medical Center, 2018

Rolf A. Brekken, Ph.D.

Aberrant expression and activity of TANK binding kinase 1 (TBK1) has been observed in numerous diseases. Here I've identified novel functions for TBK1 in pancreatic ductal adenocarcinoma (PDA) and in metabolic syndrome that promote disease progression.

Activating mutations in *KRAS* are present in 90% of human PDA cases; yet direct pharmacological inhibition of K-RAS remains a challenge, indicating a need for effective therapies. Higher levels of *TBK1* mRNA, a critical downstream mediator of oncogenic K-RAS in lung cancer, correlate with poorer outcome in PDA patients. Given these observations, I hypothesized that TBK1 is also an effector of K-RAS in PDA. *KRAS*

mutant PDA cell lines are selectively sensitive to small molecule inhibition of TBK1. In K-RAS-driven genetic mouse models of PDA, *Tbk1* supports spontaneous pancreatic tumor growth as evidenced by smaller tumors and fewer metastases in *Tbk1* mutant PDA mice relative to normal PDA mice. Additionally, *Tbk1* mutant tumors are more epithelial; an observation consistent with the reduced migratory phenotype of *Tbk1* mutant tumor cell lines and lack of detectable metastases in *Tbk1* mutant PDA animals. Mechanistic studies indicate that TBK1 is central to Axl-driven EMT and is activated with RAS in response to Axl stimulation in PDA cell lines.

The latter part of this thesis is focused on the contribution of TBK1 to mice with metabolic disorder. TBK1 is implicated in the regulation of metabolism through studies with amlexanox, an inhibitor of I κ B kinase (IKK)-related kinases. Amlexanox induced weight loss, reduced fatty liver and insulin resistance in high fat diet (HFD) fed mice and has now progressed into clinical testing for the treatment and prevention of obesity and type 2 diabetes. However, since amlexanox is a dual IKK ϵ /TBK1 inhibitor, the specific contribution of TBK1 is unclear. To distinguish metabolic functions unique to TBK1, I examined the metabolic profile of global *Tbk1* mutant mice challenged with HFD and investigated potential mechanisms for the improved metabolic phenotype. I report that systemic loss of TBK1 kinase function has a protective effect on metabolic readouts in HFD-fed mice, which is mediated by loss of an inhibitory interaction between TBK1 and the insulin receptor.

TABLE OF CONTENTS

Prior Publications.....	viii
List of Figures and Tables.....	ix
List of Abbreviations.....	x
Chapter 1. Introduction.....	1
1.1 Pancreatic Cancer.....	1
Identification of TBK1 as a RAS effector.....	1
TBK1 supports microtubule stability and mitosis in NSCLC.....	2
TBK1 promotes autophagy during pathogen infection and oncogenic stress..	4
TBK1 participates in tumor immunity.....	6
TBK1 activates AKT pro-survival signaling in melanoma and NSCLC.....	9
1.2 Metabolic Syndrome.....	13
TBK1 and IKK ϵ promote metabolic dysfunction.....	13
1.3 TBK1 inhibitors.....	14
1.4 Conclusions.....	16
Chapter 2. <i>Tbk1</i> loss in pancreatic cancer reduces tumor epithelial plasticity.....	20
2.1 TBK1 expression in pancreatic cancer.....	20
2.2 K-RAS-driven pancreatic cancer growth is disrupted by restricting TBK1 kinase activity.....	21
2.3 <i>Tbk1</i> Δ/Δ : KIC tumors are more 'epithelial'.....	23
2.4 <i>Tbk1</i> Δ/Δ : KIC tumor cells are less migratory & invasive.....	24
2.5 Evaluation of <i>Tbk1</i> loss on pancreatic cancer metastases.....	25
2.6 Re-expression of <i>Tbk1</i> in <i>Tbk1</i> Δ/Δ : KIC cells.....	27
2.7 TBK1 is central to Axl-driven EMT.....	27
Chapter 3. Loss of <i>Tbk1</i> kinase activity protects mice from diet-induced metabolic dysfunction.....	38
3.1 HFD induces TBK1 expression and activity.....	38
3.2 <i>Tbk1</i> Δ/Δ mice are resistant to DIO.....	38
3.3 <i>Tbk1</i> Δ/Δ mice are glucose and insulin tolerant on HFD.....	39
3.4 Loss of TBK1 kinase enhances insulin sensitivity on HFD.....	40
3.5 <i>Tbk1</i> Δ/Δ mice expend more energy through physical activity.....	42
3.6 HFD-fed <i>Tbk1</i> Δ/Δ mice maintain lipid homeostasis.....	44
3.7 Diet-induced inflammation is nominal in <i>Tbk1</i> Δ/Δ mice.....	45
Chapter 4. Discussion and Conclusions.....	58
Chapter 5. Experimental Procedures.....	67
Bibliography.....	78
Acknowledgements.....	90

PRIOR PUBLICATIONS

V.H. Cruz, E.N. Arner, K.W. Wynne, P.E. Scherer, R.A. Brekken. Loss of *Tbk1* kinase activity protects mice from diet-induced metabolic dysfunction. Molecular Metabolism. *In press*. <https://doi.org/10.1016/j.molmet.2018.06.007>

V.H. Cruz, R.A. Brekken. Assessment of TANK-binding kinase 1 as a therapeutic target in cancer. Journal of Cell Communication and Signaling. 2018 March 29;12(1):83-90.

K.F. Ludwig, W. Du, N. Sorrelle, K. Wnuk-Lipinska, M. Topalovski, J.E. Toombs, **V.H. Cruz**, S. Yabuuchi, N.V. Rajeshkumar, A. Maitra, J.B. Lorens, R.A. Brekken. Small molecule inhibition of Axl targets tumor immune suppression and enhances chemotherapy in pancreatic cancer. Cancer Research. 2018 Jan 1; 78 (1): 246-255.

Y. Guo, B. Updegraff, S. Park, D. Durakoglugil, **V.H. Cruz**, S. Maddux, T.H. Hwang, K.A. O'Donnell. A comprehensive *ex vivo* transposon mutagenesis screen identifies novel drivers of human leukemogenesis. Cancer Research. 2016 Feb 15;76(4):773-86.

O. Ocal, V. Pashkov, R.K. Kollipara, B.R. Heath, A.B. Artyukhin, **V.H. Cruz****, A.L. Christie, J.B. Lorens, G.H. Swift, R.A. Brekken, T.M. Wilkie. A rapid in vivo screen for pancreatic ductal adenocarcinoma therapeutics. Disease Models & Mechanisms. 2015 Oct 1;8(10):1201-11.

***Note: Last name change from Burton to Cruz.*

W. Li*, N. Hu*, **V.H. Burton***, H.H. Yang, H. Su, C. Conway, L. Wang, C. Wang, T. Ding, Y. Xu, C. Giffen, C.C. Abnet, A.M. Goldstein, S.M. Hewitt, P.R. Taylor. PLCE1 mRNA and protein expression and survival of patients with esophageal squamous cell carcinoma and gastric adenocarcinoma. Cancer Epidemiology, Biomarkers & Prevention. 2014 Aug;23(8):1579-88.

**co-first author*

Q. Du, W. Yan, **V.H. Burton**, S.M. Hewitt, L. Wang, N. Hu, P.R. Taylor, M.D. Armani, S. Mukherjee, M.R. Emmert-Buck, M.A. Tangrea. Validation of esophageal squamous cell carcinoma candidate genes from high-throughput transcriptomic studies. American Journal of Cancer Research. 2013 August; 3(4): 402–410.

P.M. Van Wynsberghe, Z. Kai, K. Massirer, **V.H. Burton**, G. Yeo and A.E. Pasquinelli. Co-transcriptional association of LIN-28 with let-7 primary transcripts regulates miRNA maturation in *C.elegans*. Nature Structural & Molecular Biology. 2011 March; 18(3): 302-8.

LIST OF FIGURES AND TABLES

Chapter 1. Introduction

Figure 1.1.....	18
Table 1.....	19

Chapter 2. *Tbk1* loss in pancreatic cancer reduces tumor epithelial plasticity

Figure 2.1.....	29
Figure 2.2.....	30
Figure 2.3.....	31
Figure 2.4.....	32
Figure 2.5.....	33
Figure 2.6.....	34
Figure 2.7.....	35
Figure 2.8.....	36
Figure 2.9.....	37

Chapter 3. Loss of *Tbk1* kinase activity protects mice from diet-induced metabolic dysfunction

Figure 3.1.....	47
Figure 3.2.....	48
Figure 3.3.....	49
Figure 3.4.....	50
Figure 3.5.....	51
Figure 3.6.....	52
Figure 3.7.....	53
Figure 3.8.....	54
Figure 3.9.....	55
Figure 3.10.....	56
Figure 3.11.....	57

LIST OF ABBREVIATIONS

AALE	Immortalized tracheobronchial epithelial cells
AKT	Protein kinase B
ALS	Amyotrophic lateral sclerosis
ATKO	Adipose tissue knockout
BRAF ⁱ	BRAF inhibitor
CCL2	Chemokine ligand 2
CCL4	Chemokine ligand 4
CCL5	Chemokine ligand 5
CCL27	Chemokine ligand 27
Cdkn2a	Cyclin-dependent kinase Inhibitor 2A
CEP1	Centrosomal protein 170
CK19	Cytokeratin 19
CMV	Cytomegalovirus
CXCL1	Chemokine (C-X-C motif) ligand 1
DAPI	4',6-diamidino-2-phenylindole
DC	Dendritic cell
DIO	Diet-induced obesity
DKO	Dendritic cell knockout
EF1	Elongation factor 1
EMT	Epithelial-to-mesenchymal transition
ER α	Estrogen receptor α
FBS	Fetal bovine serum
FTD	Frontotemporal dementia
GAPDH	Glyceraldehyde 3-phosphate dehydrogenase
GAS6	Growth arrest specific 6
GEMM	Genetically engineered mouse model
GFP	Green fluorescent protein
GSK3 β	Glycogen synthase kinase 3 β
GST	Glutathione S-transferase
GTP	Guanosine triphosphate
HFD	High fat diet
HPNE	Human pancreatic nestin expressing
IC ₅₀	Half maximal inhibitory concentration
IFN-I	Type I interferon
IFN β	Interferon β
IFNAR1	Interferon α/β receptor 1
IgG	Immunoglobulin G
IKB	Inhibitor of NF κ B
IKK	I κ B kinase
IKK α	I κ B kinase α
IKK β	I κ B kinase β
IKK ϵ	I κ B kinase ϵ
IL1	Interleukin 1
IL1R	Interleukin 1 receptor

IL1 β	Interleukin 1 β
IL6	Interleukin 6
IL12	Interleukin 12
IRF1	Interferon regulator factor 1
IRF3	Interferon regulator factor 3
IRS	Insulin receptor substrate
IR β	Insulin receptor β
IV	Intravenous
JNK	Jun N-terminal kinase
LATS1	Large tumor suppressor kinase 1
LC3	Microtubule-associated protein-1 light chain 3
LPS	Lipopolysaccharide
LSL	Lox-stop-lox
MCS	Multiple cloning site
MEFs	Mouse embryonic fibroblasts
MEKi	MEK inhibitor
MMP9	Matrix Metalloproteinase 9
mTOR	Mammalian target of rapamycin
mTOR	Mammalian target of rapamycin
MTS	3-(4,5-dimethylthiazol-2-yl)-5-(3-carboxymethoxyphenyl)-2-(4-sulfophenyl)-2H-tetrazolium)
ND	Normal chow diet
Neo	Neomycin
NF- κ B	Nuclear factor kappa B
NOD SCID	Nonobese diabetic/severe combined immunodeficiency
NSCLC	Non-small cell lung cancer
NSG	NOD SCID gamma
NUMA	Nuclear mitotic apparatus protein
OGTT	Oral glucose tolerance test
OPTN	Optineurin
p65	NF- κ B p65 subunit
PanIN	Pancreatic intraepithelial neoplasia
PBS	Phosphate-buffered saline
H&E	Hematoxylin and eosin
IgG	Immunoglobulin G
PCR	Polymerase chain reaction
PD-1	Programmed cell death protein 1
PDA	Pancreatic ductal adenocarcinoma
PDK1	3-phosphoinositide-dependent protein kinase-1
PGC1 α	PPARG co-activator 1 α
PI3K	Phosphatidylinositol-4,5-bisphosphate 3-kinase
PKC	Protein kinase C
PLK1	Polo-like kinase 1
PPARG	Peroxisome proliferator-activated receptor gamma
PTF1A	Pancreas transcription factor 1 α
qPCR	Quantitative PCR

RAL	Ras-related protein
RAS	Rat sarcoma virus
RBD	RAS-binding domain
RIPA	Radioimmunoprecipitation assay
S6K	p70 S6 kinase
SEM	Standard error of the mean
SILAC	Stable isotope labeling by amino acids in cell culture
siRNA	Small interfering RNA
STAT3	Signal transducer and activator of transcription 3
STING	Stimulator of interferon genes
TANK	TRAF family member associated NF- κ B activator
TBK1	TANK binding kinase 1
TBK1i	TBK1 inhibitor
TCGA	The cancer genome atlas
TGF β	Transforming growth factor β
TIMP3	Tissue inhibitor of metalloproteinase 3
TNF α	Tumor necrosis factor α
UCP1	Uncoupling protein 1
UCP2	Uncoupling protein 2
VCAM1	Vascular cell adhesion molecule 1
WAT	White adipose tissue
WT	Wild-type
YAP1	Yes associated protein 1
ZEB1	Zinc finger E-box binding homeobox 1
ZO1	Zonula occludens-1

Chapter 1. Introduction

1.1 Pancreatic Cancer

Pancreatic cancer is one of the most lethal and poorly understood human malignancies for which patient survival has not improved substantially in more than 40 years [22].

Each year, over 45,000 new cases are diagnosed and an almost equal number of patients succumb to this devastating disease [22]. The high incidence to death ratio is attributed in part to late diagnosis, at which point the tumor is aggressively invasive, as well as resistant to most forms of conventional chemo and radiotherapies [37].

Therefore, effective therapies are needed to enhance the long-term survival of patients with pancreatic ductal adenocarcinoma (PDA).

A major challenge in the pancreatic cancer field is the identification of signaling molecules or pathways critical for PDA growth that can be utilized to develop effective targeted therapies. An activating point mutation in the small GTPase, *KRAS* is one of the earliest genetic events seen in human PDA development and is present in 90% of PDA cases [38]. These observations support that oncogenic K-RAS is the dominant driver in PDA initiation and maintenance [46]. However, since RAS itself has not been an amenable target for the development of direct inhibitors, much effort is focused on inhibiting RAS effector signaling [30].

Identification of TANK-binding kinase 1 (TBK1) as a RAS effector

While the majority of RAS effector targeted therapies are focused on the RAF and PI3K signaling networks, there is considerable evidence supporting the serine threonine

protein kinase, TBK1 as a critical mediator of RAS-driven tumorigenesis [6, 67]. As a member of the inhibitor of kappa B kinase (IKK) family, TBK1 functions as a regulator of innate immunity. Upon pathogen recognition, TBK1 can mobilize the interferon response pathway or activate the NF- κ B pathway in host cell defense [36]. Studies in lung cancer revealed that TBK1 activation enabled tumor cells to survive under stressful conditions while ablation of TBK1 expression or activity induced apoptosis. Moreover, expression of an oncogenic *K-Ras* allele in TBK1-deficient murine embryonic fibroblasts induced immediate cell death, suggesting that TBK1 is integral for cells to tolerate transforming levels of oncogenic RAS [12, 67]. The critical contribution of TBK1 to RAS-induced cancer growth was corroborated in an RNAi screen of synthetic lethal partners of oncogenic K-RAS, where *TBK1* was identified as a top hit [6]. While RAS signaling through TBK1 is well established, the mechanism by which TBK1 promotes tumorigenesis remains unclear. Dozens of publications related to TBK1 signaling in cancer have resulted since these initial discoveries were made several years ago.

TBK1 supports microtubule stability and mitosis in non small cell lung cancer (NSCLC)

TBK1 was originally linked to cell division in a phosphoproteomics screen performed in A549 lung adenocarcinoma cells [48]. The stable isotope labeling by amino acids in cell culture (SILAC) mass spectrometry technique was used in control shRNA and shTBK1 knock-down A549 cells to define TBK1-regulated signaling networks based on quantitative differences in phosphoproteins. Pathway analyses and subsequent experimental validation revealed that TBK1 is induced at mitosis and directly

phosphorylates the mitotic kinase, Polo-like kinase 1 (PLK1). In 2015, Pillai and colleagues [69] confirmed TBK1 induction during mitosis in NSCLC cell lines. However, PLK1 overexpression did not rescue mitotic progression in cells treated with siRNA targeting TBK1. This led to a search for and ultimately identification of novel mitotic TBK1 substrates including CEP170 and NUMA, proteins that promote microtubule stability and mitosis.

Given the relatively high frequency of *KRAS* mutations in lung cancer, one consideration is whether TBK1 facilitates mitotic spindle formation independent of mutant *KRAS*. The discovery of CEP170 and NUMA as mitotic TBK1 substrates was made in both mutant and wild-type (WT) *KRAS* NSCLC lines, suggesting that mutant *KRAS* may not be initiating this function of TBK1. Thus, the identity of upstream factors that direct TBK1 to the centrosome during mitosis and induce TBK1 expression is of great interest. Evidence from recent studies indicates that TBK1 activation is dependent upon its subcellular localization as well as local TBK1 concentration [36, 56]. Numerous adaptor proteins have been shown to escort TBK1 to various signaling complexes for distinctive cellular responses. Additionally, TBK1 can autophosphorylate itself through inter-dimer interactions between locally concentrated TBK1 molecules. Moving forward, it will be important to test these findings in vivo to understand the clinical significance of targeting TBK1 in NSCLC. Mitotic defects resulting from TBK1 inhibition in vitro indicate that therapeutically targeting TBK1 would likely have a cytotoxic effect by preventing tumor cell division. Inhibiting cancer cell proliferation by blocking TBK1 activity could be

especially beneficial in combination with drugs that function independently of the cell cycle.

TBK1 promotes autophagy during pathogen infection and oncogenic stress

TBK1 has been shown to promote the intracellular degradation pathway, autophagy, which is often deregulated in human cancers [63, 102]. Autophagy is a fundamental biological process of self-digestion, whereby a cell degrades various intracellular components, including damaged or excessive proteins and organelles, as a reactive survival mechanism or as a strategy to maintain cellular energy production. Autophagy is induced by various physiological stressors including hypoxia, nutrient deprivation, high temperatures and innate immune signals [54]. Deregulation of autophagy is implicated in various disease states, including cancer. However, the function of autophagy in cancer cells is complex with reports indicating it has oncogenic and tumor-suppressive roles. Depending on the tumor source and/or stage, autophagy can function as a tumor suppressor pathway that prevents tumor formation. For example, in the initial stages of pancreatic cancer, autophagy can limit inflammation and cell injury, processes that are critical for tumor development and progression [28]. Autophagy also functions as a pro-survival pathway in pancreatic cancer, allowing tumor cells to tolerate metabolic stress and resist cell death induced by chemotherapy. In fact, several studies have reported elevated basal autophagy levels in human PDA cell lines and primary tumor tissues. Inhibition of autophagy in culture and in PDA mouse models caused marked growth suppression, indicating a large subset of PDA cells depend on autophagy [77, 103].

Originally, autophagy was thought to be a nonselective bulk degradation pathway in response to cellular stress. Recent studies have revealed that through the use of autophagic receptors and adaptors, the antibacterial form of autophagy, referred to as 'xenophagy', can selectively degrade intracellular pathogens [23, 73]. In xenophagy, TBK1 activates the adaptor proteins OPTN and p62 that bind to and escort invading pathogens for rapid autophagic clearance [43, 70, 96]. I, along with another group (Pilli, Arko-Mensah et al. 2012), observed an increase in the autophagic marker, LC3, in *Tbk1-deficient* mouse embryonic fibroblasts (MEFs) without any pathogenic stimulus (**Figure 1.1A-B**). Additionally, I detected an increase in autophagic markers, LC3 and p62, in tumor tissues collected from *Tbk1* mutant mice (*Tbk1*^{ΔΔ}) that were crossed into a genetically engineered mouse model of PDA (*Kras*^{LSL-G12D}; *Cdkn2a*^{lox/lox}; *Ptf1a*^{Cre/+}) compared to *Tbk1*^{+/+}: PDA tumors (**Figure 1.1C**). *Tbk1*^{ΔΔ} mice have a truncated form of TBK1 that lacks the catalytic domain and is expressed at very low levels globally [58]. These findings demonstrate that autophagy is altered in the absence of *Tbk1* and suggest that TBK1 may regulate autophagy induced by stimuli other than bacteria. Furthermore, it is plausible that TBK1 contributes to the pro-survival effect of autophagy in tumors, including PDA.

Similarly, a recent study by Yang et al. [102] demonstrated a link between autophagy inhibition and TBK1 signaling in pancreas cancer. They claim that a negative feedback mechanism exists between TBK1 and autophagy, whereby active TBK1 promotes basal autophagy in PDA cells and is then degraded in the autophagic process to limit over-activation of autophagy and TBK1-induced cytokine production, both of which fuel

neoplasia. Accordingly, utilization of the multitarget JAK/TBK1/IKK ϵ inhibitor CYT387 (mometinib) proved advantageous in blocking autophagy and cytokine production in a PDA cell line with high basal autophagy and in a PDA mouse model, resulting in more intact pancreatic acinar tissue and limited pre-neoplastic lesions relative to vehicle control. While the authors mention that autophagy restricts TBK1 and cytokine activity, it is not clear how cell lines with low basal levels of autophagy would respond to the multi-target inhibitor CYT387. It is intriguing to consider but currently unclear whether baseline autophagy levels could serve as a predictor of CYT387 sensitivity. Or whether inflammation could function as a biomarker for this TBK1 inhibitor. It is also unclear if mutant active *KRAS* is necessary for the negative feedback between TBK1 and autophagy in PDA cells. This is especially relevant considering that oncogenic *KRAS* can induce autophagy and is commonly mutated in PDA [29]. It is worth pointing out that CYT387 has undergone testing in multiple clinical trials including in combination with chemotherapy in PDA and in combination with the MEK inhibitor, Trametinib, in NCSLC. Results from these trials will be very informative from multiple interest points, including that of *KRAS*-driven cancers.

TBK1 participates in tumor immunity

Innate immune sensing is a critical step in promoting T-cell priming and infiltration in tumors. Better understanding of the cross talk between innate and adaptive immune systems is needed to pharmacologically facilitate enduring anti-tumor immunity. TBK1 is best known as an innate immune kinase that is downstream of the transmembrane protein stimulator of interferon genes (STING) in the type I interferon (IFN-I) response

pathway. STING senses the presence of nucleic acids from intracellular pathogen infection and in turn initiates a downstream signaling cascade that includes TBK1-mediated activation of IRF3 and Stat6, resulting in IFN-I and cytokine production [10, 42]. Multiple STING agonists have been shown to generate anti-tumor immunity through interferon β (IFN- β) production in the tumor microenvironment [15, 97]. Intratumoral injection of synthetically derived cyclic di-nucleotides to activate STING resulted in primary tumor regression in three different murine tumor models, including B16 melanoma, 4T1 mammary and CT26 colon carcinomas. In each of these models, a systemic immune response involving IFN- β and cytokine production, priming of CD8+ T cells and immunologic memory was elicited that prevented primary tumor growth and the development of distal lesions. This work supports the development of innate immune modulatory strategies for anti-tumor efficacy and implicates TBK1 as a potential anti-tumor protein.

Contrary to these findings, a recent study of dendritic cell (DC) conditional *Tbk1* knockout mice (*Tbk1-DKO*) found that *Tbk1-DKO* mice injected subcutaneously with tumor cells lived longer and had smaller tumors compared to wild-type (*WT*) control mice [99]. Bone marrow and spleen from *Tbk1-DKO* and *WT* control mice showed similar peripheral immune profiles, implying that TBK1 is not critical to myeloid cell development. Yet the assessment of anti-tumor immunity in *Tbk1-DKO* animals containing B16 melanoma tumors revealed greater T-effector cell infiltration into tumors and lymph nodes as well as synergy with anti-PD-1 treatment. These results were corroborated with two additional tumor cell lines (EG7-OVA and EL4 lymphoma cells).

Gene expression profiling of DCs isolated from *Tbk1-DKO* spleens and tumors showed enhanced interferon-responsive gene expression compared to *WT* control DCs. To see if the *Tbk1-DKO* tumor suppressive phenotype was dependent upon interferon signaling, DCs harvested from *Tbk1-DKO* mice crossed into *interferon alpha/beta receptor 1 (Ifnar1) KO* mice were utilized in DC-based tumor immunotherapy in *WT* mice with established B16 melanoma tumors. Treatment with double *TBK1^{DKO} IFNAR^{KO}* DCs allowed for tumor development unlike in the *TBK1^{DKO} IFNAR^{WT}* DC therapy group where tumor growth was restrained. Collectively, these observations support a pro-tumor function for TBK1 in DCs that suppresses IFNAR1 signaling to mediate immune tolerance and enable tumor growth.

While the interpretation of the function of TBK1 in tumor immunity from these two publications [15, 99] are conflicting, we can glean that the function of TBK1 is likely variable between different stromal cell types within a tumor and even within cancer types. Further work is needed to understand whether there are distinct tumor types that would respond better to modulation of TBK1 activity. In the previous publication [99], for example, synergy was observed in *Tbk1-DKO* animals containing B16 melanoma tumors treated with anti-PD-1. Thus, it is plausible that PD-L1 expressing tumors may show a stronger response to TBK1 inhibition. Xiao and colleagues [99] also showed greater T-effector cell tumor infiltration in tumor bearing *Tbk1-DKO* animals compared to tumor bearing *WT* control animals. Therefore, it may also be therapeutically beneficial to pretreat immune therapy non-responder patients with a TBK1 inhibitor in an effort to augment T-cell infiltration into tumors. These papers highlight the importance in

understanding the unique function of TBK1 in each relevant cell type within a tumor as well as different tumor types and mouse models. This is especially pertinent when considering the therapeutic benefit of pharmacological modulation of TBK1 in cancer patients. If TBK1 does function differently between immune cell types, then going forward it would be important to evaluate whether one cell type is more abundant in a particular tumor or has more of a dominant effect on tumor growth.

TBK1 activates AKT pro-survival signaling in melanoma and NSCLC

One of the original reports linking TBK1 with RAS signaling identified AKT as a direct substrate of TBK1 in NSCLC [67]. Follow up from these results has led to the characterization of TBK1 as a molecular vulnerability in subtypes of melanoma, in addition to NSCLC, in two recent studies [13, 21]. Eskiocak et al. [21] used a panel of melanoma cell lines annotated with drug-resistant status in screening a chemical compound library to identify molecular liabilities unique to BRAF inhibitor (BRAFi) resistant tumors. Bx795, a TBK1/PDK1 (3-phosphoinositide-dependent protein kinase-1) dual inhibitor was the top hit from the screen with selective toxicity in BRAFi resistant cell lines. Since Bx795 is a dual TBK1/PDK1 inhibitor, the mechanism of action causing toxicity in the drug resistant melanoma cell lines was unclear. Additional scaffolds targeting TBK1 were tested, including compound II, MRT6737 and momelotinib, and these showed similar toxicity profiles across the cell panel, incriminating TBK1 inhibition as the cause for cell death. Of note, TBK1 inhibitor (TBK1i) sensitivity positively correlated with MEK inhibitor resistance. TBK1 inhibitor, compound II, was selected for further testing in vivo in NSG (*Cg-Prkdc^{scid} Il2rg^{tm1Wjl}/SzJ*) mice subcutaneously

implanted with three melanoma cell lines that were already proven to be sensitive to compound II in vitro. As expected, tumor growth in these immunodeficient animals was reduced by compound II. Though compound II does show therapeutic benefit in this model, the growth curves of the treated tumors have a positive slope indicating that tumor growth is slowed but not inhibited. In these TBK1-dependent cell lines, compound II treatment reduced AKT activity, yet chemical inhibition of AKT was not sufficient to recapitulate the level of toxicity associated with TBK1 inhibition. Interestingly, two members of the hippo tumor suppressor pathway, LATS1 and YAP1, co-immunoprecipitated with TBK1. Inhibition of TBK1 activated the hippo tumor suppressor pathway while combined siRNA-mediated knock down of YAP1 with AKT inhibition resulted in apoptosis at a level comparable to compound II-mediated apoptosis. Thus, the authors concluded that the basis of TBK1 addiction in drug resistant melanoma cells is through the combined activation of AKT survival signaling and suppression of hippo tumor suppressor pathway activity.

In a NSCLC study [13], sensitivity to TBK1 inhibitors Bx795 and compound II along with gene expression data for 100 NSCLC cell lines were pooled to distinguish biological features of TBK1-dependent cell lines. This data included a screen of chemical compounds in pursuit of scaffolds with similar activity profiles. As in the melanoma study [21], the TBK1i sensitivity profiles correlated well with one another. They also were highly correlative with the profiles of multiple AKT/mTOR pathway inhibitors, particularly in the mutant *KRAS* NSCLC lines, suggesting a mechanistic relationship between TBK1 and the mTOR pathway. Subsequent experiments in fibroblasts with genetic modulation

or pharmacological inhibition of TBK1 uncovered a physical interaction between TBK1 and multiple components of the mTOR pathway. TBK1 promoted mTOR activation through direct phosphorylation of upstream activator AKT and downstream substrate S6K predominantly in the transition from the amino acid-starved to fed state. Further analysis of the TBK1i sensitive NSCLC lines revealed mutations in RAS family members and greater mesenchymal gene expression compared to the resistant lines that had a more epithelial gene expression profile. Intriguingly, TGF β treatment in a TBK1i resistant cell line induced epithelial-to-mesenchymal transition (EMT) and sensitized the cell line to TBK1i in a reversible manner. All in all, this report characterized a TBK1-dependent subset of NSCLC lines that contain mesenchymal gene expression, *RAS* class member mutations and are liable to mTOR pathway inhibitors. A limitation of this study is that the mechanism of TBK1 dependency in the subset of NSCLC lines is attributed to TBK1-mediated activation of the mTOR/AKT pro-survival pathway that was observed primarily in fibroblasts. This investigation sheds light on the effect of TBK1 inhibition in a relevant stromal cell type which is informative considering small molecule inhibitors do not target cancer cells exclusively. However, additional studies to validate these interactions in lung cancer cell lines would substantiate the proposed mechanism in the NSCLC context. Additionally, it would be interesting to examine the non-tumor cell autonomous consequences of inhibiting TBK1-mediated mTOR activation in tumor associated fibroblasts or other stromal cells on overall tumor growth.

These two studies [13, 21] highlight the potential of TBK1 as a therapeutic target in BRAF/MEKi resistant melanoma together with mutant *RAS* NSCLC. Moving forward, it will be essential to evaluate the therapeutic benefit of TBK1 inhibition in preclinical cancer models, particularly in immune-competent animals. The melanoma tumor xenograft studies were performed in immunodeficient animals so there is a gap in understanding how TBK1 inhibition will affect the immune-competent tumor microenvironment. Also, the TBK1-dependent melanoma cell lines were BRAF/MEKi resistant and displayed an “innate immune” expression profile. This specific combination of drug resistance and gene expression is associated with a decreased response to immune therapy [41]. Therefore, TBK1 inhibition may be a viable alternative to the subset of melanoma patients who don’t respond to immune therapy. It is also possible that pretreatment of these patients with TBK1i could enhance immune therapy response. An unexplored question stemming from the melanoma study is whether *NRAS* mutation status, which can be found in up to 30% of melanoma patients, had any correlation with TBK1i sensitivity. One group observed that TBK1 is active in mutant *NRAS* melanoma and promoted migration and invasion of these cells [90]. The group also demonstrated cooperation between TBK1 and MEK inhibition to promote apoptosis in mutant *NRAS* MEKi resistant melanomas, suggesting clinical utility for combined TBK1/MEK inhibition. While mutant *NRAS* is common in melanoma, *KRAS* activating mutations dominate PDA and to a lesser extent colon and lung cancers, respectively. Given the high sensitivity to TBK1i seen in NSCLCs with *RAS* class mutations it would also be appropriate to investigate TBK1 dependency in these other *RAS*-driven cancers.

1.2 Metabolic Syndrome

The prevalence of obesity has expanded dramatically over the last 30 years worldwide and has contributed to the increasing health burden of associated complications, including insulin resistance, type 2 diabetes, cardiovascular disease, hypertension, liver steatosis and dyslipidemia [5, 71, 98]. A primary pathology of obesity and metabolic disorders is the induction of chronic low-grade, unresolved inflammation in organs pertinent to energy homeostasis. This so-called “meta-inflammation” consists of increased levels of proinflammatory cytokines and macrophage infiltration in white adipose tissue [99] and is coincident with the manifestation of insulin resistance [9, 44, 64]. While the etiology of insulin resistance is complicated and multifaceted, numerous studies have demonstrated that blocking inflammatory mediators through genetic or pharmacological means results in improved insulin and glucose tolerance [3, 33, 40, 88, 94, 106].

TBK1 and IKK ϵ promote metabolic dysfunction

NF- κ B is a major transcriptional driver of inflammation that is activated in response to cytokines and pathogenic stimuli to promote the upregulation of inflammatory and immune regulatory gene expression. Not surprisingly, NF- κ B is chronically active in many inflammatory diseases and over the past two decades, has gained significant attention in the metabolism field due to its high-level activity in affected tissues [4, 11]. Most metabolic studies have centered on canonical NF- κ B activators, such as IKK α and IKK β ; however, Chiang and colleagues [11] reported that the noncanonical activators, IKK ϵ and TBK1, are more highly expressed than canonical activators in metabolically

affected tissues of obese animals. Subsequent investigations revealed that *Ikkbe*^{-/-} mice and mice treated with amlexanox (a dual IKKε/TBK1 small molecule inhibitor) are protected from diet-induced obesity (DIO) and associated metabolic syndrome conditions [11, 75]. This protection is thought to result from loss of TBK1 and IKKε metabolic functions in repressing adaptive energy expenditure in a diet-driven inflammatory state. However, due to the nature of amlexanox as a dual IKKε and TBK1 inhibitor and the embryonic lethality of *Tbk1*^{-/-} mice, distinguishing metabolic functions unique to TBK1 remains a challenge [8]. As amlexanox enters the clinical space for the treatment of obesity and type 2 diabetes in human trials, it has become increasingly important to understand the implications of systemic TBK1 inhibition during metabolic stress.

1.3 TBK1 inhibitors

Over the past decade, research and interest in TBK1 have expanded along with the identification and development of small molecules targeting TBK1. There are at least six distinct small molecules that are known to inhibit TBK1 including Bx795, compound II, CYT387, MRT67307, GSK2292978A and amlexanox. Though most of these compounds are quite potent towards TBK1 and homolog IKKε, not all of them are highly selective. Bx795 inhibits the serine/threonine kinase, PDK1, in addition to TBK1 and IKKε. CYT387 or momelotinib was originally described as a selective JAK inhibitor but was recently discovered to inhibit TBK1 with low nanomolar potency [109]. Three years ago, momelotinib began testing in combination with either chemotherapy or Trametinib (MEKi) in multiple clinical trials for metastatic *KRAS* mutant NSCLC and PDA

(NCT02258607, NCT02244489, NCT02101021). Unfortunately all three trials were terminated early by the sponsor, Gilead Sciences without the release of further information.

The only other TBK1i known to enter clinical trial testing in human patients is amlexanox in a phase 2 study for the treatment of type 2 diabetes, nonalcoholic fatty liver disease or obesity (NCT01975935, NCT01842282). Amlexanox was identified in a compound library screen for inhibitors of TBK1/IKK ϵ , which had previously been shown to promote metabolic syndrome in an obese rodent model [11, 75]. Takeda developed amlexanox in the 1980s for the treatment of asthma and conjunctivitis in Japan. Though the mechanism of action was unknown until recently, amlexanox is still sold in Japan for treating asthma. Despite the fact that TBK1 inhibition in patients with metabolic syndrome is a different biology than cancer, the side effects from systemic TBK1 inhibition in this trial are applicable to the evaluation of TBK1 as a viable therapeutic target in cancer patients. In the open label trial to ensure the safe administration of amlexanox, there were no serious adverse events reported [65]. However, mild to moderate events included two rash incidents that resolved in the presence of continued amlexanox treatment. The rashes, confirmed as perivascular inflammation by biopsy, are reminiscent of the reported phenotype seen in the previously mentioned [58] kinase dead *Tbk1* ^{$\Delta\Delta$} mice. These mice exhibited mild levels of immune cell infiltrates in multiple organs and tissues including skin. It is likely that modulation of the innate immune kinase TBK1 will result in some form of an altered immune reactivity. The question then becomes in what way and how will that affect diseases that are exacerbated by

inflammation? Aside from that, the mild side effects observed from the amlexanox trial are promising in terms of tolerability of systemic TBK1 inhibition, at least in the context of amlexanox.

1.4 Conclusions

The multifunctional kinase, TBK1, mediates numerous signaling pathways that result in malignant growth and metabolic disease (**Table 1**). In the context of cancer, TBK1 facilitates cell division in lung cancer cells through its interaction with mitotic substrates PLK1, CEP170 and NUMA to promote microtubule stability and mitosis. TBK1 can also promote autophagy in pancreatic cancer cells to silence proinflammatory signals that illicit an immune response. Furthermore, the DC-specific function of TBK1 suppresses IFNAR1 signaling to enable tumor growth. In a subset of melanoma and *RAS* mutant NSCLC cancers, TBK1 has been implicated in the activation of AKT/mTOR signaling to promote cancer cell survival. Given the prominent activity of mutant K-RAS in pancreatic cancer and the requirement of TBK1 for cells to tolerate transforming levels of oncogenic RAS, I hypothesized that TBK1 is critical to K-RAS driven pancreatic cancer growth. In my studies, I found that TBK1 is highly expressed in pancreatic cancer and is negatively associated with survival outcomes in human pancreatic cancer patients. Further, loss of TBK1 kinase function in preclinical mouse models of *K-Ras* mutant PDA resulted in lighter tumor load and fewer metastatic events indicating that TBK1 activity contributes directly to the aggressive and metastatic properties of pancreatic cancer. Taken together, my results highlight TBK1 inhibition as a novel approach to targeting *KRAS* mutant pancreatic cancer.

In a metabolic setting, homologs TBK1 and IKK ϵ are induced in response to high fat diet challenge [11, 75]. IKK ϵ in particular, regulates lipid and glucose metabolism by sustaining a state of chronic, low-grade inflammation through NF- κ B in obese mice [11, 61, 74, 75]. Given that both TBK1 and IKK ϵ can activate the immune response transcription factor, NF- κ B, I suspected that TBK1 also functions to maintain metabolic balance under HFD feeding. Therefore, I set out to investigate TBK1-dependent contributions to metabolism in a metabolically challenged rodent model. I did this utilizing a *Tbk1* mutant mouse that harbors two copies of a null *Tbk1* allele (*Tbk1* $^{\Delta/\Delta}$) [58]. This particular “null allele” encodes a truncated TBK1 protein that is catalytically inactive and expressed at low levels, thereby allowing analysis of global TBK1 kinase loss in vivo. Recently, Zhao and colleagues [108] reported the metabolic effects of an adipocyte specific *Tbk1*-deficient animal model. Here, I focus on the analysis of a global loss-of-function mutant, which provides an opportunity to evaluate the function of TBK1 in a wider context than just the adipocyte. Overall, loss of TBK1 kinase activity improved the health of HFD-challenged mice by alleviating the repression of insulin receptor signaling, resulting in enhanced insulin sensitivity and glucose absorption. These results imply that targeting TBK1 in metabolic syndrome patients may be beneficial and warrant further testing of TBK1 pharmacological inhibitors in human trials.

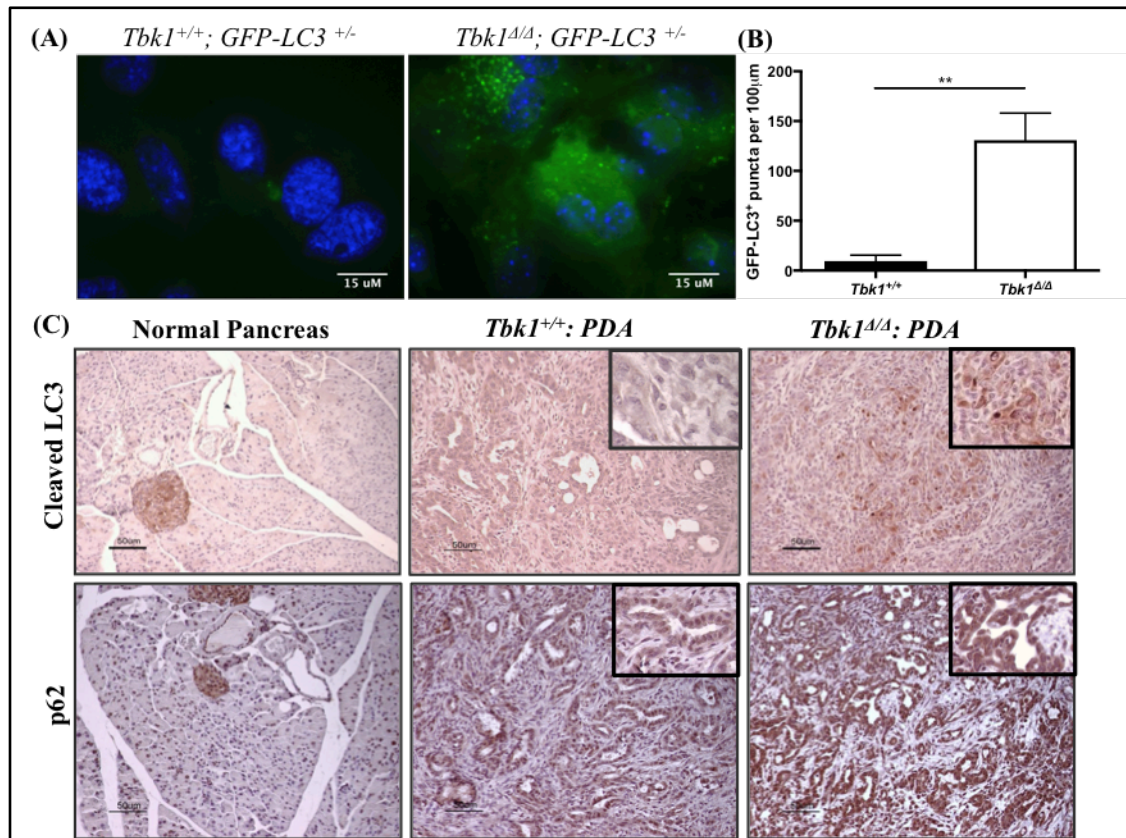


Figure 1.1. Autophagy is dysregulated in the absence of *Tbk1*. (A) MEFs isolated at E13.5 days were cultured in DMEM-10% serum. (B) GFP-LC3⁺ puncta were quantified in a minimum of four microscopic fields per cell line (3 cell lines/genotype) at 100x. Results are presented as mean ± SEM. **p<0.01, student's t-test. (C) Tumor tissues from *Tbk1*^{+/+}; PDA and *Tbk1*^{Δ/Δ}; PDA mice were stained for autophagy markers LC3 and p62 to analyze autophagic flux. Images are representative of 4 images/tumor, 5 tumors/genotype.

Table 1. Summary of TBK1-mediated malignant growth signaling.

Upstream/Predictor	Downstream/Substrate	Context	Reference
-	PLK1	NSCLC	Kim, J. Y. et al. 2013
-	CEP170, NUMA	NSCLC*	Pillai, S. et al. 2015
KRAS, IL1	CCL5, IL6	PDA	Zhu, Z. et al. 2014, Yang, S. et al. 2016
STING	IRF3	Melanoma	Corrales, L. et al. 2015
-	IFNAR1, STAT3	Melanoma, Lymphoma	Xiao, Y. et al. 2017
BRAF ⁱ /MEK ⁱ resistance	AKT, YAP1, LATS1	Melanoma	Eskiocak, B. et al. 2017
RAS class	S6K, AKT	NSCLC, Fibroblasts	Cooper, J. M. et al. 2017

- Undefined/unmentioned by authors

* Experiments were carried out primarily in NSCLC cell lines but some experiments were validated in cell lines of other origins including myeloid leukemia, Daudi Burkitt lymphoma, HeLa, AALE cells.

Chapter 2: *Tbk1* loss in pancreatic cancer reduces tumor epithelial plasticity

2.1 TBK1 expression in pancreatic cancer

TBK1 is expressed in numerous epithelial tumors including breast, lung and colon [6, 50, 81, 101]. Up until now, the function and activity of TBK1 in human pancreatic cancer has not been characterized extensively. Evaluation of TBK1 expression and activity in a panel of human pancreatic cancer cell lines revealed high activity as seen by pTBK1 expression in *KRAS* mutant PDA cell lines relative to wild-type *KRAS* cell lines (**Figure 2.1A**). This included the Human Pancreatic Nestin Expressing (HPNE) cell line which is an immortalized, untransformed pancreatic ductal epithelial line that is *KRAS* wild-type and had relatively high levels of TBK1 but limited expression of pTBK1 under basal conditions. Mouse embryonic fibroblasts (MEFs) isolated from *Tbk1* mutant mice (*Tbk1*^{Δ/Δ}) served as a negative control with no detectable expression of TBK1 or pTBK1. Additionally, I observed higher TBK1 protein levels in spontaneous pancreatic tumors from genetically engineered mouse models (GEMMs) compared to normal pancreas from littermate controls (**Figure 2.1B**). I have previously shown that *TBK1* expression is associated with poor prognosis in pancreatic cancer patients (stages I-II) from the Cancer Genome Atlas (TCGA) [16]. From this cohort (n=84), gene expression was divided into top 25% and bottom 75% percentiles for Kaplan Meier survival analyses. While expression of TBK1 homolog, *IKBKE*, showed no correlation with survival, high expression of *TBK1* showed a strong trend towards poorer overall survival in this patient cohort (p=0.07) (**Figure 2.1C-D**). Though not causative, this data strengthens the importance of TBK1 in *human pancreatic cancer*.

2.2 K-RAS-driven pancreatic cancer growth is disrupted by restricting TBK1 kinase activity

After observing high TBK1 activity in human PDA cell lines with mutant active *KRAS*, I tested cell line dependency on TBK1 for viability. I did this using the small molecule inhibitor of TBK1 kinase activity, compound II. Compound II is a 6-aminopyrazolopyrimidine derivative with an IC_{50} of 13 nM and 59 nM against TBK1 and IKK ϵ , respectively [67]. Compound II has 100- to 1000-fold less activity against other purified recombinant protein kinases tested, including PI3K and mTOR family members. Following a 96-hour exposure to compound II, viability of human and mouse PDA cell lines was measured using the colorimetric based MTS assay system (**Figure 2.2A**). Remarkably, cell lines harboring a *KRAS* mutation (shown in red) segregated distinctly from wild-type *KRAS* cell lines (shown in blue) with an IC_{50} of around 1 μ M. Interestingly, the *KRAS* wild-type PDA cell line, Hs766T, which previously showed no TBK1 activity, was the least sensitive to TBK1 inhibition with an IC_{50} above 20 μ M. In this panel, MCF-7 is a *KRAS* wild-type cancer cell line that was previously shown by Ou et al. [67] to be less sensitive to compound II and therefore served as a negative control with an IC_{50} of 5 μ M. Additionally I tested two murine cell lines (*KPC*-M09 and *Tbk1*^{+/+}: *KIC*-B) that were isolated from spontaneous pancreatic tumors in GEMMs containing an oncogenic *K-Ras* allele that proved to be more sensitive to compound II than the human PDA cell lines. *Tbk1* ^{Δ/Δ} : *KIC*-A cells were also isolated from a spontaneous pancreatic tumor that formed in a GEMM; however, these cells lack functional TBK1 and therefore served as an additional negative control with an IC_{50} of 7 μ M. The selective sensitivity of

mutant *KRAS* PDA cell lines to TBK1 inhibition in culture led us to speculate whether TBK1 was essential to RAS-driven PDA tumorigenesis in vivo.

To assess the contribution of TBK1 to PDA progression in vivo, I crossed the *Tbk1* mutant mice (*Tbk1*^{Δ/Δ}) that harbor two copies of a null *Tbk1* allele into a GEMM of PDA [58]. The GEMM of PDA recapitulates human pancreatic cancer with the introduction of PDA-related genetic alterations into the mouse pancreas through cre-lox technology. The cre-loxP system is driven by the pancreas specific, *Ptf1a* (*p48*) gene promoter to delete a conditional *Cdkn2a* (*INK4A/ARF*) tumor suppressor allele and activate an oncogenic *K-Ras* allele, *LSL-Kras*^{G12D}, resulting in *KIC* (*LSL-Kras*^{G12D/+}; *Cdkn2a*^{Lox/Lox}; *p48*^{Cre}) mice that present with low grade ductal lesions by 3 weeks of age [1, 2, 7]. These lesions develop into small pancreatic adenocarcinomas by 6 weeks old and between 7 and 11 weeks, all *KIC* mice are moribund. I hypothesized that TBK1 was critical for RAS-mediated oncogenesis in pancreatic cancer so I expected with this model that *Tbk1*^{Δ/Δ}: *KIC* mice would have smaller tumors and outlive *Tbk1*^{+/+}: *KIC* mice. In comparing tumor sizes, I observed that tumors from *Tbk1*^{Δ/Δ}: *KIC* mice were between 20-40% smaller than *Tbk1*^{+/+}: *KIC* tumors at multiple time points, yet there was no difference in overall survival between the two groups (**Figure 2.2B-C**). Malnutrition resulting from loss of normal exocrine pancreas function and pancreatic enzyme insufficiency contributes to early death in the *KIC* model [110]. Thus, I cannot exclude the possibility that the anti-tumor effects of *Tbk1* loss are surpassed by the aggressiveness of the *KIC* model causing the mice to succumb to malnutrition.

2.3 *Tbk1*^{Δ/Δ}: KIC tumors are more ‘epithelial’

To better understand TBK1-dependent mechanisms of tumor cell growth contributing to larger tumors in *Tbk1*^{+/+}: KIC mice, I did gene expression analysis in RNA isolated from 8-week-old *Tbk1*^{Δ/Δ}: KIC & *Tbk1*^{+/+}: KIC tumors. One of the most significant and top dysregulated gene networks between *Tbk1*^{Δ/Δ}: KIC & *Tbk1*^{+/+}: KIC tumors identified by Ingenuity Pathway Analysis (Qiagen) was the “Cancer/cellular movement” network. This network included a large number of genes involved in epithelial-to-mesenchymal transition (EMT). In comparison to *Tbk1*^{+/+}: KIC tumors, all three *Tbk1*^{Δ/Δ}: KIC tumors showed a trend of lower expression of mesenchymal genes, such as Vimentin and MMP9 (Matrix Metalloproteinase 9), and higher expression of epithelial genes including Claudins 3, 4 and 10 and TIMP3 (Tissue Inhibitor of Metalloproteinase 3) (**Figure 2.3A**). This ‘EMT’ gene expression signature was consistent with alcian blue staining of *Tbk1*^{Δ/Δ}: KIC & *Tbk1*^{+/+}: KIC tumors from 8 weeks. Alcian blue stains mucins that are expressed within the ductal epithelial cells within the early panIN (pancreatic intraepithelial neoplasia) lesions [1]. Representative images show that *Tbk1*^{Δ/Δ}: KIC tumors contain more Alcian blue positive epithelial cells compared to *Tbk1*^{+/+}: KIC tumors that are more undifferentiated (**Figure 2.3B**). Furthermore, I evaluated collagen deposition in 8-week-old tumors through trichrome staining. Collagen deposition, a major hallmark of pancreatic cancer, promotes EMT in PDA and is upregulated in response to epithelial plasticity [1, 82]. *Tbk1*^{+/+}: KIC tumors showed higher levels of fibrillar collagen than *Tbk1*^{Δ/Δ}: KIC tumors by trichrome histology and quantification (**Figure 2.3C**).

To confirm the epithelial phenotype observed in *Tbk1^{Δ/Δ}*: KIC tumors is specific to the tumor cells, I isolated single cell clones from *Tbk1^{Δ/Δ}*: KIC & *Tbk1^{+/+}*: KIC tumors. In total 3 cell lines per genotype were generated, each from individual tumors. In accordance with gene expression data from *Tbk1^{+/+}*: KIC tumors, each cell line isolated from these tumors showed evidence of EMT with an elongated spindle-like cell shape, a characteristic often associated with mesenchymal cells. Moreover, cell lines from *Tbk1^{Δ/Δ}*: KIC tumors exhibited a 'cobblestone' morphology, which is a feature consistent with epithelial cells. These differences in morphology between *Tbk1^{Δ/Δ}*: KIC & *Tbk1^{+/+}*: KIC tumor cell lines were observed in 2D culture and in organotypic culture after the cells were plated on a mixed layer of collagen and matrigel to simulate the extracellular matrix (**Figure 2.3D**). Evaluation of EMT-related markers revealed largely higher expression of epithelial proteins, ZO-1 and E-cadherin and lower expression of mesenchymal proteins Vimentin, Slug and Snail in *Tbk1^{Δ/Δ}*: KIC cell lines (**Figure 2.3E**). Altogether, these results illustrate a unique epithelial signature in *Tbk1^{Δ/Δ}*: KIC cells and have implications for functional differences in tumor cell motility.

2.4 *Tbk1^{Δ/Δ}*: KIC tumor cells are less migratory & invasive

Epithelial plasticity changes commonly correspond with alterations in tumor cell motility and invasiveness [51]. Based on previous findings that *Tbk1^{Δ/Δ}*: KIC tumors & cell lines are less mesenchymal in gene expression and morphology I hypothesized that functional TBK1 is important for PDA tumor cell migration. To compare motility and invasiveness between *Tbk1^{Δ/Δ}*: KIC & *Tbk1^{+/+}*: KIC tumor cell lines, I performed a series of wound healing and transwell migration assays. Despite the fact that *Tbk1^{Δ/Δ}*: KIC cell

lines grow faster in culture, they did not migrate as well as *Tbk1*^{+/+}: KIC cells (**Figure 2.4A**). For each cell line, migration at 24 hours was plotted against total cell population doublings (**Figure 2.4B**). The negative correlation in this plot demonstrates that enhanced migration seen in *Tbk1*^{+/+}: KIC cells is not a result of faster growth rates. Transwell migration assays also revealed a 20-50% decrease in invasive capacity in *Tbk1*^{Δ/Δ}: KIC cell lines when compared *Tbk1*^{+/+}: KIC cells at multiple time points (24 and 72 hours) (**Figure 2.4C-D**). These results further highlight the reduced migratory ability of *Tbk1*^{Δ/Δ}: KIC cells.

2.5 Evaluation of *Tbk1* loss on pancreatic cancer metastases

Next I asked whether the reduction in tumor cell motility with kinase dead *Tbk1* translated to fewer metastases in vivo. The KIC mouse model of PDA is an aggressive model with an average life span of ~10 weeks [1, 2, 7]. As such, these mice rarely developed gross metastases, making this model less than ideal for comparing metastatic burden. However, it is worth mentioning that livers from *Tbk1*^{+/+} (n=14) and *Tbk1*^{Δ/Δ} (n=12) KIC mice were examined for micro-metastases. Lesions were identified in 6 livers from *Tbk1*^{+/+} animals but no lesions were found in livers from *Tbk1*-mutant mice (**Figure 2.5A-C**). To more robustly study the effect of *Tbk1* loss on metastatic potential, I employed two different animal models. First, I exploited an experimental metastasis model where *Tbk1*^{+/+} or *Tbk1*^{Δ/Δ}: KIC cell lines were injected intravenously (i.v.) into NOD SCID mice. With this model, I was able to evaluate how well *Tbk1*^{Δ/Δ}: KIC tumor cells could extravasate and grow in lung tissue following i.v. injection. Twelve days after i.v. injection, mice were sacrificed, and lungs were fixed in Bouin's solution

for visualization of gross tumor nodules (**Figure 2.6A**). Lungs from mice injected with *Tbk1*^{Δ/Δ}: *KIC* cells showed a 10-fold reduction in tumor colonies relative lungs from mice injected with *Tbk1*^{+/+}: *KIC* cells (**Figure 2.6C**). This dramatic difference was apparent grossly, by H&E and by lung weight where *Tbk1*^{Δ/Δ}: *KIC* injected lungs were 36% lighter than lungs injected with *Tbk1*^{+/+}: *KIC* cells (**Figure 2.6A-D**).

While the experimental metastasis assay results were quite striking, the effect of *Tbk1* loss on spontaneous metastatic development was also of great interest. Therefore, I crossed *Tbk1*^{Δ/Δ} mice into an alternative PDA GEMM called *KPC* (*LSL-Kras*^{G12D/+}; *LSL-Trp53*^{R172H/+}; *p48*^{Cre}). The *KPC* model differs from the *KIC* model in that it contains a dominant negative p53 point mutation instead of loss of the tumor suppressor, *Cdkn2a* [39]. *KPC* mice have a longer median survival (5 months) allowing more time for tumor cells to metastasize [39, 91]. Although not statistically significant, *Tbk1*^{Δ/Δ}: *KPC* mice live one month longer than *Tbk1*^{+/+}: *KPC* mice, shifting the median survival from 5 months to 6 months (p=0.15) (**Figure 2.6E**). Primary tumor burden was significantly reduced in *Tbk1*^{Δ/Δ}: *KPC* animals relative to *Tbk1*^{+/+}: *KPC* animals (**Figure 2.6F**). Liver and lung metastases were evaluated grossly and by H&E, alcian blue and CK19 staining, all of which showed fewer metastatic lesions in *Tbk1*^{Δ/Δ}: *KPC* mice compared to *Tbk1*^{+/+}: *KPC* mice (**Figure 2.6G-H**). Consistent with the *KIC* model and the experimental metastasis model, loss of functional *Tbk1* in the *KPC* GEM model restricted tumor cell metastases.

2.6 Re-expression of *Tbk1* in *Tbk1*^{Δ/Δ}: KIC cells

To confirm that TBK1 promotes pancreatic tumor cell motility, we stably re-expressed full-length human *TBK1* by lentiviral infection in *Tbk1*^{Δ/Δ}: KIC tumor cells and assayed for invasive and migratory activity. Re-expression of *TBK1* in *Tbk1*^{Δ/Δ}: KIC tumor cells was confirmed by western blot (**Figure 2.7A**). Though the level of *TBK1* re-expression in *Tbk1*^{Δ/Δ}: KIC tumor cell lines was substantially lower than endogenous TBK1 levels in *Tbk1*^{+/+}: KIC cell lines, we did detect a partial rescue of the migratory phenotype in *Tbk1*^{Δ/Δ}: KIC cells infected with TBK1-expressing lentivirus (pCDH-TBK1) compared to empty vector (pCDH-Empty vector) expressing cells in vitro (**Figure 2.7B-C**). Further, *Tbk1*^{Δ/Δ}: KIC cell lines rescued with pCDH-TBK1 formed 2-3x as many lung tumor nodules resulting in greater diseased lung burden than pCDH-Empty vector-infected cells after i.v. injection (**Figure 2.7D-E**). These results demonstrate that *Tbk1* loss is responsible for the migratory and invasive deficiency in *Tbk1*^{Δ/Δ}: KIC cells and highlight a novel function for TBK1 in promoting a migratory program in tumor cells.

2.7 TBK1 is central to Axl-driven EMT

Pancreatic tumor cells frequently exploit EMT programs during metastatic dissemination [51, 66]. However, the absence of functional TBK1 in pancreatic tumor cells limits EMT, invasion and metastases. We recently reported that TBK1 is downstream of the receptor tyrosine kinase, Axl, a receptor associated with EMT in PDA [49, 55].

Pharmacological inhibition of Axl led to concentration dependent decreases of TBK1 activity while stimulation of Axl with its ligand, Gas6, resulted in TBK1 activation [55]. To determine if TBK1 is central to Axl-driven EMT we evaluated Axl signaling in *Tbk1*^{Δ/Δ}:

KIC tumor cells. Axl was stimulated in *Tbk1^{Δ/Δ}: KIC* and *Tbk1^{+/+}: KIC* cells with AF854, an activating anti-Axl antibody [107], and resulting cell lysates were probed for epithelial (E-cadherin, Claudin-1), mesenchymal (N-cadherin, Slug) and Axl signaling targets (AKT). Axl activation induced N-Cadherin and Slug protein 2 to 3 fold, respectively, in *Tbk1^{+/+}: KIC* tumor cells while having no effect on mesenchymal markers in *Tbk1^{Δ/Δ}: KIC* tumor cells (**Figure 2.8A**). Furthermore, pAKT levels increased 5-fold in *Tbk1^{+/+}: KIC* cells and remained unaltered in *Tbk1^{Δ/Δ}: KIC* tumor cells upon AF854 treatment, indicating that TBK1 may be upstream of AKT. Next, we investigated Axl-induced RAS activation in *Tbk1^{+/+}: KIC* cell lines as a possible link between the Axl and TBK1 signaling cascade. *Tbk1^{+/+}: KIC-A* and *Tbk1^{+/+}: KIC-D* cells treated with AF854 resulted in a substantial increase of GTP-bound RAS, demonstrating that RAS activity is augmented by Axl activation (**Figure 2.8B**). These results are the first to show that Axl activates RAS, which leads to downstream activation of TBK1 and AKT.

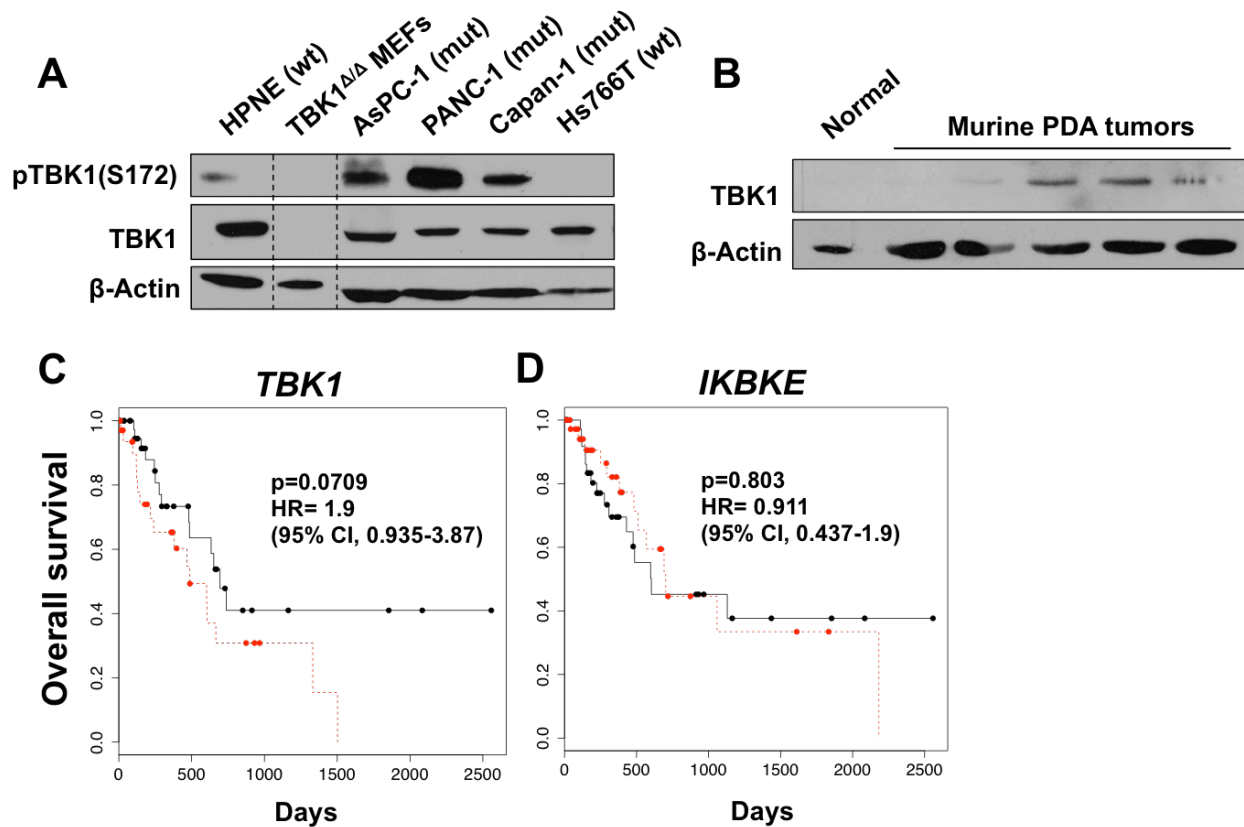


Figure 2.1. TBK1 is highly expressed in pancreatic cancer and correlates with worse overall survival. (A) Total and pTBK1(S172) expression in human PDA cell line lysates with either wild-type *KRAS* (wt) or mutant active *KRAS* (mut). HPNE is an immortalized, untransformed pancreatic ductal epithelial cell line. Lysates from *Tbk1*^{Δ/Δ} mouse embryonic fibroblasts (MEFs) served as a negative control. β-actin was used as a loading control. Dotted line indicates where blot was cropped, however, all samples were run on the same gel and exposed simultaneously. (B) Total TBK1 expression in murine PDA tumors relative to normal pancreas from a non-tumor bearing littermate control. (C) *TBK1* and (D) *IKBKE* gene expression (mRNA) in pancreatic cancer patient survival data from the TCGA [16]. Gene expression was divided into top 25% and bottom 75% percentiles. For statistical analysis, cox regression was used to calculate hazard ratios and KM -survival analyses.

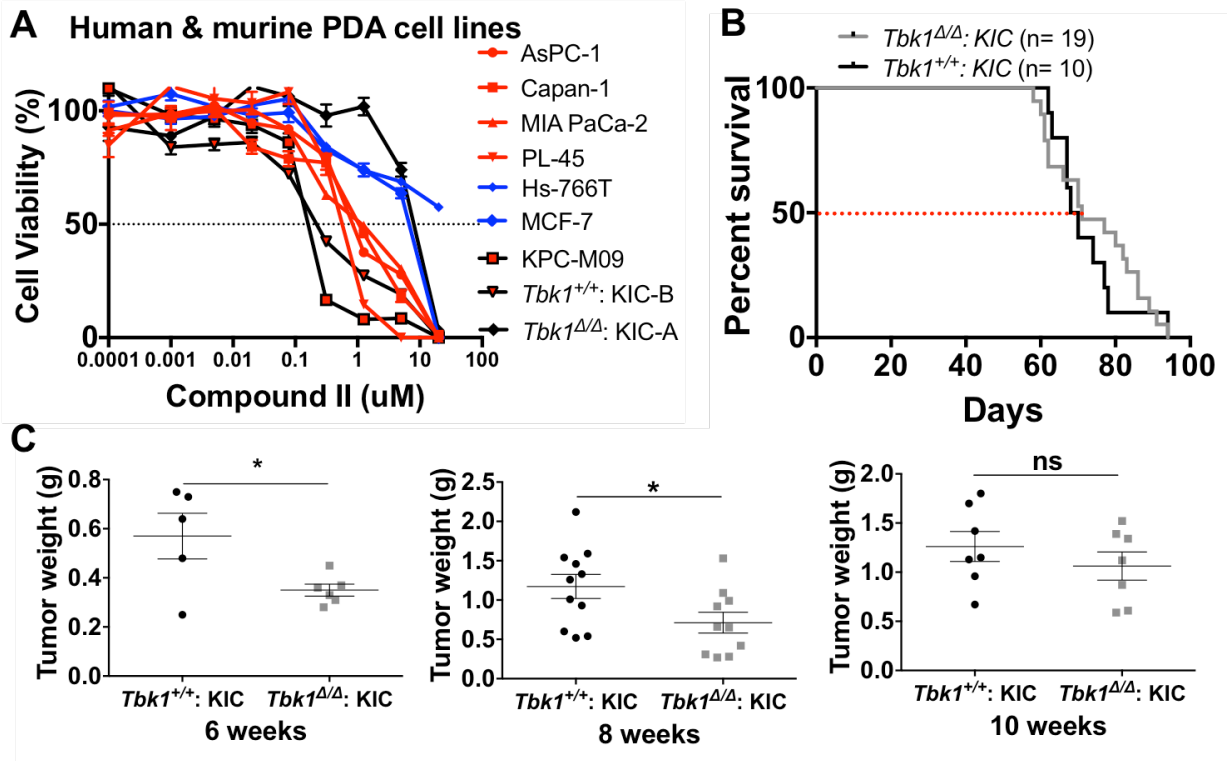


Figure 2.2. TBK1 promotes PDA tumor growth. (A) Dose response curves of human and murine PDA cell lines treated with TBK1 inhibitor, compound II. Red indicates a human *KRAS* mutant cell line, blue indicates a human *KRAS* wild-type cell line, and black indicates a murine PDA cell line. Error bars represent SEM from triplicate experiments. **(B)** Kaplan-Meier survival curve of *Tbk1*^{Δ/Δ}: KIC and *Tbk1*^{+/+}: KIC mice. Log rank mantel cox test was used for survival comparison. **(C)** Endpoint tumor weights at 6, 8 and 10 weeks in *Tbk1*^{Δ/Δ}: KIC and *Tbk1*^{+/+}: KIC. Results are representative of mean +/- SEM. Unpaired t-test *, p<0.05, ns, not significant

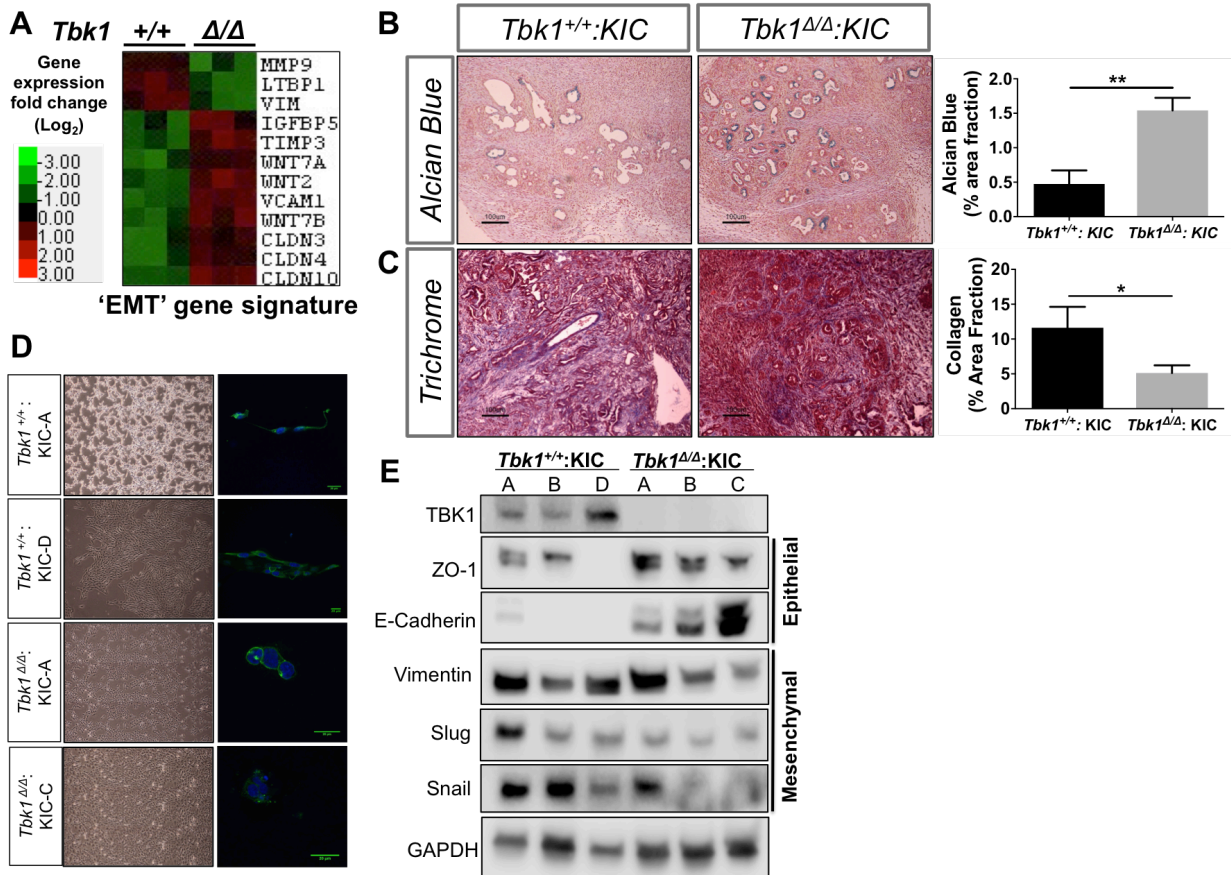


Figure 2.3. *Tbk1*^{Δ/Δ}: KIC tumors are more 'epithelial'. (A) Heatmap representing gene expression fold change (log₂) of EMT-related genes from *Tbk1*^{Δ/Δ}: KIC and *Tbk1*^{+/+}: KIC tumors. Color key indicates gene expression fold change. n=3 tumors/genotype, p<0.05 for all genes between *Tbk1*^{Δ/Δ}: KIC and *Tbk1*^{+/+}: KIC tumors. (B) Representative images of alcian blue and (C) trichrome stained tumors from eight week old *Tbk1*^{Δ/Δ}: KIC and *Tbk1*^{+/+}: KIC mice. Scale bar indicates 100 μm. n ≥ 4 mice/group, 4 images/mouse. Results are representative of mean +/- SEM. Unpaired t-test * p<0.05, ** p<0.01. (D) Representative brightfield and confocal images of single cell clones isolated from *Tbk1*^{Δ/Δ}: KIC and *Tbk1*^{+/+}: KIC tumors plated on plastic (brightfield images) or on a mixed layer of collagen and matrigel (confocal). In confocal images, nuclei were labeled with DAPI (blue) and F-actin was labeled with phalloidin (green). Scale bar indicates 20 μm. (E) Protein lysates isolated from *Tbk1*^{Δ/Δ}: KIC and *Tbk1*^{+/+}: KIC cell lines were immunoblotted for indicated epithelial and mesenchymal markers. GAPDH was used as a loading control.

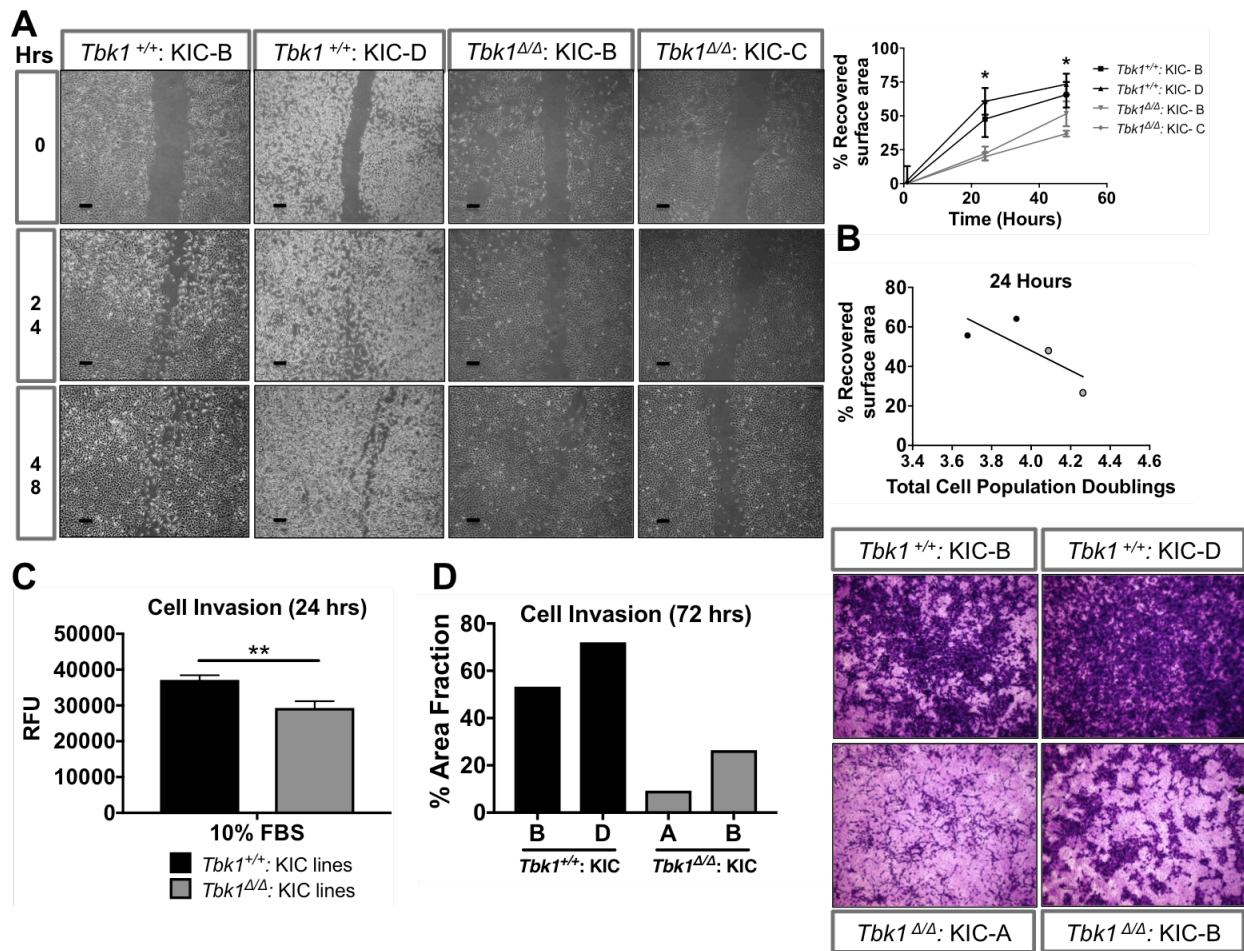


Figure 2.4. *Tbk1*^{Δ/Δ}: KIC tumor cells are less migratory & invasive than *Tbk1*^{+/+}: KIC cells. (A) Images and quantification of recovered surface area of *Tbk1*: KIC cell lines at 0, 24 and 48 hours post scratch in wound healing assay. Recovered surface area was calculated as percentage of covered area at 24 or 48 hours over originally scratched area. Images and quantification are representative of 3-wells/cell line. Scale bars indicate 100 μM. **(B)** From initial time of plating, total cell population doublings were calculated for each cell line in **(A)** and correlated to each respective cell lines' recovered surface area. Black dots indicate *Tbk1*^{+/+}: KIC cell lines and grey dots indicate *Tbk1*^{Δ/Δ}: KIC cell lines. **(C)** Quantification (expressed as relative fluorescent units) of *Tbk1*: KIC cells that passed through transwell membranes 24 hours after plating in serum free media. **(D)** Quantification and images of crystal violet stained *Tbk1*: KIC cells that passed through the transwell membranes after 72 hours. Quantification was measured as percent area fraction of membrane covered in cells (stained in purple). For both **(C)** and **(D)** outer wells of transwell assays were filled with 10% FBS containing media as the chemoattractant. Results are representative of mean +/- SEM. Unpaired t-test * p<0.05, ** p<0.01.

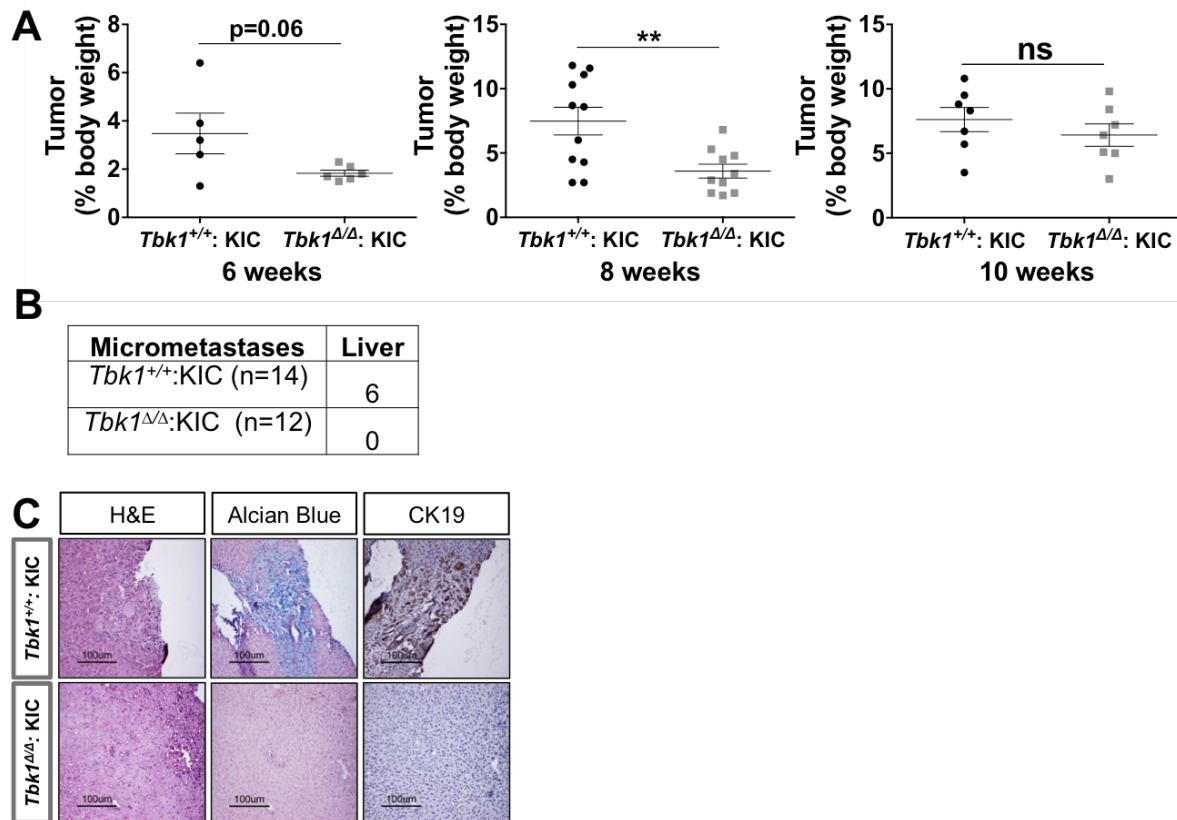


Figure 2.5. *Tbk1*^{Δ/Δ}: KIC mice have less overall tumor burden than *Tbk1*^{+/+}: KIC mice. (A) Tumor as percentage of body weight measurements at 6, 8 and 10 weeks in *Tbk1*^{Δ/Δ}: KIC and *Tbk1*^{+/+}: KIC. Results are representative of mean +/- SEM. Unpaired t-test *, p<0.05, ns, not significant. (B) Number of mice from (A) with liver micrometastases. (C) Representative liver histology in mice from (A) including H&E, alcian blue and CK19 staining.

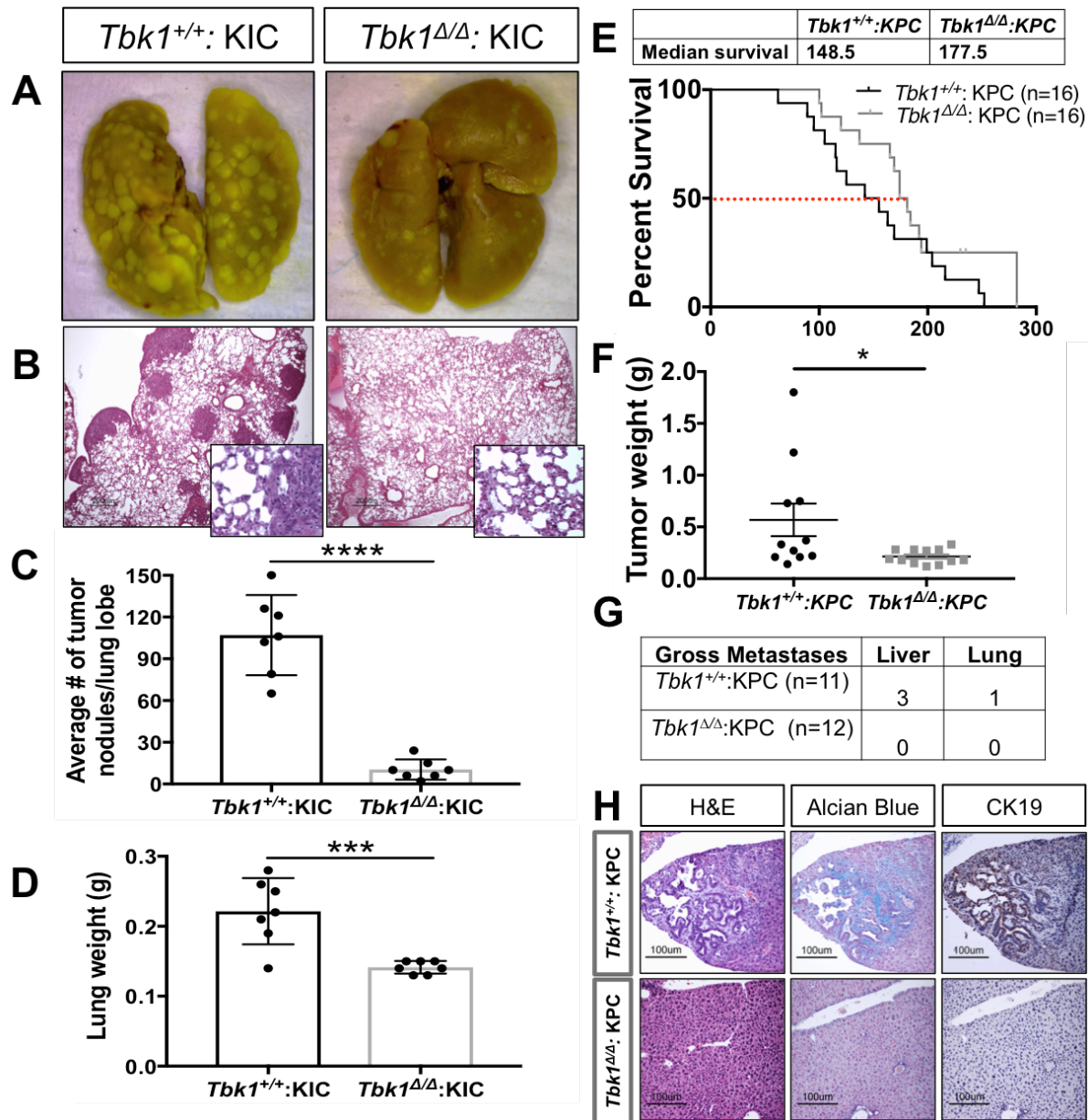


Figure 2.6. *Tbk1* loss in PDA shows a reduction in metastatic events. (A) Representative images of gross lungs from NOD SCID mice sacrificed 12 days after i.v. injection with *Tbk1*^{+/+} or *Tbk1*^{Δ/Δ}: KIC tumor cells (100,000 cells injected per mouse, n= 7 mice/group). **(B)** H&E section of lungs from **(A)** highlighting tumor nodules. Scale bar indicates 200 μm. **(C)** Number of tumor nodules per lung lobe from **(A)**. **(D)** Lung weights from **(A)**. **(E)** Kaplan-Meier survival curve of *Tbk1*^{Δ/Δ}: KPC and *Tbk1*^{+/+}: KPC mice (n=16 mice/group). Log rank mantel cox test was used for survival comparison, p=0.15. **(F)** Tumor weights of *Tbk1*^{Δ/Δ}: KPC and *Tbk1*^{+/+}: KPC mice. **(G)** Number of mice from **(F)** with gross metastases in indicated organs. **(H)** Representative liver histology in mice from **(F)** including H&E, alcian blue and CK19 staining. Scale bar indicates 100 μm. Results are representative of mean +/- SEM. Unpaired t-test *, p<0.05, ***, p<0.001, ****, p<0.0001.

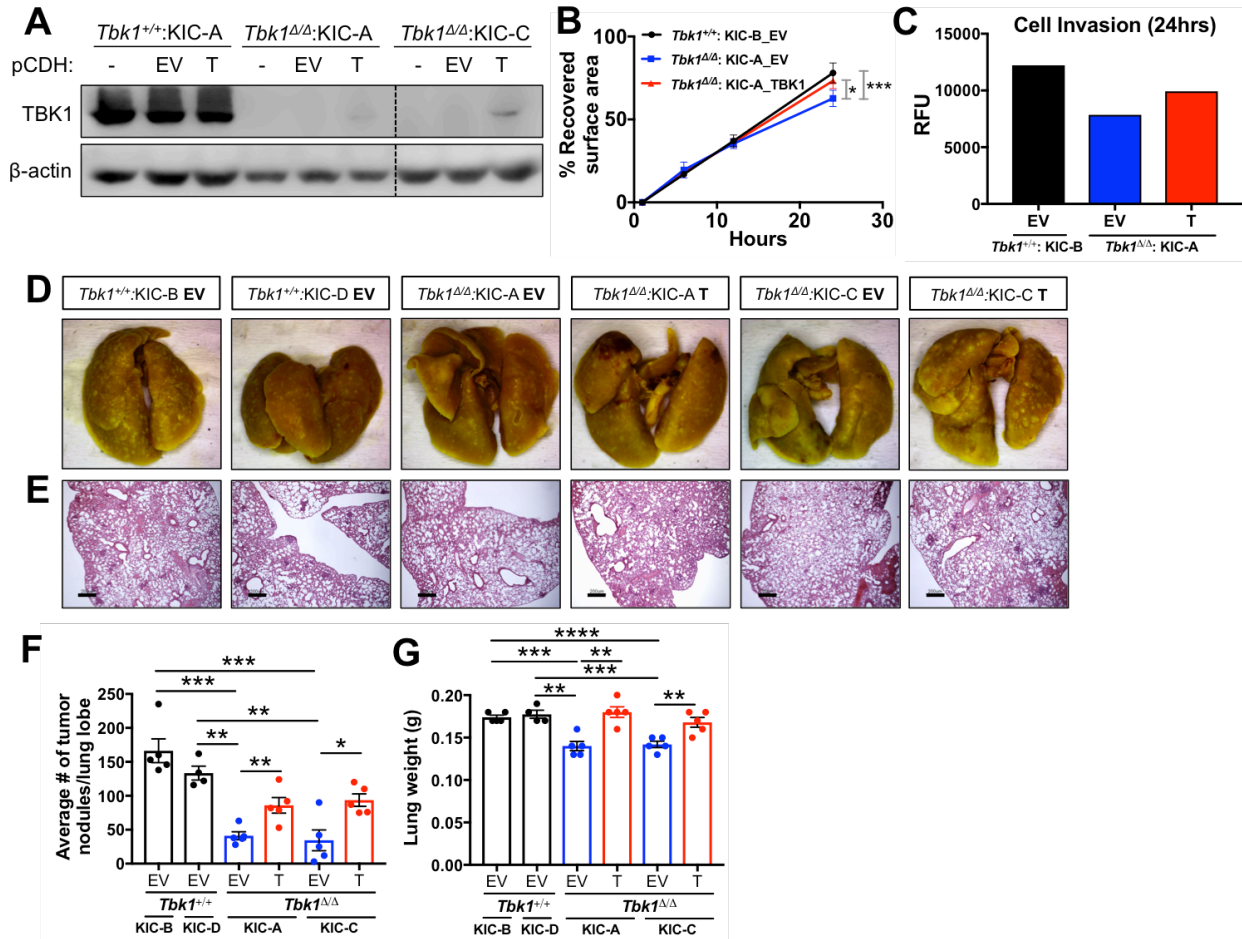


Figure 2.7. Re-expression of *Tbk1* partially reverses migratory deficit in *Tbk1*^{Δ/Δ}: *KIC* cells. (A) Protein lysates isolated from *Tbk1*^{Δ/Δ}: *KIC* and *Tbk1*^{+/+}: *KIC* cell lines infected with either pCDH-empty vector (EV) or pCDH-TBK1 (T) were immunoblotted for TBK1. β-actin was used as a loading control. Dotted line indicates where blot was cropped, however, all samples were run on the same gel and exposed simultaneously. (B) Recovered surface area quantification of *Tbk1*: *KIC* cell lines infected with pCDH-Empty vector or pCDH-TBK1 at indicated time points post scratch in wound healing assay. Recovered surface area was calculated as percentage of covered area over originally scratched area. Images and quantification are representative of 3-wells/cell line. (C) Quantification (expressed as relative fluorescent units) of *Tbk1*: *KIC* cell lines infected with pCDH-empty vector or pCDH-TBK1 that passed through transwell membranes 24 hours after plating in serum free media. Outer wells of transwell assays were filled with 10% FBS containing media as the chemoattractant. (D) Representative images of gross lungs from NOD SCID mice sacrificed 7 days after i.v. injection with *Tbk1*: *KIC* cell lines infected with pCDH-empty vector or pCDH-TBK1 (100,000 cells injected per mouse, n= 4-5 mice/group). (E) H&E section of lungs from (D) highlighting tumor nodules. Scale bars indicate 200 μm. (F) Number of tumor nodules per lung lobe from (D). (G) Lung weights from (D).

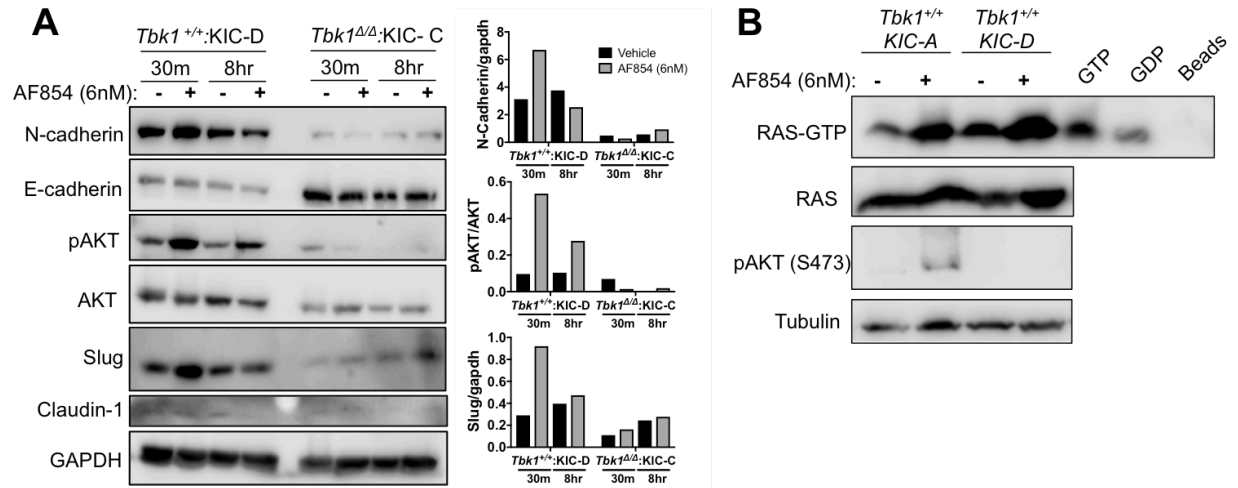


Figure 2.8. TBK1 promotes EMT downstream of Axl. (A) Protein lysates isolated from *Tbk1*: KIC cell lines treated with AF854 (6 nM) for 30 minutes or 8 hours were immunoblotted for indicated proteins and quantified. **(B)** Active RAS assay in *Tbk1*^{+/+}: KIC cell lines treated with AF854 (6 nM) for 30 minutes. GAPDH and Tubulin were used as a loading controls.

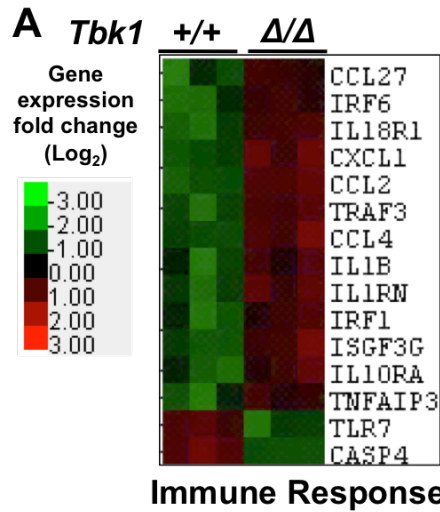


Figure 2.9. *Tbk1* ^{Δ/Δ} : KIC tumors contain higher pro-inflammatory gene expression than *Tbk1*^{+/+}: KIC tumors. (A) Heatmap representing gene expression fold change (log₂) of inflammatory genes from *Tbk1* ^{Δ/Δ} : KIC and *Tbk1*^{+/+}: KIC tumors. Color key indicates gene expression fold change. n=3 tumors/genotype, p<0.05 for all genes between *Tbk1* ^{Δ/Δ} : KIC and *Tbk1*^{+/+}: KIC tumors.

Chapter 3: Loss of *Tbk1* kinase activity protects mice from diet-induced metabolic dysfunction

3.1 HFD induces TBK1 expression and activity

Prolonged consumption of a HFD results in increased expression of IKK ϵ and TBK1 in murine liver and WAT [11, 75]. To confirm and extend these results, I evaluated IKK ϵ and TBK1 expression in liver and subcutaneous WAT tissue collected from HFD-fed C57BL/6 mice. Consistent with earlier reports, TBK1 mRNA levels increased nearly 6- and 3-fold, respectively, in liver and WAT of HFD-fed animals (**Figure 3.1A-B**).

Surprisingly, IKK ϵ transcript levels were not elevated in either set of tissues post HFD, even though IL-6, which is known to be abundant in obese settings, was increased in liver and WAT, confirming the presence of metabolic inflammation in these HFD-fed animals [19, 78]. In addition to confirming TBK1 induction at the protein level in liver tissues, I also observed an increase in TBK1 activity as seen by higher levels of pTBK1 and downstream TBK1 targets, pIRF3 and pp65 (**Figure 3.1C**). Interestingly, a previous study [62] reported that TBK1 interacts with insulin receptor β subunit (IR β) in livers of obese rats. Concurrent with elevated TBK1 activity, I also detected a robust increase in IR β -associated TBK1 by co-immunoprecipitation in liver lysates from HFD-fed mice compared to normal chow diet (ND) fed animals (**Figure 3.1D**). This heightened association could be indicative of a novel insulin-related function for TBK1.

3.2 *Tbk1* ^{Δ/Δ} mice are resistant to DIO

Upon observing the induction of TBK1 expression, activity and IR β interaction on HFD feeding, I sought to resolve TBK1 contributions to metabolism that are distinct from its homolog, IKK ϵ . I did this by utilizing *Tbk1* ^{Δ/Δ} animals [58]. To examine the outcome of

metabolic stress in a *Tbk1*-deficient setting, I placed *Tbk1*^{Δ/Δ} and *Tbk1*^{+/+} mice on HFD for 10 weeks. Weight measurements for each group were collected weekly and compared to age-matched ND-fed *Tbk1*^{Δ/Δ} and *Tbk1*^{+/+} mice (**Figure 3.2A**). By 8 weeks of age (4 weeks into the study), I documented a 25% increase in total body weight in HFD-fed *Tbk1*^{+/+} mice compared to ND. Similar to HFD-fed *Ikkbe*^{-/-} mice and amlexanox-treated mice, *Tbk1*^{Δ/Δ} mice showed only a modest increase in total body weight on HFD relative to ND-fed mice and overall maintained significantly lighter body weights than HFD-fed *Tbk1*^{+/+} mice through the end of the study (**Figure 3.2A-B**). To confirm that these differences in body weight and fat mass are not due to *Tbk1*^{Δ/Δ} mice eating less than *Tbk1*^{+/+} mice, I evaluated daily food intake relative to body weight. While no significant difference was observed, *Tbk1*^{Δ/Δ} mice showed a minor increase in the ratio of HFD intake to body weight, eliminating the possibility of reduced consumption (**Figure 3.2C**). Additionally, there were no differences in body weight and length between ND-fed *Tbk1*^{Δ/Δ} and *Tbk1*^{+/+} mice, indicating that resistance to the diet-induced obesity (DIO) phenotype seen with *Tbk1*^{Δ/Δ} mice is unique to this particular metabolic stress (**Figure 3.3A-B**). Next, I analyzed plasma leptin levels, which are usually elevated in obese individuals due to their higher percentage of body fat. I observed approximately a 40% reduction in circulating leptin in HFD *Tbk1*^{Δ/Δ} mice relative to *Tbk1*^{+/+} mice, further highlighting the lower percentage of body fat in *Tbk1*^{Δ/Δ} mice (**Figure 3.2D**).

3.3 *Tbk1*^{Δ/Δ} mice are glucose and insulin tolerant on HFD

Given that the association of TBK1 with IRβ was augmented on HFD and that the loss

of TBK1 protected mice from diet-induced weight gain, I examined the insulin-producing pancreatic beta cells in *Tbk1*^{+/+} and *Tbk1*^{Δ/Δ} mice. Increased adipose tissue load resulting from excessive nutrient intake often leads to enhanced demands on pancreatic beta cells for insulin production. Pancreatic islets respond to the greater demand for insulin by increasing in number and in size. HFD-fed *Tbk1*^{Δ/Δ} mice were resistant to the increase in islet number and size that was observed in HFD-fed *Tbk1*^{+/+} mice (**Figure 3.4A-C**). These results suggested that *Tbk1*^{Δ/Δ} mice are more tolerant of glucose and insulin on HFD compared to *Tbk1*^{+/+} mice. Oral glucose tolerance tests (OGTTs) were performed in fasted (4 hrs) ND- and HFD-fed *Tbk1*^{+/+} and *Tbk1*^{Δ/Δ} mice. As expected, significantly higher blood glucose measurements were observed in HFD-fed *Tbk1*^{+/+} mice compared with ND-fed mice (*Tbk1*^{+/+} and *Tbk1*^{Δ/Δ}) during the course of the OGTT. However, in contrast to HFD-fed *Tbk1*^{+/+} mice, the high levels of blood insulin and glucose found in HFD-fed *Tbk1*^{Δ/Δ} mice returned to basal values by 60 min and 120 min respectively, post oral gavage of glucose. These results indicate that TBK1 deficiency ameliorates diet-induced pancreatic islet stress and improves systemic glucose homeostasis, which is akin to the phenotype of previously reported *lkbke*^{-/-} mice and amlexanox-treated animals (**Figure 3.4D-E**).

3.4 Loss of TBK1 kinase enhances insulin sensitivity on HFD

Munoz et al. [62] also reported that TBK1 can directly phosphorylate serine 994 (S994) of IRβ in livers from obese rats. This particular serine site can be phosphorylated by the serine kinase, protein kinase C (PKC, isoforms β2 and θ) and has been implicated as an inhibitory phosphorylation site that blocks insulin receptor tyrosine kinase activity and

subsequent downstream signaling [83, 84]. Within metabolically diseased tissues from obese patients, there is a high level of proinflammatory cytokines that can drive activation of stress kinases, including Jun N-terminal kinase (JNK), IKK β and PKC [57, 59]. These kinases are thought to respond to inflammation by constraining the activity of the insulin receptor directly or indirectly through insulin receptor substrates (IRSs) via inhibitory phosphorylation, ultimately bringing insulin signaling down to baseline [14, 32, 80]. Given that TBK1 is a serine/threonine IKK (I κ B kinase) family member that is responsive to inflammatory stimuli and is capable of phosphorylating the insulin receptor, I hypothesized that TBK1 negatively regulates insulin signaling through phosphorylation of S994 on IR β .

I examined the phosphorylation status of IR β (S994) in liver tissue from ND- and HFD-fed *Tbk1*^{+/+} and *Tbk1* ^{Δ/Δ} mice with an antibody specific for pIR β (S994). A modest but specific pIR β (S994) signal was detectable only in livers from *Tbk1*^{+/+} mice in the HFD-fed group (**Figure 3.5A**). Furthermore, co-immunoprecipitation of TBK1 in liver lysates showed TBK1- IR β association after HFD feeding and also revealed a pIR β (S994) band exclusively in HFD *Tbk1*^{+/+} livers (**Figure 3.5B**). These results confirm that S994 of IR β is phosphorylated in HFD-fed mouse livers and indicate that TBK1 is likely the upstream kinase responsible. Loss of this inhibitory signal in HFD-fed *Tbk1* ^{Δ/Δ} tissue suggests that insulin signaling is intact in HFD-fed *Tbk1* ^{Δ/Δ} animals. We tested this directly by injecting the mice with insulin (1 unit /kg of body weight) or PBS and collected tissues 15 min later for protein isolation. Liver and subcutaneous WAT protein lysates were probed for downstream insulin signaling proteins and phosphoproteins.

AKT2 is considered to be the more insulin-responsive isoform of AKT (Protein kinase B, PKB) [35]. In comparison to livers and WAT from ND mice, insulin-induced AKT2 and downstream GSK3 β (Glycogen synthase kinase 3 β) activation were appreciably lower in HFD *Tbk1*^{+/+} tissues (**Figure 3.5C-D**). On the other hand, tissues from insulin-treated HFD *Tbk1* ^{Δ/Δ} mice maintained consistent AKT2 activation at a level comparable to ND animals. Therefore, loss of TBK1 kinase activity in the context of a metabolic challenge results in the preservation of insulin sensitivity that is normally dampened as a result of HFD.

This difference in insulin sensitivity between *Tbk1*^{+/+} and *Tbk1* ^{Δ/Δ} mice was confirmed by analysis of total IRS1 protein levels across liver, subcutaneous WAT and skeletal muscle. Persistent inhibitory phosphorylation of IRS1 leads to its degradation and ultimately insulin resistance [14]. In light of the observation that *Tbk1* ^{Δ/Δ} mice are more responsive to insulin, I suspected they would have more IRS1 protein present in metabolic tissues relative to HFD-fed *Tbk1*^{+/+} mice. In the HFD-fed *Tbk1*^{+/+} group, there was a consistent loss of detectable IRS1 in all 10 tissues examined. Whereas in HFD fed *Tbk1* ^{Δ/Δ} mice, IRS1 was easily detectable in 7 out of 12 tissues examined (**Figure 3.5E**). Altogether, these findings are consistent with the differences observed in the OGTTs and help to explain why HFD-fed *Tbk1* ^{Δ/Δ} mice were more glucose tolerant than *Tbk1*^{+/+} mice.

3.5 *Tbk1* ^{Δ/Δ} mice expend more energy through physical activity

If the lack of functional TBK1 on HFD generates greater insulin responsiveness and

subsequent glucose absorption in *Tbk1* mutant mice, these animals are likely more efficient in storing and/or expending that energy. Total energy expenditure is composed of voluntary, or physical activity and involuntary events, which includes basal metabolic rate and thermogenesis. Thermogenesis was increased in *Ikbke*^{-/-} mice and amlexanox-treated mice compared to control mice and was determined to be the primary difference contributing to their improved phenotype. The expression of thermogenic genes *Ucp1*, *Ucp2*, *Pparg* and *Ppargc1a* were not significantly upregulated in HFD-fed *Tbk1*^{Δ/Δ} WAT and livers relative to *Tbk1*^{+/+} mice (**Figure 3.6A-B**). However, the thermogenic differences detected in *Ikbke*^{-/-} mice and amlexanox-treated mice were at week 14 of HFD. Considering the 10-week duration of my HFD study, it is possible that differences in thermogenesis were not given sufficient time to manifest.

I evaluated alternative forms of energy expenditure by monitoring *Tbk1*^{+/+} and *Tbk1*^{Δ/Δ} mice in metabolic cages over a 72-hour period. While there were no significant differences between ND-fed groups (**Figure 3.7**), HFD-fed *Tbk1*^{Δ/Δ} mice were more active than *Tbk1*^{+/+} mice as quantified by their increased movement (beam breaks) throughout the cages (**Figure 3.8A**). Accordingly, *Tbk1*^{Δ/Δ} mice also had 22% higher oxygen consumption, 25% higher carbon dioxide production and 23% higher heat production, demonstrating greater energy expenditure overall (**Figure 3.8B**). Of note, the greatest differences in activity and energy expenditure took place during the dark cycles when the animals were awake. Since mice are nocturnal animals, any differences in resting metabolic rate between the two groups would be apparent during the light or daytime hours. *Tbk1*^{Δ/Δ} mice had only a modest increase in movement and

energy expenditure during light cycles, indicating that the enhanced nighttime physical activity observed in *Tbk1^{Δ/Δ}* mice could account for their increased energy expenditure relative to *Tbk1^{+/+}* mice.

Alongside beam break and energy expenditure measurements, body composition analysis of *Tbk1^{+/+}* and *Tbk1^{Δ/Δ}* mice was performed utilizing a nuclear MRI mini spec instrument. Lean and fat mass composition were similar between ND mice, while HFD-fed *Tbk1^{+/+}* animals had 70% more fat mass and 15% less lean mass compared to ND mice (**Figure 3.8C-D**). In contrast, HFD-fed *Tbk1^{Δ/Δ}* mice contained fat and lean body masses nearly equivalent to ND-fed mice, possibly due in part to their higher energy expenditure. Overall, these findings are in agreement with the insulin and glucose tolerant state of *Tbk1^{Δ/Δ}* mice and indicate that they consume more energy via increased activity, accounting for greater lean mass and reduced fat mass.

3.6 HFD-fed *Tbk1^{Δ/Δ}* mice maintain lipid homeostasis

Differences in fat mass and lipid accumulation were also examined. HFD induces adipocyte enlargement and proliferation in WAT. In subcutaneous fat pads collected from HFD-fed *Tbk1^{+/+}* mice, I observed larger adipocytes compared to those collected from ND-fed *Tbk1^{+/+}* mice (**Figure 3.9A**). While I did see larger adipocytes in fat pads from HFD-fed *Tbk1^{Δ/Δ}* mice, overall they contained a greater abundance of small adipocytes relative to HFD-fed *Tbk1^{+/+}* fat tissue (**Figure 3.9A-B**). Additionally, cholesterol levels were measured from plasma of ND- and HFD-fed *Tbk1^{+/+}* and *Tbk1^{Δ/Δ}* mice. As expected, a prolonged fat diet led to a nearly 40% increase in circulating

cholesterol in *Tbk1*^{+/+} mice (**Figure 3.9C**). Yet, *Tbk1*^{Δ/Δ} mice maintained cholesterol levels comparable to mice on ND. Furthermore, I performed oil red O staining on frozen liver sections to assess liver steatosis. Consistent with previous results, HFD *Tbk1*^{+/+} mice displayed a striking level of hepatic lipid deposition while *Tbk1*^{Δ/Δ} livers showed a 65% reduction in oil red O staining (**Figure 3.9D-E**). Despite prolonged consumption of a HFD, *Tbk1*^{Δ/Δ} mice preserve lipid homeostasis and maintain a consistently healthier phenotype.

3.7 Diet-induced inflammation is nominal in *Tbk1*^{Δ/Δ} mice

Chronic low-grade inflammation, also referred to as “meta-inflammation,” is a hallmark of metabolic syndrome and strongly associates with insulin resistance. It is characterized by a high degree of immune cell infiltration, primarily macrophages, and local cytokine production in metabolically diseased tissues. Meta-inflammation is thought to stem from pathological adipocyte tissue expansion in an obese state where the tissue becomes poorly oxygenated or hypoxic. Hypoxia leads to fibrosis and necrotic cell death in adipose tissue, which provokes local macrophage activation and/or polarization to an “M1” proinflammatory state. Inflammation is augmented by adipocytes and macrophages that generate proinflammatory cytokines to promote macrophage mobilization from bone marrow and local infiltration into adipose tissue and other metabolically diseased tissues [85].

In light of TBK1’s well-established role in mediating innate immunity and *Tbk1*^{Δ/Δ} mice being resistant to diet-induced lipogenesis, I suspected *Tbk1*^{Δ/Δ} mice would have limited

meta-inflammation on HFD. In WAT stained for cd11b/c, I observed quantitatively fewer macrophages in HFD fed *Tbk1*^{Δ/Δ} mice relative to *Tbk1*^{+/+} mice (**Figure 3.10A**). This difference in macrophage infiltration was confirmed in RNA isolated from WAT of HFD-fed *Tbk1*^{Δ/Δ} mice, where I detected substantial reductions in gene expression of macrophage markers *Cd11c* and *Adgre1* (F4/80) and proinflammatory cytokines *Tnfa*, *Il6* and *Il12* relative to HFD *Tbk1*^{+/+} mice (**Figure 3.10B**). Analysis of protein expression from liver lysates also revealed a reduction in IL-6 and IL-1β in HFD-fed *Tbk1*^{Δ/Δ} animals compared to *Tbk1*^{+/+} (**Figure 3.10C**). Furthermore, WAT and liver protein lysates were analyzed for differences in cytokine expression by multiplex immunoassays. Cytokine levels showed little variance between ND-fed groups, which is consistent with the relatively mild immune phenotype of *Tbk1*^{Δ/Δ} animals (**Figure 3.11A-B**) [58]. Among the HFD-fed animals, *Tbk1*^{Δ/Δ} mice had less cytokine accumulation compared to *Tbk1*^{+/+} mice and in particular, IL-6, IL-1β and TNFα levels were consistently lower in WAT and liver tissues from *Tbk1*^{Δ/Δ} mice (**Figure 3.10D-E**).

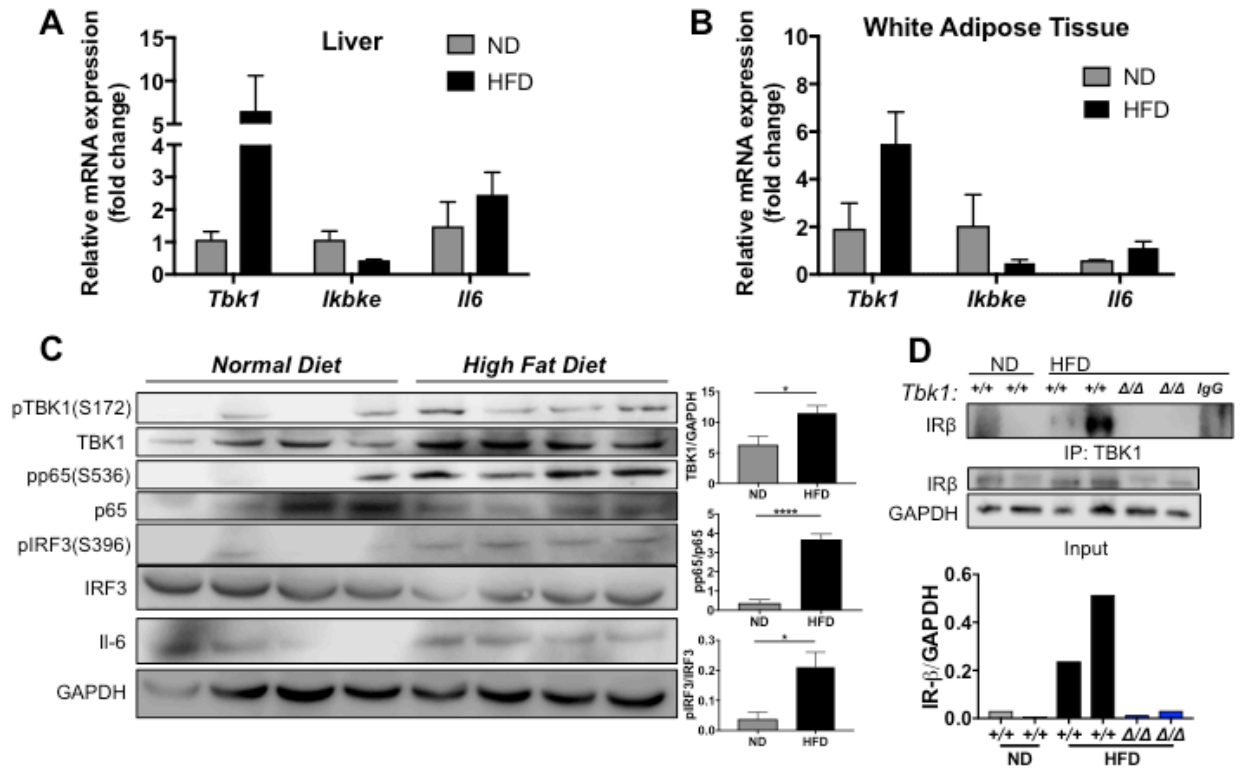


Figure 3.1. Prolonged consumption of HFD induces TBK1 and promotes interaction with IR. mRNA expression of genes encoding *Tbk1*, *Ikbke* and *Il6* in liver (A) and WAT (B) of *C57BL/6* mice fed for 10 weeks with HFD or ND as indicated (n = 4 mice/group). Results are representative of mean \pm SEM. Note: $p = 0.06$ for *Tbk1* expression in WAT between ND and HFD. (C) Protein lysates from livers of ND- and HFD-fed *C57BL/6* mice that were fasted overnight were immunoblotted with indicated antibodies and quantified. GAPDH was used as a loading control. (D) Liver lysates from ND- or HFD-fed mice were immunoprecipitated with an antibody against TBK1, followed by immunoblotting and quantification of IR β . Normal rabbit IgG was used as a control for specificity (IgG lane). Tissue lysates for immunoprecipitation were immunoblotted with antibodies against IR β for input and GAPDH as a loading control. Statistical analysis by Student's *t*-test. * $p < 0.05$, **** $p < 0.0001$

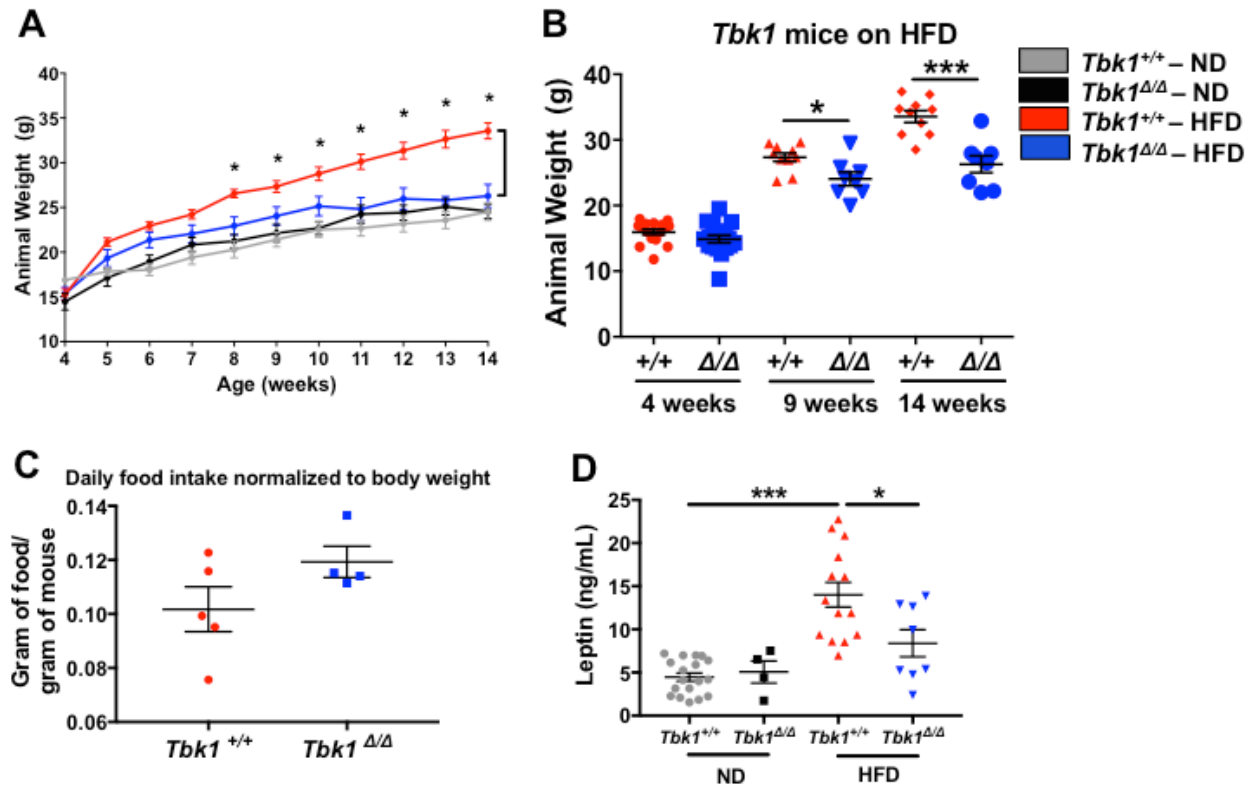


Figure 3.2. *Tbkl*^{Δ/Δ} mice are protected from HFD-induced weight gain. (A) Weekly body weights of *Tbkl*^{+/+} and *Tbkl*^{Δ/Δ} mice fed ND or HFD from 4 to 14 weeks of age (n = 7-10 mice/group). (B) Body weights of HFD-fed *Tbkl*^{+/+} and *Tbkl*^{Δ/Δ} mice at 4, 9 and 14 weeks of age. (C) Average daily food consumption of 14-week-old HFD-fed *Tbkl*^{+/+} and *Tbkl*^{Δ/Δ} mice was measured as gram of food per gram of mouse. (D) Circulating leptin levels were assayed in plasma from *Tbkl*^{+/+} and *Tbkl*^{Δ/Δ} mice as indicated. All mice are from 129S5 background. Results are representative of mean +/- SEM. Statistical analysis by Student's *t*-test. **p* < 0.05, ****p* < 0.001

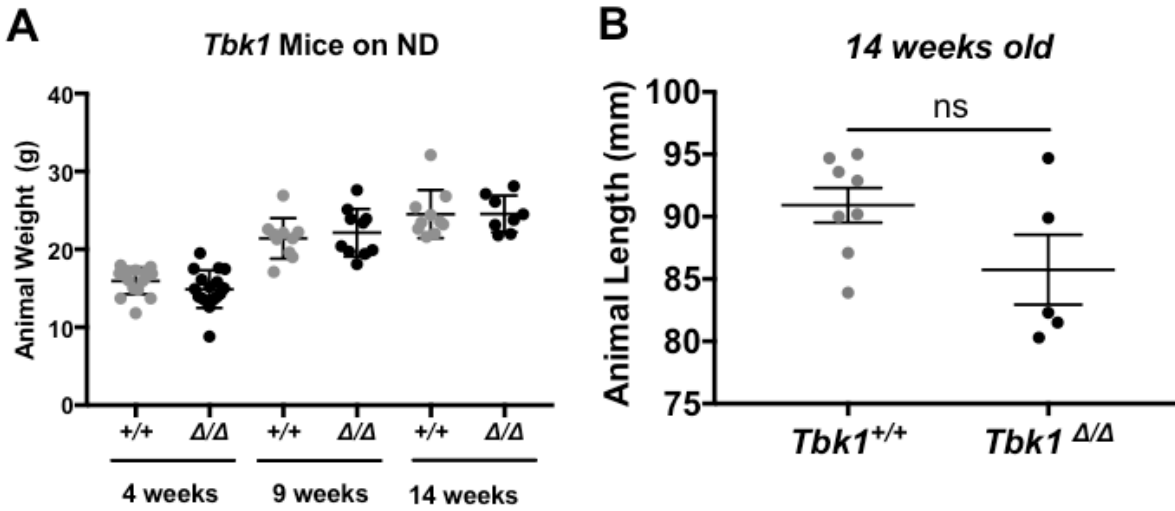


Figure 3.3. ND-fed *Tbk1* mice maintain similar body mass. (A) Body weights of ND-fed *Tbk1*^{+/+} and *Tbk1*^{Δ/Δ} mice at 4, 9 and 14 weeks of age. **(B)** Animal body length measured from nose to rump in *Tbk1*^{+/+} and *Tbk1*^{Δ/Δ} mice. All mice are from 129S5 background. Results are representative of mean +/- SEM. Statistical analysis by Student's *t*-test. *ns*, not significant

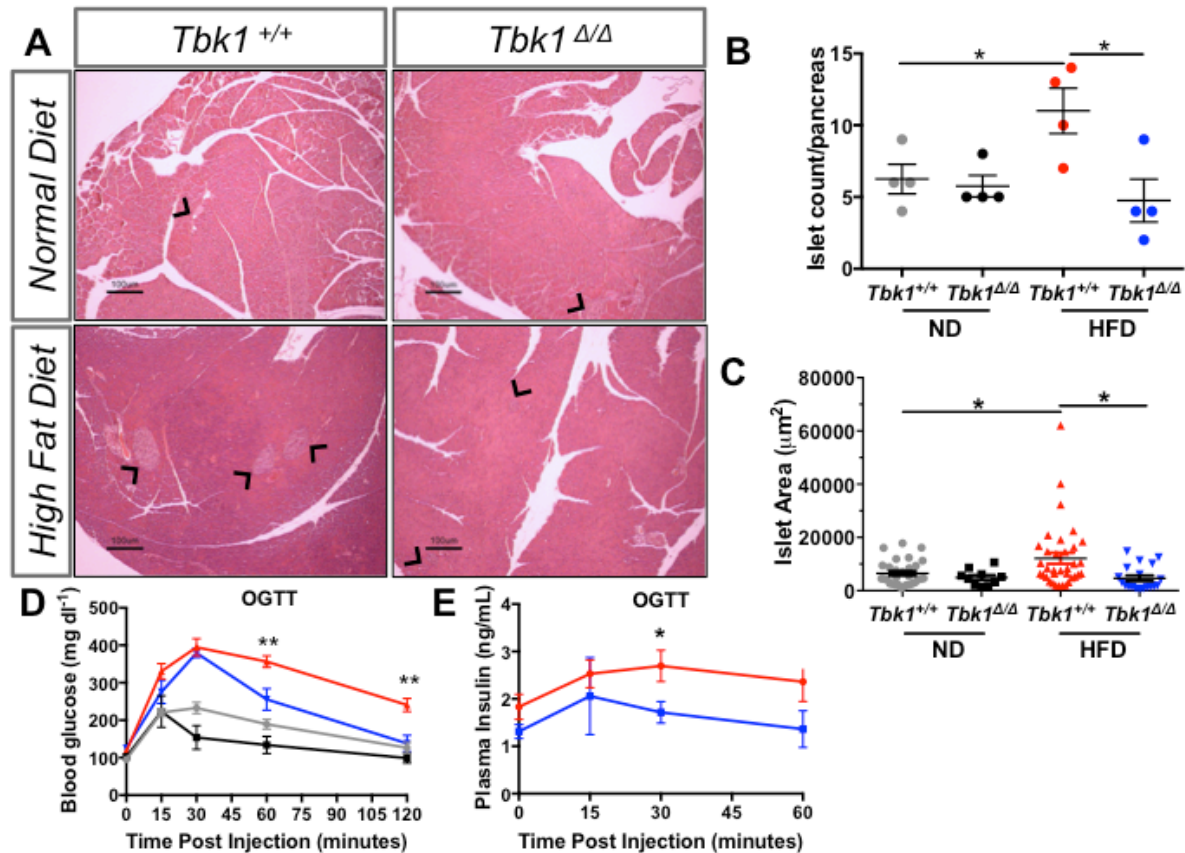


Figure 3.4. HFD-fed *Tbk1*^{Δ/Δ} mice maintain glucose and insulin sensitivity. (A) Representative images of pancreata from adult *Tbk1*^{Δ/Δ} and *Tbk1*^{+/+} mice after 10 weeks on ND or HFD. Black arrows point to pancreatic islets. Scale bar indicates 100 μm . (B) Number of islets counted per pancreas (4x section) in *Tbk1*^{Δ/Δ} and *Tbk1*^{+/+} mice on ND or HFD (n = 4 mice/group). (C) Area of each islet from (B) measured in microns². (D) Blood glucose and (E) plasma insulin measurements at indicated times after oral glucose injection for OGTT in ND- or HFD-fed *Tbk1*^{Δ/Δ} and *Tbk1*^{+/+} mice. For blood glucose, n = 4-10 mice/ND group and 8-12 mice/HFD group. For blood insulin, n \geq 5 mice/group with exception at 15 minutes where n = 3 mice/group. All mice are from 129S5 background. Results are representative of mean \pm SEM. Statistical analysis by Student's *t*-test. **p* < 0.05 and ***p* < 0.01 for HFD-fed *Tbk1*^{+/+} mice compared to HFD-fed *Tbk1*^{Δ/Δ} mice. OGTT, oral glucose tolerance test

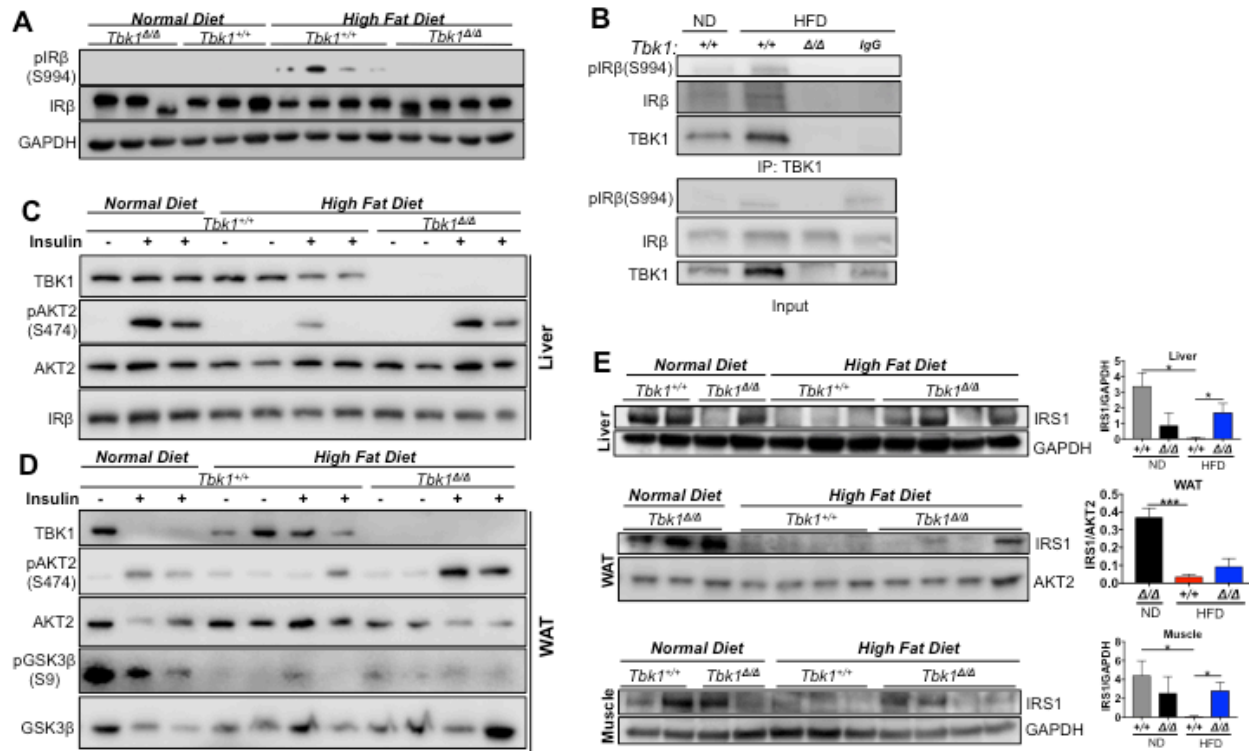


Figure 3.5. Loss of TBK1 kinase activity diminishes insulin receptor interaction and enhances insulin sensitivity on HFD. (A) Liver lysates from ND or HFD-fed *Tbk1*^{Δ/Δ} and *Tbk1*^{+/+} mice were probed for pIRβ(S994) and IRβ. GAPDH is shown as a loading control. (B) Liver lysates from ND- or HFD-fed *Tbk1*^{+/+} and *Tbk1*^{Δ/Δ} mice were immunoprecipitated with an antibody against TBK1 and assayed for IRβ and pIRβ(S994). Normal rabbit IgG was used as a control for specificity (IgG lane). Lysates for immunoprecipitation were immunoblotted with antibodies against pIRβ(S994), IRβ, and TBK1 for input. Liver (C) and WAT (D) lysates from ND- or HFD-fed *Tbk1*^{Δ/Δ} and *Tbk1*^{+/+} mice injected intraperitoneally with insulin (1 U/kg of body weight) or water as a control were probed for indicated proteins. All mice in these experiments were fasted overnight before sacrifice. (E) Total IRS1 protein levels in liver, WAT and muscle tissue lysates from 14-week-old HFD-fed *Tbk1*^{Δ/Δ} and *Tbk1*^{+/+} mice were detected by immunoblot and quantified. GAPDH, IRβ and AKT2 were used as internal loading controls. All mice are from 129S5 background. Statistical analysis by Student's *t*-test. **p* < 0.05, ****p* < 0.001

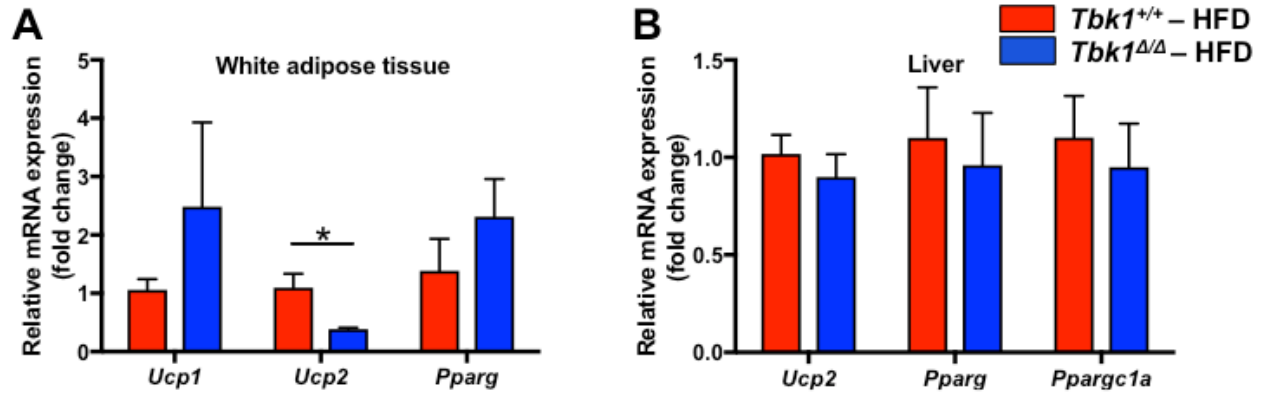


Figure 3.6. Thermogenic gene expression is unchanged between HFD-fed *Tbk1* mice. qPCR analysis of thermogenic related gene expression including *Ucp1*, *Ucp2*, *Pparg* and *Ppargc1a* in (A) white adipose tissue and (B) liver of HFD-fed *Tbk1*^{Δ/Δ} and *Tbk1*^{+/+} mice (n = 4-5 mice/group and all mice are from 129S5 background). Results are representative of mean +/- SEM. Statistical analysis by Student's *t*-test. **p* < 0.05

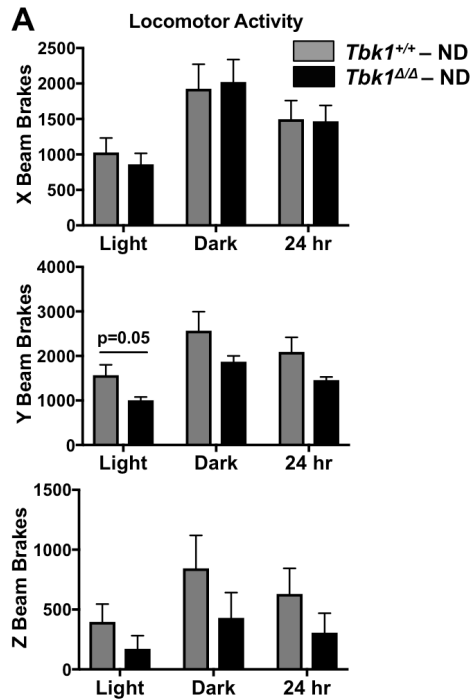


Figure 3.7. ND-fed *Tbk1* mice have similar activity profiles. (A) Movement throughout the cage as measured by beam breaks collected from 14-week-old *Tbk1*^{+/+} and *Tbk1*^{Δ/Δ} mice fed ND in a metabolic chamber over a 3-day period (n = 5 mice/group and all mice are from 129S5 background).

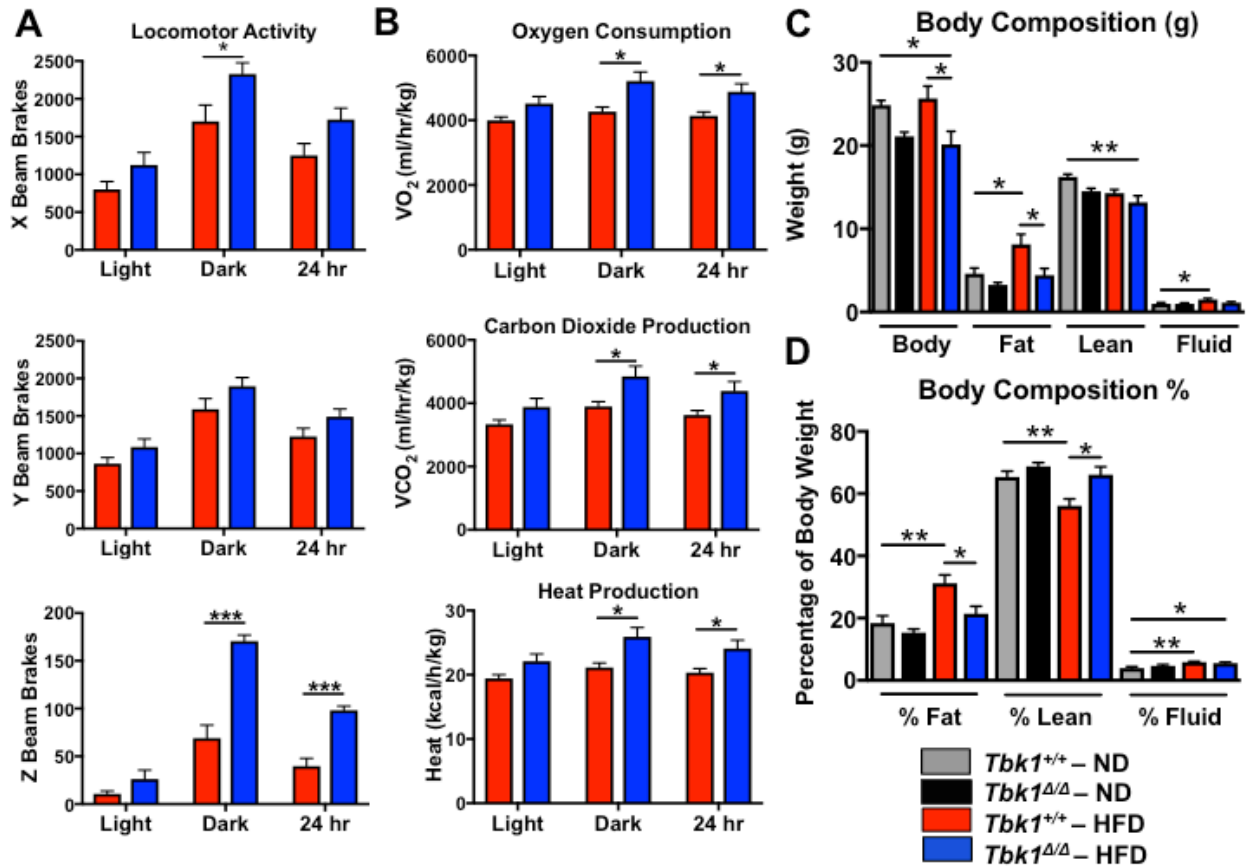


Figure 3.8. *Tbk1*^{Δ/Δ} mice are more active than *Tbk1*^{+/+} mice. Movement throughout the cage (A) and energy expenditure measurements (B) were collected from 14-week-old *Tbk1*^{+/+} and *Tbk1*^{Δ/Δ} mice fed HFD in a metabolic chamber over a 3-day period. (C) Total body weight, fat mass, lean mass and fluid in *Tbk1*^{Δ/Δ} and *Tbk1*^{+/+} mice fed either ND or HFD at 14 weeks of age. (D) Fat and lean mass and bodily fluids as a percentage of total body weight in mice from (C). Results are representative of mean \pm SEM; n = 5 mice/group and all mice are from 129S5 background. Statistical analysis by Student's *t*-test. **p* < 0.05, ***p* < 0.01, ****p* < 0.001

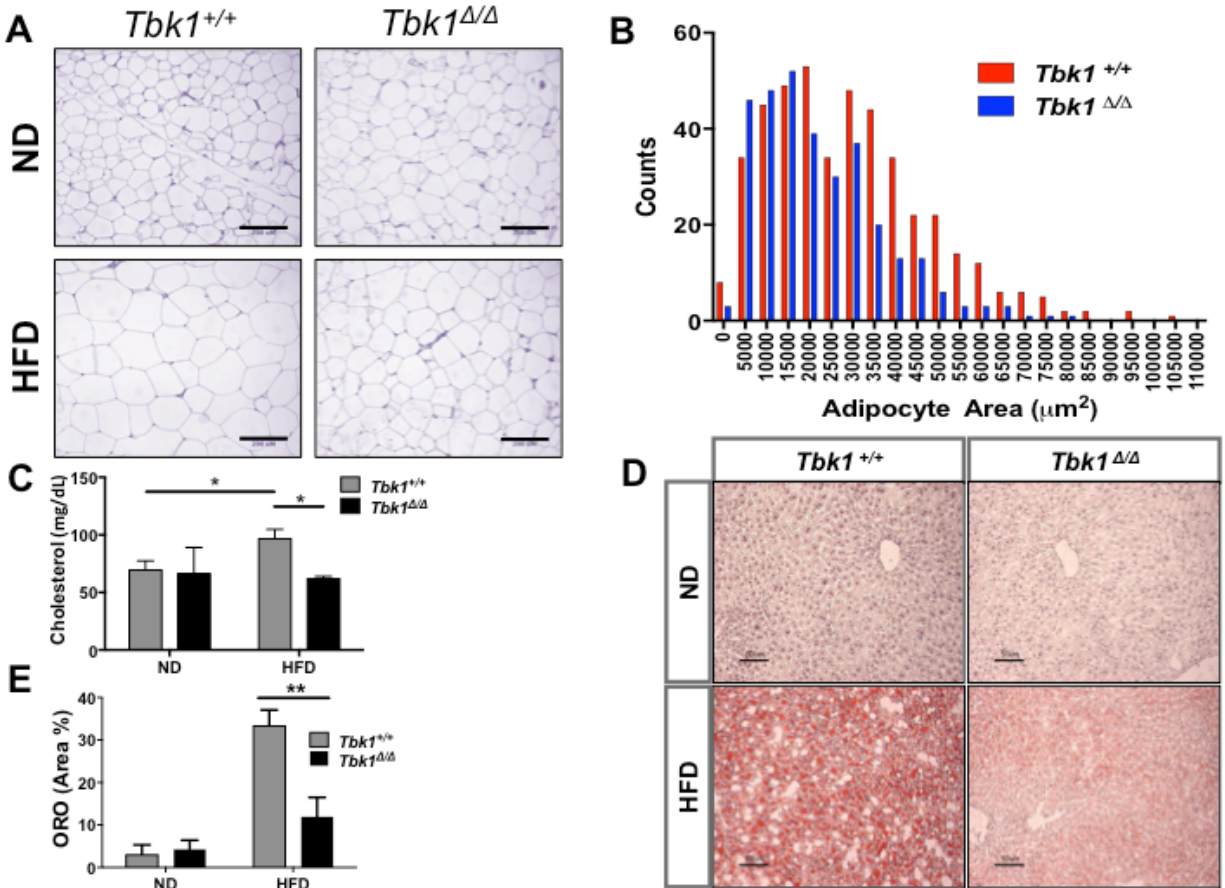


Figure 3.9. HFD-fed *Tbk1^{Δ/Δ}* mice maintain lipid homeostasis. (A) Representative 20x images of H&E stained subcutaneous white adipose tissue from *Tbk1^{Δ/Δ}* and *Tbk1^{+/+}* mice after 10 weeks on ND or HFD. Scale bar indicates 200 μm. (B) Adipocyte area count in fat pads of *Tbk1^{Δ/Δ}* and *Tbk1^{+/+}* mice fed HFD (n = 4-8 mice/group). (C) Total cholesterol levels were measured in murine plasma using Vitros chemistry systems (Ortho Clinical Diagnostics, Raritan, NJ) (n = 6 mice/group). (D-E) Representative images and relative quantification of oil red O stained livers from *Tbk1^{Δ/Δ}* and *Tbk1^{+/+}* mice (n = 4-6 mice/group). Scale bar indicates 50 μm. All mice are from 129S5 background. Results are representative of mean +/- SEM. Statistical analysis by Student's *t*-test. **p* < 0.05, ***p* < 0.01

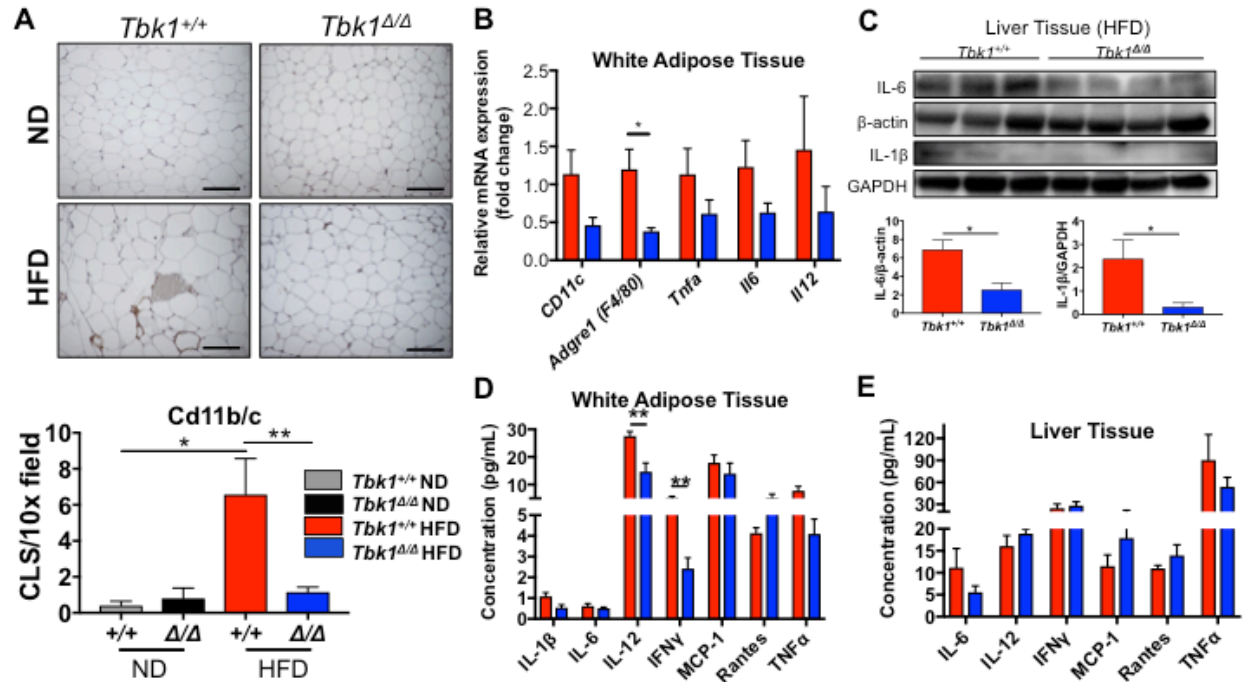


Figure 3.10. *Tbk1^{Δ/Δ}* mice have less inflammation relative to *Tbk1^{+/+}* mice on HFD. (A) Representative 20x images and quantification of *cd11b/c* stained subcutaneous white adipose tissue from *Tbk1^{Δ/Δ}* and *Tbk1^{+/+}* mice after 10 weeks on ND or HFD (n = 4-8 mice/group). Scale bar indicates 200 μm and 'CLS' refers to crown like structures. (B) mRNA expression of genes encoding *Cd11c*, *Adgre1*, *Tnfa*, *Il6* and *Il12* in subcutaneous WAT of *Tbk1^{Δ/Δ}* and *Tbk1^{+/+}* mice fed with HFD as indicated (n = 4-6 mice/group). (C) Liver tissue lysates from 14-week-old HFD-fed *Tbk1^{Δ/Δ}* and *Tbk1^{+/+}* mice were immunoblotted with antibodies against IL-6 and IL-1β. β-actin and GAPDH were used as internal loading controls. Indicated cytokines from WAT (D) and liver tissue (E) lysates of HFD-fed *Tbk1^{+/+}* and *Tbk1^{Δ/Δ}* mice were measured by Bio-Rad multiplex array (n = 4-8 mice/group for WAT, n = 8-12 mice/group for liver). All mice are from 129S5 background. Results are representative of mean +/- SEM. Statistical analysis by Student's *t*-test. **p* < 0.05, ***p* < 0.01

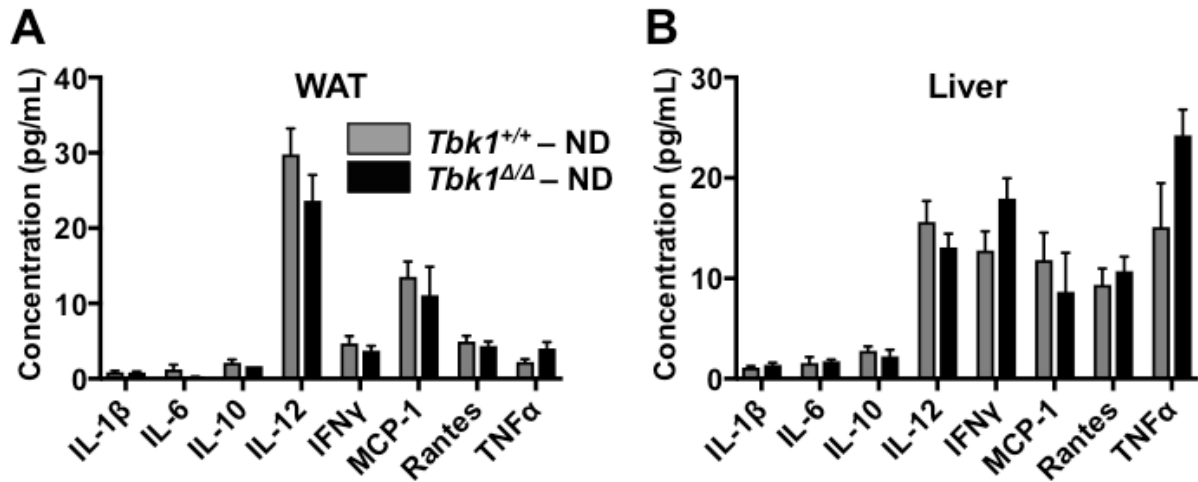


Figure 3.11. Immune expression is unvaried between ND-fed *Tbk1* mice. Indicated cytokines from WAT (**A**) and liver tissue (**B**) lysates of ND-fed *Tbk1*^{+/+} and *Tbk1*^{Δ/Δ} mice were measured by Bio-Rad multiplex array (n = 4-8 mice/group and all mice are from 129S5 background). Results are representative of mean +/- SEM. Statistical analysis by Student's *t*-test.

Chapter 4. Discussion and Conclusions

In the last decade, a growing body of evidence has accumulated implicating aberrant TBK1 activity in a wide range of disease states including macular degeneration, glaucoma, metabolic syndrome, systemic lupus erythematosus (lupus), neurodegenerative brain disorders such as amyotrophic lateral sclerosis (ALS) and frontotemporal dementia (FTD) and various cancer types [17, 25, 34, 60, 76, 89]. My investigations of TBK1 activity within two of these diseases have uncovered novel functions for the serine threonine kinase that may provide insight into the etiology of some of these other diseases.

In pancreatic cancer, I demonstrated that TBK1 is a major effector of mutant active K-RAS which is the dominant oncogenic driver of PDA and mutated in more than 90% of human PDA cases [38, 46]. No other common epithelial cancer has a single gene with comparable mutation frequency, yet efforts made to target mutant RAS proteins have not been met with success [30]. Therefore, targeting signaling components downstream of RAS that are required for RAS-mediated oncogenesis is a viable therapeutic alternative [20]. TBK1 is abundantly expressed in *KRAS* mutant PDA tumors and cell lines and correlates with worse survival in human patients with pancreatic cancer. In addition, pharmacological inhibition of TBK1 with the selective inhibitor compound II limited human and murine pancreatic tumor cell growth in a mutant *KRAS*-selective manner. Assessment of *Tbk1* loss in multiple clinically relevant GEMMs of PDA revealed that PDA mice lacking kinase active TBK1 have significantly smaller and more epithelial tumors resulting in fewer metastatic incidents relative to PDA mice with wild-

type *Tbk1*. Mechanistic studies established that TBK1 promotes EMT downstream of Axl in PDA, providing insight into a novel function for TBK1. Further, these studies suggest that therapies targeting TBK1 could be used to exploit *KRAS* mutant tumors.

It is estimated that nearly 90% of cancer mortalities are due to metastases, yet TBK1 studies to date have evaluated the effect of TBK1 inhibition only on primary tumor burden [93]. EMT is a hallmark of metastasis in pancreatic cancer and is critical to cancer cell dissemination [26, 72, 92]. Within this morphological cellular program, epithelial cancer cells lose contact with the basement membrane and neighboring cells while gaining a more mesenchymal and invasive phenotype [53, 72]. My results show that tumors and isogenic cell lines from the *KIC* pancreatic GEMM lacking functional TBK1 are more epithelial in gene expression and morphology than *KIC* tumors containing wild-type *Tbk1*. These findings, in combination with the mechanistic studies demonstrating that TBK1 is downstream of the EMT driver Axl, indicate that EMT in pancreatic tumor cells is halted by *Tbk1* loss. TBK1 has been linked to EMT in other cancer types. In contrast to my results, knockdown of TBK1 in ER α -positive breast cancer cells reportedly induced EMT and enhanced tumor growth and lung metastasis by suppressing ER α expression [101]. However, in two separate recent studies, gene expression analysis revealed that a mesenchymal gene signature in melanoma and NSCLC cell lines was associated with sensitivity to TBK1 inhibition (TBK1i) [13, 21]. Further analysis revealed mutations in *RAS* family members as a common feature of NSCLC cell lines that showed sensitivity to TBK1i while NSCLC cells that were resistant to TBK1i had a more epithelial gene expression profile and less frequent

activating RAS mutations [13]. The mesenchymal gene signature in TBK1i sensitive NSCLC lines is consistent with my observations in K-RAS-driven *Tbk1*^{+/+}: KIC tumors that have undergone EMT. Moreover, the epithelial gene expression profile of TBK1-resistant NSCLC cells lines matches the epithelial phenotype of *Tbk1*^{Δ/Δ}: KIC tumors that grew out independent of TBK1. Though the precise mechanism of how TBK1 promotes EMT is unclear, TBK1 can directly activate AKT [67]. AKT activation can drive EMT via induction of Snail and Slug that transcriptionally repress E-cadherin and induction of Vimentin, Twist1 and Matrix Metalloproteinases -2 and -9 that promote tumor cell invasion [27, 53, 100]. Currently, our lab is focused on understanding the interaction between TBK1 and AKT driving the mesenchymal phenotype in PDA and identification of additional TBK1 substrates that promote EMT programs.

Interestingly, *Tbk1* mutant KIC and KPC tumors were smaller than *Tbk1* wild-type tumors, indicating that *Tbk1* loss affects primary tumor growth in addition to tumor cell motility. TBK1 is central to numerous biological processes that could affect growth of the primary tumor including cell division, autophagy, innate immune response and AKT/mTOR signaling [13, 16, 21, 48, 69, 99, 102, 109]. In the context of pancreatic cancer, TBK1 has been reported to promote basal levels of autophagy as a means of silencing cytokine production [102]. These findings imply that inhibition or loss of TBK1 in PDA could increase cytokine production, ultimately driving immune activation and potentially an anti-tumor immune response. While I did not investigate the immune landscape of the PDA GEMMs, I did find via gene expression analysis that *Tbk1*^{Δ/Δ}: KIC tumors displayed higher expression of a number of pro-inflammatory genes relative to

Tbk1^{+/+}: KIC tumors (**Figure 2.9**). Pro-inflammatory genes with increased expression in *Tbk1*^{Δ/Δ}: KIC tumors included *Cxcl1*, *Ccl2*, *Ccl4*, *Ccl27*, *Irf1* and *Il1b*. The elevated pro-inflammatory gene expression in *Tbk1*^{Δ/Δ}: KIC tumors could be indicative of a heightened inflammatory state and/or an anti-tumor immune response to some degree. While these results are not sufficient to conclude that *Tbk1* loss promotes anti-tumor immunity in PDA, the idea is not unreasonable given that *Tbk1*^{Δ/Δ} mice have been shown to produce higher levels of pro-inflammatory cytokines in response to immune challenge [58]. An important consideration with the *Tbk1*^{Δ/Δ} PDA models is that the global *Tbk1* mutation eliminates TBK1 kinase activity and significantly reduces *Tbk1* expression in all cell types including immune cells, which could impact immune responses to tumor challenge. In fact, a recent study demonstrated that dendritic cell (DC) conditional *Tbk1* knockout mice (*Tbk1*-DKO) injected subcutaneously with B16 melanoma cells lived longer and had smaller tumors compared to wild-type *Tbk1* control mice [99]. Assessment of B16 melanoma tumors from *Tbk1*-DKO animals revealed enhanced interferon-responsive gene expression and greater T-effector cell infiltration into tumors and lymph nodes, confirming anti-tumor immunity conferred by dendritic cell *Tbk1* loss. Collectively, these observations support a pro-tumor immune function for TBK1 that could contribute to the larger tumor sizes in *Tbk1* wild-type PDA mice.

Recent evidence implicating TBK1 in the regulation of insulin receptor activity led to my investigation of a novel function for TBK1 in metabolism [10, 24, 31, 36, 62]. My data corroborate previously reported upregulation of TBK1 expression on HFD and also

show increased pIRF3, indicating heightened TBK1 kinase activity as well. In the DIO model, I confirmed the inhibitory interaction between TBK1 and IR β and demonstrate that insulin sensitivity is maintained under HFD conditions in the absence of functional TBK1, supporting a previously unappreciated function of TBK1 in regulating insulin receptor activity. *Tbk1* ^{Δ/Δ} mice are resistant to DIO and I suspect this stems primarily from their enhanced insulin sensitivity, allowing for more efficient glucose uptake and utilization. Accordingly, these mice exhibited greater energy expenditure primarily in the form of enhanced physical activity, which accounts for their leaner body composition. These results provide a mechanistic basis for the overall protective effect on the metabolism and general health of *Tbk1* ^{Δ/Δ} mice challenged with a HFD.

An important consideration with this study is that the *Tbk1* ^{Δ/Δ} mice contain a global mutation in *Tbk1*, thereby inhibiting its kinase activity and significantly reducing its overall expression in all cell types. Thus, it is unclear if the *Tbk1* ^{Δ/Δ} mouse phenotype is due to *Tbk1* loss in a specific subset or subsets of tissues or cell types. Interestingly, conditional deletion of *Tbk1* in adipose tissue (*Tbk1* ATKO) resulted in higher macrophage and proinflammatory cytokine gene expression on HFD [108]. In contrast to my model, HFD-fed *Tbk1* ATKO mice were insulin resistant and glucose intolerant. This information, in conjunction with the restricted inflammatory response produced by lipopolysaccharide (LPS) stimulated macrophages from the *Tbk1* ^{Δ/Δ} mice, leads us to speculate whether myeloid cell loss of TBK1 is critical to maintaining insulin sensitivity under metabolic stress [58, 105]. In a similar vein, myeloid cell specific knockout of *Ikkb* (IKK β gene) in HFD fed mice resulted in improved insulin resistance and lower

adiposity, supporting the central contribution of myeloid cells in the development of systemic insulin resistance [3]. With the *Tbk1^{Δ/Δ}* model, I conclude that the observed phenotype is the effect of systemically eliminating TBK1 catalytic activity. From a clinical perspective, global loss of TBK1 kinase function could be biologically analogous in some respects to the effects of small molecule inhibition of TBK1 system wide.

The relationship between inflammation and insulin resistance is complex and somewhat controversial. In particular, modulating the expression of certain inflammatory signaling molecules such as IKK β , JNK, TNF α , IL-1R or IL-6 in different tissues or by different methods has led to inconsistent metabolic outcomes [104]. For example, liver specific JNK activation improved insulin sensitivity, yet activation of JNK in other tissues, including adipose tissue, skeletal muscle and brain, impaired insulin action, suggesting JNK regulation of insulin sensitivity is tissue specific [45, 79, 104]. Considering the well-established functions of TBK1 in mediating inflammation and innate immunity, I cannot rule out the possibility that some of the healthier metabolic parameters seen in *Tbk1^{Δ/Δ}* mice could be due in part to reduced inflammation, especially given that *Tbk1^{Δ/Δ}* macrophages show only a partial response to LPS challenge [58]. While these results are consistent with the argument that inflammation leads to insulin resistance, the scope of this study limits the use of the inflammatory phenotype to function as an indicator of metabolic health in *Tbk1^{Δ/Δ}* mice. Regardless, these results strongly suggest that TBK1 promotes metabolic dysfunction through negative regulation of insulin receptor signaling, thus aiding in insulin resistance.

This feature of TBK1 is reminiscent of other kinases that have been previously shown to inhibit insulin signaling in response to cytokine activation. In particular, IKK β , JNK, PKC, and S6K have each been shown to phosphorylate IRS proteins at unique sites that limit insulin-stimulated activity [14, 32, 80]. Accordingly, *S6K1-deficient* mice demonstrate a comparable phenotype to *Tbk1 Δ/Δ* mice on HFD with lower body weights and insulin hypersensitivity [86, 87]. The opposition of insulin-stimulated anabolic processes common to all of these kinases is indicative of an evolutionary conserved role in reserving energy during times of inflammatory stress for resolving inflammation.

In summary, I have characterized the phenotype of mice globally lacking catalytically active TBK1 under metabolic challenge, which, prior to this mouse, was impossible due to embryonic lethality in *Tbk1 $^{-/-}$* mice [8, 58]. Overall, loss of TBK1 kinase activity benefited mice challenged with HFD. One way that TBK1 promotes metabolic syndrome progression is by directly impeding insulin receptor signaling, resulting in systemic insulin resistance and limited glucose absorption. While work from others has begun to elucidate the tissue specific effects of TBK1, it is unclear whether additional TBK1 substrates could be mediating these metabolic effects [108]. A recent study from Kumari and colleagues [52] revealed that the TBK1 substrate, IRF3, transcriptionally drives adipose inflammation during periods of overnutrition. IRF3 was upregulated and more active in metabolic tissues from obese mice, matching my observations, while *Irf3 $^{-/-}$* mice were protected from DIO, exhibited reduced inflammation and showed improved insulin sensitivity on HFD. This finding helps elaborate the function of TBK1 under metabolic stress, but also highlights the need for further investigation of TBK1 targets in

regulating metabolism.

Lastly, these results, in conjunction with other previous reports, imply that TBK1 inhibition may provide benefits to patients with metabolic syndrome and warrants further testing of pharmacological inhibitors of TBK1 in human trials [11, 61, 74, 75, 108]. The TBK1/IKK ϵ inhibitor amlexanox just completed testing in clinical trials beginning with a safety trial of six patients where no serious adverse events were reported from drug treatment (NCT01842282) [65]. The safety trial was followed by a randomized, double-blind, placebo-controlled trial of 42 obese patients with type 2 diabetes or nonalcoholic fatty liver disease who received amlexanox or placebo for 12 weeks (NCT01975935). A subset of patients constituting one-third of the participants in the blinded study responded with a clinically significant reduction in blood glucose. Interestingly, molecular analysis of fat tissue biopsies collected from patients at the beginning of the study revealed greater inflammation in the responder group compared to non-responders. Though it is unclear whether this high level of inflammation in the responder group showed any sort of resolution by the end of the study, further development and confirmation of this inflammatory gene signature could lead to its utilization as a predictive tool for patient response to amlexanox or potentially other TBK1 inhibitors. Future studies are needed with larger patient groups to validate the efficacy of amlexanox, determine the appropriate dosage and dosing schedule and evaluate whether amlexanox treatment has long-term benefits.

Altogether, my work has led to the identification of novel TBK1 functions in pancreatic cancer and metabolic syndrome that promote disease progression. Here I provide clinically relevant evidence of the effects of global *Tbk1* loss in all cell types with HFD-fed *Tbk1*^{Δ/Δ} mice and *Tbk1*^{Δ/Δ} PDA models, which in many respects is biologically analogous to the effects of pharmacologically inhibiting TBK1 systemically. These results suggest that therapeutic inhibition of TBK1 may be a useful strategy to control tumor cell invasion and metastasis in RAS-driven pancreatic cancer and promote insulin sensitivity in metabolic syndrome or type 2 diabetes patients.

Chapter 5. Experimental Procedures

Animals

Tbk1^{Δ/Δ} mice were generated in a pure 129S5 strain as previously described [58] and were generously provided by Pfizer (Cambridge, MA). NOD SCID mice were purchased from the UT Southwestern Mouse Breeding Core (Dallas, TX). *Tbk1*^{Δ/Δ}, *Tbk1*^{+/+}, *LSL-Kras*^{G12D/+}; *Cdkn2a*^{Lox/Lox} (KI) and *Cdkn2a*^{Lox/Lox}; *p48*^{Cre} (IC) mice were generated as previously described [2, 7, 58]. *Tbk1*^{Δ/Δ} and *Tbk1*^{+/+} mice were used to breed with KI and IC mice to generate *Tbk1*^{+/+}; *LSL-Kras*^{G12D/+}; *Cdkn2a*^{Lox/Lox}; *p48*^{Cre} (*Tbk1*^{+/+}: KIC) mice and *Tbk1*^{Δ/Δ}: KIC mice. *LSL-Trp53*^{R172H/+} mice were obtained from National Cancer Institute (NCI) Mouse Repository [39]. *Tbk1*^{Δ/Δ} and *Tbk1*^{+/+} mice were also used to breed with *LSL-Kras*^{G12D/+}; *LSL-Trp53*^{R172H/+} (KP) and *p48*^{Cre} mice to generate *Tbk1*^{+/+}; *LSL-Kras*^{G12D/+}; *LSL-Trp53*^{R172H/+}; *p48*^{Cre} (KPC) mice and *Tbk1*^{Δ/Δ}: KPC mice. All mice were bred and maintained in a pathogen-free barrier facility with access to food and water *ad libitum*. All protocols for mouse use and euthanasia were reviewed and approved by the Institutional Animal Care and Use Committee of the University of Texas Southwestern Medical Center (Dallas, TX).

Animal studies

All experiments in the metabolism studies were conducted using littermate-controlled male mice. HFD experiments were initiated at 4 weeks of age. Mice were fed a normal chow diet (16% protein diet, irradiated) (Teklad Global Diets; Envigo, East Millstone, NJ), or a 60% HFD (D12492; Research Diets, Inc., New Brunswick, NJ). Tissue and blood were collected in the fasted state. Before the metabolic cage studies, the mice

were housed individually in metabolic chambers for 1 week for acclimation. Metabolic measurements were obtained continuously using TSE metabolic chambers (TSE Labmaster System; TSE Systems, Bad Homburg, Germany) in an open-circuit indirect calorimetry system where the mice had access to water and either ND or 60% HFD *ad libitum*. The fat mass and the bone-free lean body composition were measured in nonanesthetized mice using an Echo 3-in-1 nuclear magnetic resonance (MRI) mini Spec instrument (Bruker, Rheinstetten, Germany). For oral glucose tolerance tests (OGTTs), mice were fasted for 4 hours prior to administration of glucose (2 g/kg body weight by oral gavage). Mice did not have access to food throughout the experiment. Blood from the tail was measured for glucose content using Contour glucometer strips (Bayer) at 0, 15, 30, 60, 90 and 120 min post oral gavage. Blood was collected and prepared for plasma to measure the concentration of leptin at 0 min and insulin at 0, 15, 30, 60, 90 and 120 min post oral gavage with commercial ELISA kits (Millipore, Burlington, MA). For insulin signaling assays, mice were fasted overnight for insulin injection the next day by i.p. (1 U/kg body weight, insulin). At 15 min post insulin injection, mice were sacrificed and tissues (liver, subcutaneous WAT, skeletal muscle) were harvested and immediately snap-frozen in liquid nitrogen.

All cancer-related murine studies were conducted using littermate-controlled mice. All mice were fed a normal chow diet (16% protein diet, irradiated) (Teklad Global Diets; Envigo, East Millstone, NJ). For endpoint studies, *Tbk1*^{+/+}: *KIC* and *Tbk1*^{Δ/Δ}: *KIC* mice were sacrificed and entire tissues including pancreas/tumor, liver, lungs and spleen were harvested and weighed at 6, 8 and 10 weeks old, n = 5-11 mice per time point per

group. *Tbk1*^{+/+}: *KPC* and *Tbk1*^{Δ/Δ}: *KPC* mice were sacrificed between 4 and 5 months, n ≥ 8 mice per time point per group. For all survival studies, mice were carefully monitored and sacrificed when they appeared moribund. For lung colonization studies, *Tbk1*^{+/+}: *KIC* and *Tbk1*^{Δ/Δ}: *KIC* cells (1x10⁵) were resuspended in 200 μl PBS and injected intravenously into the tail vein of 8 week-old female NOD SCID mice. Lungs were harvested at 7 or 12 days post injection and fixed in Bouin's fixative for gross analysis of tumor nodules. Tumor colonization was analyzed by H&E.

Cell Lines

Human cancer cell lines (AsPC-1, Capan-1, Hs766T, MCF7, MIA PaCa-2, PANC-1 and PL-45) were obtained from ATCC (Manassas, VA). HPNE (Human Pancreatic Nestin Expressing) cells were obtained from the UT MD Anderson Cancer Center (Houston, TX). The *KPC*-M09 cell line was isolated from a spontaneous tumor originating in a *KPC* mouse as previously described [55]. All cell lines were cultured in DMEM or RPMI (Invitrogen, Carlsbad, CA) containing 10% FBS and maintained in a humidified incubator with 5% CO₂ at 37°C. The human cell lines were DNA fingerprinted for provenance using the Power-Plex 1.2 kit (Promega) and confirmed to be the same as the DNA fingerprint library maintained by ATCC. All cell lines were confirmed to be free of *mycoplasma* (e-Myco kit, Boca Scientific) before use.

Isogenic cell lines were derived from individual tumors of 8 week old *Tbk1*^{+/+}: *KIC* and *Tbk1*^{Δ/Δ}: *KIC* mice. Each tumor was minced and digested with 1% collagenase type I, DMEM, 10 mM HEPES and 1% FBS at 37°C to obtain a single-cell suspension. Cell

suspensions were centrifuged at low speed to pellet large debris, resuspended in wash buffer, and passed through a 70 μ M cell strainer. The resulting cell suspension was plated at low density to isolate tumor cell populations using cloning rings. Cells were confirmed to be tumor cells by immunocytochemistry and PCR. These cell lines were expanded and stained for tumor cell markers. Cell lines were confirmed to be pathogen-free before use. Clones *Tbk1*^{+/+}: KIC-A, *Tbk1*^{+/+}: KIC-B, *Tbk1*^{+/+}: KIC-D, *Tbk1* ^{Δ/Δ} : KIC-A, *Tbk1* ^{Δ/Δ} : KIC-B, *Tbk1* ^{Δ/Δ} : KIC-C were used in subsequent experiments. Cells were cultured in DMEM containing 10% FBS and maintained at 37°C in a humidified incubator with 5% CO₂ and 95% air.

RNA isolation and quantitative RT-PCR

Tissues were excised from mice and snap-frozen with liquid nitrogen. Total RNA was isolated after tissue homogenization in TRIzol (Thermo Fisher, Waltham, MA) and RNA was extracted using RNeasy RNA extraction kit (Qiagen, Germantown, MD). RNA was quantified using a NanoDrop instrument (Thermo Fisher). Complementary DNA was prepared by reverse transcribing 1 μ g of RNA with iScript cDNA synthesis kit (Bio-Rad, Hercules, CA). Supplementary Table 1 lists the primer sets used for quantitative RT-PCR. qPCR was performed on a CFX96 Touch Real-Time PCR Detection System (Bio-Rad), with iQ SYBR Green Supermix (Bio-Rad). Results were measured using the comparative threshold cycle [47] method, with β -actin used for normalization. Fold changes and statistical significance were calculated from three independent replicates.

Microarray analysis

Tumor tissues were excised from 8 week old *Tbk1^{Δ/Δ}* & *Tbk1^{+/+}*: *K1C* mice and snap-frozen with liquid nitrogen (n= 3 tumors per genotype). Total RNA was isolated and quantified as previously mentioned. RNA was checked for quality with a Bioanalyzer Instrument (Agilent). Gene expression was analyzed on a MouseWG-6 v2.0 Expression BeadChip (Illumina, San Diego, CA) through the UT Southwestern Microarray Core (Dallas, TX). Gene expression data analysis was performed through IPA software (Ingenuity Pathway Analysis, Qiagen). Java TreeView (Alok Saldanha) and Cluster 3.0 software (Michael Eisen, Berkeley Lab) were employed for hierarchical clustering gene expression analysis [47].

Immunoblotting

Tissues and cells were lysed in ice-cold RIPA buffer (50 mM Tris-Cl, 150 mM NaCl, 1% Nonidet P-40, 0.5% sodium deoxycholate, and 0.1% SDS) containing cocktails of protease (Thermo Fisher Scientific) and phosphatase inhibitors (Sigma-Aldrich, St. Louis, MO) and centrifuged for 20 min at 13,000 × *g* at 4°C. Total protein concentration was calculated using a bicinchoninic acid assay kit (Thermo Fisher Scientific). Proteins were resolved by SDS-PAGE and transferred to a methanol-activated polyvinylidene difluoride membrane. All primary and secondary antibodies were diluted in 5% donkey serum in TBS with 0.05% tween. Primary antibodies used included the following: anti-pAKT(S473) (Cell Signaling, #4060), anti-AKT (Cell Signaling, #9272), anti-pAKT2(S474) (Cell Signaling, #8599), anti-AKT2 (Cell Signaling, #3063), anti-pAxl(Y779) (R&D, AF2228), anti-Axl (Santa Cruz, sc-1096), anti-Claudin1 (Cell

Signaling, #13255), anti-E-Cadherin (Cell Signaling, #3195), anti-pGSK3 β (S9) (Cell Signaling, #9323), anti-GSK3 β (Cell Signaling, #9315), anti-IKK ϵ (Biochain, Z5020108), anti-IL1 β (Abcam, ab34837), anti-IL6 (Epitomics, 1957-1), anti-pIR β (S994) (Thermo Fisher, purified custom antibody), anti-IR β (Cell Signaling, #3025), anti-pIRF3(S396) (Cell Signaling, #4947), anti-IRF3 (Santa Cruz Biotechnology, sc-9082), anti-IRS1 (Cell Signaling, #3407), anti-N-Cadherin (Cell Signaling, #13116), anti-pp65(S536) (Cell Signaling, #3031), anti-Ras (Abcam, ab108602), anti-Snail (Cell Signaling, #3879), anti-Slug (Cell Signaling, #9585), anti-pTBK1(S172) (Cell Signaling, #5483), anti-TBK1 (Abcam, ab40676), anti-Vimentin (Cell Signaling, #5741), anti-Zeb1 (Cell Signaling, #3396), anti-ZO-1 (Cell Signaling, #8193). Anti- β -actin (Sigma-Aldrich, A2066), anti-GAPDH (Cell Signaling, #2118) and anti-Tubulin (Abcam, ab4047) were used as loading controls for all Western blots shown. Horseradish peroxidase-conjugated donkey anti-rabbit, donkey anti-mouse and donkey anti-goat IgG (1:10,000; Jackson ImmunoResearch Laboratories, West Grove, PA) were used as a secondary antibodies. Membranes were exposed with Clarity Western ECL Blotting Substrate (Bio-Rad) and visualized with the Odyssey Fc imager (LI-COR Biotechnology, Lincoln, NE).

Immunoprecipitation

Briefly, liver tissue lysates were prepared by lysis in TNET buffer (150 mM NaCl, 5 mM EDTA, 50 mM Tris pH 8.0, 1% Triton X) plus protease and phosphatase inhibitor cocktails (Thermo Scientific) and 1 mM PMSF. Liver tissue lysate concentrations were assayed using a bicinchoninic acid assay and then equilibrated with lysis buffer. Lysates were pre-cleared by incubation with 20 μ L of Protein A/G agarose beads (Thermo

Scientific) for 90 min at 4°C followed by centrifugation. Pre-cleared lysates (250 µg/sample) were then incubated with rabbit anti-TBK1 (Cell Signaling, #3031) or rabbit IgG control (Cell Signaling, #2729) and 30 µL of Protein A/G agarose beads and rotated overnight at 4°C. Immunoprecipitates were washed three times in TNET buffer then heated to 95°C for 5 min in standard SDS sample buffer. Samples were separated by SDS-PAGE followed by Western blot analysis.

Histology and Immunohistochemistry

For cancer studies, pancreas tumors, livers, lungs, spleens and kidneys were excised and fixed with 10% neutral buffered formalin solution overnight and embedded in paraffin for sectioning. For metabolism studies, fat pads, livers, and pancreas tissues were excised and either frozen in liquid nitrogen and embedded in optimum cutting temperature compound (OCT, Tissue-Tek; EMS, Hatfield, PA) for frozen sections or fixed with 10% neutral buffered formalin solution overnight and embedded in paraffin for sectioning. Frozen liver sections (10 µm) were air-dried overnight and then fixed in 10% neutral buffered formalin for 10 min at room temperature. After brief rinsing with water and then 60% isopropanol, frozen liver sections were stained with oil red O for 15 min and counterstained with hematoxylin.

All formalin-fixed paraffin embedded tissues were sectioned at 5 µm thickness. After sectioning, slides were deparaffinized with xylene and rehydrated in decreasing ethanol dilution series followed by H&E stain or antigen retrieval with 0.01 mol/L citric acid buffer (pH 6.0) for immunohistochemistry. Sections for immunohistochemical analysis were

blocked with 20% aquablock and incubated with rabbit anti-cd11b/c (Novus Biologicals, NB110-40766) or rabbit anti-Ck19 (ab15463) in blocking solution (5% BSA in TBS with 0.05% tween) at 4°C overnight. Horseradish peroxidase–conjugated donkey anti-rabbit IgG (Jackson ImmunoResearch Laboratories, West Grove, PA) was used as a secondary antibody. Negative controls included omission of primary antibody. Masson's Trichrome and Alcian Blue stains were performed on formalin-fixed, paraffin-embedded *KIC* tumor sections by the Molecular Pathology Core (UT Southwestern, Dallas, TX). All slides were visualized with a Nikon Eclipse E600 microscope (Nikon, Melville, NY) and color images were captured using a Nikon Digital Dx1200me camera and ACT-1 software. Images were analyzed using NIS Elements AR 2.3 Software (Nikon).

***In vitro* drug response assay**

Assays were performed in 96-well format as described [18]. Briefly, cells were plated on day 0 and compound II [67] was added on day 1 in four fold dilutions starting at 20 μ M (highest dose). For each assay, eight different drug concentrations were tested with eight replicates per concentration. Relative cell number was determined by adding MTS (Promega, Madison, WI, final concentration 333 μ g/ml), incubating for 1 to 3 hours at 37°C, and reading absorbance at 490 nm plate reader (Spectra Max 190, Molecular Devices, Downington, PA). Drug sensitivity curves and IC50s were calculated using in-house software. Response was validated in replicate plates ($n \geq 4$).

Wound healing and invasion assays

Wound healing assays were conducted in 6-well plates. Monolayers of cells were grown in low-serum media until 90% confluency was reached. Each well was scratched with a P200 pipette tip to create an artificial wound, washed with PBS to remove residual cells and replaced with fresh media containing 10% FBS. Cells were photographed at indicated timepoints after wounding. Wound closure was measured as a percentage of original wound width with MRI Wound Healing Tool macro (ImageJ).

Invasion assays were carried out with QCM ECMatrix Cell Invasion Assays (EMD Millipore, Burlington, MA). In brief, cells were serum starved overnight and then seeded the next day on transwell inserts (8 μ M pore size) that are lined with a reconstituted basement membrane matrix of proteins derived from the Engelbreth Holm-Swarm [110] mouse tumor. The inner chambers were filled with medium containing 2.5% FBS while the outer chambers were filled with medium containing 10% FBS as the chemoattractant. After the indicated time points, invaded cells on the bottom of the insert membrane are dissociated from the membrane when incubated with cell detachment buffer and subsequently lysed and detected by CyQuant GR dye.

Organotypic culture and immunocytochemistry

For each cell line, 2000 cells were plated in 8-well chamber slides onto a base layer of Matrigel (5 mg/ml) and collagen I (1.5–2.1 mg/ml) and cultured for 3 to 4 days in a humidified 37°C incubator as previously described [95]. For immunocytochemistry, cultures were fixed in 2% formalin (Sigma-Aldrich) in PBS for 20 min, permeabilized

with 0.5% Triton X-100 in PBS for 10 min at room temperature, incubated with Alexa Fluor 488 Phalloidin 488 (A12379, Invitrogen) in immunofluorescence buffer as described [68] for 1 hr at room temperature and mounted using ProLong Gold antifade reagent with DAPI (Invitrogen). Images were acquired using a confocal laser-scanning microscope (LSM880, Zeiss) through UT Southwestern Live Cell Imaging Core (Dallas, TX).

Active RAS Assay

Active RAS in cell lysates was measured via precipitation with GST-tagged RAF-RBD beads (Ras Pull-down Activation Assay Biochem Kit; Cytoskeleton, Denver, CO, USA). Lysates were prepared and precipitation was performed per manufacturer instructions. Subsequently, pull-down samples and respective whole cell lysates were immunoblotted with anti-RAS (pan) and indicated loading controls.

Reagents

The mammalian expression plasmid pCDH-CMV-MCS-TBK1-EF1-NEO was generously provided by Drs. Peiqing Shi and James Chen (UT Southwestern Medical Center, Dallas, TX). Lentiviral-based expression constructs were packaged by cotransfection of HEK293T cells with psPAX2 and pMD2.G packaging system (4:2:1). Polyethylenimine (PEI) was used for transfection at 3:1 ratio of total DNA. Transfection media was replaced with 10% complete DMEM 24 hours post transfection, and incubated a further 24 hours prior to viral particle collection. *Tbk1*^{+/+} and *Tbk1*^{Δ/Δ}: KIC cells were seeded at a density of 1x10⁶ cells per 10 cm dish. Twenty-four hours later, the cells were infected

with lentiviral particles and polybrene (10 µg/ml). 24-hours post-infection, cells were given fresh medium containing G418 (400 µg/mL, Invivogen) for selection and maintained in culture under selection for 3 weeks following initial infection. AF854 (R&D systems, Minneapolis, MN) was previously shown to activate mouse Axl and was used at indicated concentrations to stimulate mouse Axl [107]. Compound II was synthesized by William G. Bornmann (UT MD Anderson Cancer Center) and found to be a potent inhibitor of TBK1 and IKKε in a chemical compound screen as previously described [67].

Clinical Data Set

Gene expression data and survival analyses of 84 pancreatic cancer patients with annotated clinical outcomes were downloaded from the Cancer Genome Atlas (TCGA). For survival analyses, gene expression data was divided into the top 25 percent and bottom 75 percent. Cox regression was used to calculate hazard ratios and Kaplan-Meier survival analyses. Significance for these plots was determined using the logrank test.

Statistics

Statistical analyses were performed using GraphPad Prism (GraphPad, La Jolla, CA). Results are expressed as mean ± SEM. All data were analyzed by *t*-test. Significance was accepted at $p < 0.05$, with asterisks denoting *p*-value levels: *, $p < 0.05$; **, $p < 0.01$; ***, $p < 0.001$; and ****, $p < 0.0001$.

Bibliography

- [1] Aguilera, K. Y., L. B. Rivera, H. Hur, J. G. Carbon, J. E. Toombs, C. D. Goldstein, M. T. Dellinger, D. H. Castrillon and R. A. Brekken (2014). "Collagen signaling enhances tumor progression after anti-VEGF therapy in a murine model of pancreatic ductal adenocarcinoma." Cancer Res **74**(4): 1032-1044.
- [2] Aguirre, A. J., N. Bardeesy, M. Sinha, L. Lopez, D. A. Tuveson, J. Horner, M. S. Redston and R. A. DePinho (2003). "Activated Kras and Ink4a/Arf deficiency cooperate to produce metastatic pancreatic ductal adenocarcinoma." Genes Dev **17**(24): 3112-3126.
- [3] Arkan, M. C., A. L. Hevener, F. R. Greten, S. Maeda, Z. W. Li, J. M. Long, A. Wynshaw-Boris, G. Poli, J. Olefsky and M. Karin (2005). "IKK-beta links inflammation to obesity-induced insulin resistance." Nat Med **11**(2): 191-198.
- [4] Baker, R. G., M. S. Hayden and S. Ghosh (2011). "NF-kappaB, inflammation, and metabolic disease." Cell Metab **13**(1): 11-22.
- [5] Barazzoni, R., G. Gortan Cappellari, M. Ragni and E. Nisoli (2018). "Insulin resistance in obesity: an overview of fundamental alterations." Eat Weight Disord **23**(2): 149-157.
- [6] Barbie, D. A., P. Tamayo, J. S. Boehm, S. Y. Kim, S. E. Moody, I. F. Dunn, A. C. Schinzel, P. Sandy, E. Meylan, C. Scholl, S. Frohling, E. M. Chan, M. L. Sos, K. Michel, C. Mermel, S. J. Silver, B. A. Weir, J. H. Reiling, Q. Sheng, P. B. Gupta, R. C. Wadlow, H. Le, S. Hoersch, B. S. Wittner, S. Ramaswamy, D. M. Livingston, D. M. Sabatini, M. Meyerson, R. K. Thomas, E. S. Lander, J. P. Mesirov, D. E. Root, D. G. Gilliland, T. Jacks and W. C. Hahn (2009). "Systematic RNA interference reveals that oncogenic KRAS-driven cancers require TBK1." Nature **462**(7269): 108-112.
- [7] Bardeesy, N. and R. A. DePinho (2002). "Pancreatic cancer biology and genetics." Nat Rev Cancer **2**(12): 897-909.
- [8] Bonnard, M., C. Mirtsos, S. Suzuki, K. Graham, J. Huang, M. Ng, A. Itie, A. Wakeham, A. Shahinian, W. J. Henzel, A. J. Elia, W. Shillinglaw, T. W. Mak, Z. Cao and W. C. Yeh (2000). "Deficiency of T2K leads to apoptotic liver degeneration and impaired NF-kappaB-dependent gene transcription." Embo j **19**(18): 4976-4985.
- [9] Calay, E. S. and G. S. Hotamisligil (2013). "Turning off the inflammatory, but not the metabolic, flames." Nat Med **19**(3): 265-267.
- [10] Chen, H., H. Sun, F. You, W. Sun, X. Zhou, L. Chen, J. Yang, Y. Wang, H. Tang, Y. Guan, W. Xia, J. Gu, H. Ishikawa, D. Gutman, G. Barber, Z. Qin and Z. Jiang

- (2011). "Activation of STAT6 by STING is critical for antiviral innate immunity." Cell **147**(2): 436-446.
- [11] Chiang, S. H., M. Bazuine, C. N. Lumeng, L. M. Geletka, J. Mowers, N. M. White, J. T. Ma, J. Zhou, N. Qi, D. Westcott, J. B. Delproposto, T. S. Blackwell, F. E. Yull and A. R. Saltiel (2009). "The protein kinase IKKepsilon regulates energy balance in obese mice." Cell **138**(5): 961-975.
- [12] Chien, Y., S. Kim, R. Bumeister, Y. M. Loo, S. W. Kwon, C. L. Johnson, M. G. Balakireva, Y. Romeo, L. Kopelovich, M. Gale, Jr., C. Yeaman, J. H. Camonis, Y. Zhao and M. A. White (2006). "RalB GTPase-mediated activation of the IkkappaB family kinase TBK1 couples innate immune signaling to tumor cell survival." Cell **127**(1): 157-170.
- [13] Cooper, J. M., Y. H. Ou, E. A. McMillan, R. M. Vaden, A. Zaman, B. O. Bodemann, G. Makkar, B. A. Posner and M. A. White (2017). "TBK1 Provides Context-Selective Support of the Activated AKT/mTOR Pathway in Lung Cancer." Cancer Res **77**(18): 5077-5094.
- [14] Copps, K. D. and M. F. White (2012). "Regulation of insulin sensitivity by serine/threonine phosphorylation of insulin receptor substrate proteins IRS1 and IRS2." Diabetologia **55**(10): 2565-2582.
- [15] Corrales, L., L. H. Glickman, S. M. McWhirter, D. B. Kanne, K. E. Sivick, G. E. Katibah, S. R. Woo, E. Lemmens, T. Banda, J. J. Leong, K. Metchette, T. W. Dubensky, Jr. and T. F. Gajewski (2015). "Direct Activation of STING in the Tumor Microenvironment Leads to Potent and Systemic Tumor Regression and Immunity." Cell Rep **11**(7): 1018-1030.
- [16] Cruz, V. H. and R. A. Brekken (2018). "Assessment of TANK-binding kinase 1 as a therapeutic target in cancer." J Cell Commun Signal **12**(1): 83-90.
- [17] Cui, K., S. Zhang, X. Liu, Z. Yan, L. Huang, X. Yang, R. Zhu and A. Sang (2018). "Inhibition of TBK1 reduces choroidal neovascularization in vitro and in vivo." Biochem Biophys Res Commun.
- [18] Dineen, S. P., C. L. Roland, R. Greer, J. G. Carbon, J. E. Toombs, P. Gupta, N. Bardeesy, H. Sun, N. Williams, J. D. Minna and R. A. Brekken (2010). "Smac mimetic increases chemotherapy response and improves survival in mice with pancreatic cancer." Cancer Res **70**(7): 2852-2861.
- [19] Eder, K., N. Baffy, A. Falus and A. K. Fulop (2009). "The major inflammatory mediator interleukin-6 and obesity." Inflamm Res **58**(11): 727-736.
- [20] Engelman, J. A., L. Chen, X. Tan, K. Crosby, A. R. Guimaraes, R. Upadhyay, M. Maira, K. McNamara, S. A. Perera, Y. Song, L. R. Chirieac, R. Kaur, A.

- Lightbown, J. Simendinger, T. Li, R. F. Padera, C. Garcia-Echeverria, R. Weissleder, U. Mahmood, L. C. Cantley and K. K. Wong (2008). "Effective use of PI3K and MEK inhibitors to treat mutant Kras G12D and PIK3CA H1047R murine lung cancers." Nat Med **14**(12): 1351-1356.
- [21] Eskiocak, B., E. A. McMillan, S. Mendiratta, R. K. Kollipara, H. Zhang, C. G. Humphries, C. Wang, J. Garcia-Rodriguez, M. Ding, A. Zaman, T. I. Rosales, U. Eskiocak, M. P. Smith, J. Sudderth, K. Komurov, R. J. Deberardinis, C. Wellbrock, M. A. Davies, J. A. Wargo, Y. Yu, J. K. De Brabander, N. S. Williams, L. Chin, H. Rizos, G. V. Long, R. Kittler and M. A. White (2017). "Biomarker Accessible and Chemically Addressable Mechanistic Subtypes of BRAF Melanoma." Cancer Discov **7**(8): 832-851.
- [22] Ferlay, J., H. R. Shin, F. Bray, D. Forman, C. Mathers and D. M. Parkin (2010). "Estimates of worldwide burden of cancer in 2008: GLOBOCAN 2008." Int J Cancer **127**(12): 2893-2917.
- [23] Fimia, G. M., G. Kroemer and M. Piacentini (2013). "Molecular mechanisms of selective autophagy." Cell Death Differ **20**(1): 1-2.
- [24] Fitzgerald, K. A., S. M. McWhirter, K. L. Faia, D. C. Rowe, E. Latz, D. T. Golenbock, A. J. Coyle, S. M. Liao and T. Maniatis (2003). "IKKepsilon and TBK1 are essential components of the IRF3 signaling pathway." Nat Immunol **4**(5): 491-496.
- [25] Freischmidt, A., T. Wieland, B. Richter, W. Ruf, V. Schaeffer, K. Muller, N. Marroquin, F. Nordin, A. Hubers, P. Weydt, S. Pinto, R. Press, S. Millecamps, N. Molko, E. Bernard, C. Desnuelle, M. H. Soriani, J. Dorst, E. Graf, U. Nordstrom, M. S. Feiler, S. Putz, T. M. Boeckers, T. Meyer, A. S. Winkler, J. Winkelmann, M. de Carvalho, D. R. Thal, M. Otto, T. Brannstrom, A. E. Volk, P. Kursula, K. M. Danzer, P. Lichtner, I. Dikic, T. Meitinger, A. C. Ludolph, T. M. Strom, P. M. Andersen and J. H. Weishaupt (2015). "Haploinsufficiency of TBK1 causes familial ALS and fronto-temporal dementia." Nat Neurosci **18**(5): 631-636.
- [26] Gaianigo, N., D. Melisi and C. Carbone (2017). "EMT and Treatment Resistance in Pancreatic Cancer." Cancers (Basel) **9**(9).
- [27] Grille, S. J., A. Bellacosa, J. Upson, A. J. Klein-Szanto, F. van Roy, W. Lee-Kwon, M. Donowitz, P. N. Tsichlis and L. Larue (2003). "The protein kinase Akt induces epithelial mesenchymal transition and promotes enhanced motility and invasiveness of squamous cell carcinoma lines." Cancer Res **63**(9): 2172-2178.
- [28] Gukovsky, I., N. Li, J. Todoric, A. Gukovskaya and M. Karin (2013). "Inflammation, autophagy, and obesity: common features in the pathogenesis of pancreatitis and pancreatic cancer." Gastroenterology **144**(6): 1199-1209.e1194.

- [29] Guo, J. Y., H. Y. Chen, R. Mathew, J. Fan, A. M. Strohecker, G. Karsli-Uzunbas, J. J. Kamphorst, G. Chen, J. M. Lemons, V. Karantza, H. A. Collier, R. S. Dipaola, C. Gelinas, J. D. Rabinowitz and E. White (2011). "Activated Ras requires autophagy to maintain oxidative metabolism and tumorigenesis." Genes Dev **25**(5): 460-470.
- [30] Gysin, S., M. Salt, A. Young and F. McCormick (2011). "Therapeutic strategies for targeting ras proteins." Genes Cancer **2**(3): 359-372.
- [31] Hacker, H. and M. Karin (2006). "Regulation and function of IKK and IKK-related kinases." Sci STKE **2006**(357): re13.
- [32] Haeusler, R. A., T. E. McGraw and D. Accili (2018). "Biochemical and cellular properties of insulin receptor signalling." Nat Rev Mol Cell Biol **19**(1): 31-44.
- [33] Han, M. S., D. Y. Jung, C. Morel, S. A. Lakhani, J. K. Kim, R. A. Flavell and R. J. Davis (2013). "JNK expression by macrophages promotes obesity-induced insulin resistance and inflammation." Science **339**(6116): 218-222.
- [34] Hasan, M., N. Dobbs, S. Khan, M. A. White, E. K. Wakeland, Q. Z. Li and N. Yan (2015). "Cutting Edge: Inhibiting TBK1 by Compound II Ameliorates Autoimmune Disease in Mice." J Immunol **195**(10): 4573-4577.
- [35] Hay, N. (2011). "Akt isoforms and glucose homeostasis - the leptin connection." Trends Endocrinol Metab **22**(2): 66-73.
- [36] Helgason, E., Q. T. Phung and E. C. Dueber (2013). "Recent insights into the complexity of Tank-binding kinase 1 signaling networks: the emerging role of cellular localization in the activation and substrate specificity of TBK1." FEBS Lett **587**(8): 1230-1237.
- [37] Hezel, A. F., A. C. Kimmelman, B. Z. Stanger, N. Bardeesy and R. A. Depinho (2006). "Genetics and biology of pancreatic ductal adenocarcinoma." Genes Dev **20**(10): 1218-1249.
- [38] Hingorani, S. R., E. F. Petricoin, A. Maitra, V. Rajapakse, C. King, M. A. Jacobetz, S. Ross, T. P. Conrads, T. D. Veenstra, B. A. Hitt, Y. Kawaguchi, D. Johann, L. A. Liotta, H. C. Crawford, M. E. Putt, T. Jacks, C. V. Wright, R. H. Hruban, A. M. Lowy and D. A. Tuveson (2003). "Preinvasive and invasive ductal pancreatic cancer and its early detection in the mouse." Cancer Cell **4**(6): 437-450.
- [39] Hingorani, S. R., L. Wang, A. S. Multani, C. Combs, T. B. Deramautd, R. H. Hruban, A. K. Rustgi, S. Chang and D. A. Tuveson (2005). "Trp53R172H and KrasG12D cooperate to promote chromosomal instability and widely metastatic pancreatic ductal adenocarcinoma in mice." Cancer Cell **7**(5): 469-483.

- [40] Hirosumi, J., G. Tuncman, L. Chang, C. Z. Gorgun, K. T. Uysal, K. Maeda, M. Karin and G. S. Hotamisligil (2002). "A central role for JNK in obesity and insulin resistance." *Nature* **420**(6913): 333-336.
- [41] Hugo, W., H. Shi, L. Sun, M. Piva, C. Song, X. Kong, G. Moriceau, A. Hong, K. B. Dahlman, D. B. Johnson, J. A. Sosman, A. Ribas and R. S. Lo (2015). "Non-genomic and Immune Evolution of Melanoma Acquiring MAPKi Resistance." *Cell* **162**(6): 1271-1285.
- [42] Ishikawa, H. and G. N. Barber (2008). "STING is an endoplasmic reticulum adaptor that facilitates innate immune signalling." *Nature* **455**(7213): 674-678.
- [43] Jo, E. K., J. M. Yuk, D. M. Shin and C. Sasakawa (2013). "Roles of autophagy in elimination of intracellular bacterial pathogens." *Front Immunol* **4**: 97.
- [44] Johnson, A. R., J. J. Milner and L. Makowski (2012). "The inflammation highway: metabolism accelerates inflammatory traffic in obesity." *Immunol Rev* **249**(1): 218-238.
- [45] Jurczak, M. J., A. H. Lee, F. R. Jornayvaz, H. Y. Lee, A. L. Birkenfeld, B. A. Guigni, M. Kahn, V. T. Samuel, L. H. Glimcher and G. I. Shulman (2012). "Dissociation of inositol-requiring enzyme (IRE1 α)-mediated c-Jun N-terminal kinase activation from hepatic insulin resistance in conditional X-box-binding protein-1 (XBP1) knock-out mice." *J Biol Chem* **287**(4): 2558-2567.
- [46] Karnoub, A. E. and R. A. Weinberg (2008). "Ras oncogenes: split personalities." *Nat Rev Mol Cell Biol* **9**(7): 517-531.
- [47] Keil, C., Leach, Robert William, Faizaan, Shaik Mohammed, Bezawada, Srikanth, Parsons, Lance, & Baryshnikova, Anastasia. (2016, October 13). Treeview 3.0 (alpha 3) - Visualization and analysis of large data matrices. Zenodo. <http://doi.org/10.5281/zenodo.160573>.
- [48] Kim, J. Y., E. A. Welsh, U. Oguz, B. Fang, Y. Bai, F. Kinose, C. Bronk, L. L. Remsing Rix, A. A. Beg, U. Rix, S. A. Eschrich, J. M. Koomen and E. B. Haura (2013). "Dissection of TBK1 signaling via phosphoproteomics in lung cancer cells." *Proc Natl Acad Sci U S A* **110**(30): 12414-12419.
- [49] Kirane, A., K. F. Ludwig, N. Sorrelle, G. Haaland, T. Sandal, R. Ranaweera, J. E. Toombs, M. Wang, S. P. Dineen, D. Micklem, M. T. Dellinger, J. B. Lorens and R. A. Brekken (2015). "Warfarin Blocks Gas6-Mediated Axl Activation Required for Pancreatic Cancer Epithelial Plasticity and Metastasis." *Cancer Res* **75**(18): 3699-3705.
- [50] Korherr, C., H. Gille, R. Schafer, K. Koenig-Hoffmann, J. Dixelius, K. A. Eglund, I. Pastan and U. Brinkmann (2006). "Identification of proangiogenic genes and

- pathways by high-throughput functional genomics: TBK1 and the IRF3 pathway." Proc Natl Acad Sci U S A **103**(11): 4240-4245.
- [51] Krebs, A. M., J. Mitschke, M. Lasierra Losada, O. Schmalhofer, M. Boerries, H. Busch, M. Boettcher, D. Mougiakakos, W. Reichardt, P. Bronsert, V. G. Brunton, C. Pilarsky, T. H. Winkler, S. Brabletz, M. P. Stemmler and T. Brabletz (2017). "The EMT-activator Zeb1 is a key factor for cell plasticity and promotes metastasis in pancreatic cancer." Nat Cell Biol **19**(5): 518-529.
- [52] Kumari, M., X. Wang, L. Lantier, A. Lyubetskaya, J. Eguchi, S. Kang, D. Tenen, H. C. Roh, X. Kong, L. Kazak, R. Ahmad and E. D. Rosen (2016). "IRF3 promotes adipose inflammation and insulin resistance and represses browning." J Clin Invest **126**(8): 2839-2854.
- [53] Larue, L. and A. Bellacosa (2005). "Epithelial-mesenchymal transition in development and cancer: role of phosphatidylinositol 3' kinase/AKT pathways." Oncogene **24**(50): 7443-7454.
- [54] Levine, B. and D. J. Klionsky (2004). "Development by self-digestion: molecular mechanisms and biological functions of autophagy." Dev Cell **6**(4): 463-477.
- [55] Ludwig, K. F., W. Du, N. B. Sorrelle, K. Wnuk-Lipinska, M. Topalovski, J. E. Toombs, V. H. Cruz, S. Yabuuchi, N. V. Rajeshkumar, A. Maitra, J. B. Lorens and R. A. Brekken (2018). "Small-Molecule Inhibition of Axl Targets Tumor Immune Suppression and Enhances Chemotherapy in Pancreatic Cancer." Cancer Res **78**(1): 246-255.
- [56] Ma, X., E. Helgason, Q. T. Phung, C. L. Quan, R. S. Iyer, M. W. Lee, K. K. Bowman, M. A. Starovasnik and E. C. Dueber (2012). "Molecular basis of Tank-binding kinase 1 activation by transautophosphorylation." Proc Natl Acad Sci U S A **109**(24): 9378-9383.
- [57] Maher, J. J., P. Leon and J. C. Ryan (2008). "Beyond insulin resistance: Innate immunity in nonalcoholic steatohepatitis." Hepatology **48**(2): 670-678.
- [58] Marchlik, E., P. Thakker, T. Carlson, Z. Jiang, M. Ryan, S. Marusic, N. Goutagny, W. Kuang, G. R. Askew, V. Roberts, S. Benoit, T. Zhou, V. Ling, R. Pfeifer, N. Stedman, K. A. Fitzgerald, L. L. Lin and J. P. Hall (2010). "Mice lacking Tbk1 activity exhibit immune cell infiltrates in multiple tissues and increased susceptibility to LPS-induced lethality." J Leukoc Biol **88**(6): 1171-1180.
- [59] McLaughlin, T., S. E. Ackerman, L. Shen and E. Engleman (2017). "Role of innate and adaptive immunity in obesity-associated metabolic disease." J Clin Invest **127**(1): 5-13.

- [60] Moore, A. S. and E. L. Holzbaur (2016). "Dynamic recruitment and activation of ALS-associated TBK1 with its target optineurin are required for efficient mitophagy." Proc Natl Acad Sci U S A **113**(24): E3349-3358.
- [61] Mowers, J., M. Uhm, S. M. Reilly, J. Simon, D. Leto, S. H. Chiang, L. Chang and A. R. Saltiel (2013). "Inflammation produces catecholamine resistance in obesity via activation of PDE3B by the protein kinases IKKepsilon and TBK1." Elife **2**: e01119.
- [62] Munoz, M. C., J. F. Giani, M. A. Mayer, J. E. Toblli, D. Turyn and F. P. Dominici (2009). "TANK-binding kinase 1 mediates phosphorylation of insulin receptor at serine residue 994: a potential link between inflammation and insulin resistance." J Endocrinol **201**(2): 185-197.
- [63] Newman, A. C., C. L. Scholefield, A. J. Kemp, M. Newman, E. G. McIver, A. Kamal and S. Wilkinson (2012). "TBK1 kinase addiction in lung cancer cells is mediated via autophagy of Tax1bp1/Ndp52 and non-canonical NF-kappaB signalling." PLoS One **7**(11): e50672.
- [64] Odegaard, J. I. and A. Chawla (2013). "Pleiotropic actions of insulin resistance and inflammation in metabolic homeostasis." Science **339**(6116): 172-177.
- [65] Oral, E. A., S. M. Reilly, A. V. Gomez, R. Meral, L. Butz, N. Ajluni, T. L. Chenevert, E. Korytnaya, A. H. Neidert, R. Hench, D. Rus, J. F. Horowitz, B. Poirier, P. Zhao, K. Lehmann, M. Jain, R. Yu, C. Liddle, M. Ahmadian, M. Downes, R. M. Evans and A. R. Saltiel (2017). "Inhibition of IKKvarepsilon and TBK1 Improves Glucose Control in a Subset of Patients with Type 2 Diabetes." Cell Metab **26**(1): 157-170.e157.
- [66] Ostapoff, K. T., B. K. Cenik, M. Wang, R. Ye, X. Xu, D. Nugent, M. M. Hagopian, M. Topalovski, L. B. Rivera, K. D. Carroll and R. A. Brekken (2014). "Neutralizing murine TGFbetaR2 promotes a differentiated tumor cell phenotype and inhibits pancreatic cancer metastasis." Cancer Res **74**(18): 4996-5007.
- [67] Ou, Y. H., M. Torres, R. Ram, E. Formstecher, C. Roland, T. Cheng, R. Brekken, R. Wurz, A. Tasker, T. Polverino, S. L. Tan and M. A. White (2011). "TBK1 directly engages Akt/PKB survival signaling to support oncogenic transformation." Mol Cell **41**(4): 458-470.
- [68] Pearson, G. W. and T. Hunter (2007). "Real-time imaging reveals that noninvasive mammary epithelial acini can contain motile cells." J Cell Biol **179**(7): 1555-1567.
- [69] Pillai, S., J. Nguyen, J. Johnson, E. Haura, D. Coppola and S. Chellappan (2015). "Tank binding kinase 1 is a centrosome-associated kinase necessary for microtubule dynamics and mitosis." Nat Commun **6**: 10072.

- [70] Pilli, M., J. Arko-Mensah, M. Ponpuak, E. Roberts, S. Master, M. A. Mandell, N. Dupont, W. Ornatowski, S. Jiang, S. B. Bradfute, J. A. Bruun, T. E. Hansen, T. Johansen and V. Deretic (2012). "TBK-1 promotes autophagy-mediated antimicrobial defense by controlling autophagosome maturation." *Immunity* **37**(2): 223-234.
- [71] Poirier, P., T. D. Giles, G. A. Bray, Y. Hong, J. S. Stern, F. X. Pi-Sunyer and R. H. Eckel (2006). "Obesity and cardiovascular disease: pathophysiology, evaluation, and effect of weight loss: an update of the 1997 American Heart Association Scientific Statement on Obesity and Heart Disease from the Obesity Committee of the Council on Nutrition, Physical Activity, and Metabolism." *Circulation* **113**(6): 898-918.
- [72] Puls, T. J., X. Tan, C. F. Whittington and S. L. Voytik-Harbin (2017). "3D collagen fibrillar microstructure guides pancreatic cancer cell phenotype and serves as a critical design parameter for phenotypic models of EMT." *PLoS One* **12**(11): e0188870.
- [73] Reggiori, F., M. Komatsu, K. Finley and A. Simonsen (2012). "Autophagy: more than a nonselective pathway." *Int J Cell Biol* **2012**: 219625.
- [74] Reilly, S. M., M. Ahmadian, B. F. Zamarron, L. Chang, M. Uhm, B. Poirier, X. Peng, D. M. Krause, E. Korytnaya, A. Neidert, C. Liddle, R. T. Yu, C. N. Lumeng, E. A. Oral, M. Downes, R. M. Evans and A. R. Saltiel (2015). "A subcutaneous adipose tissue-liver signalling axis controls hepatic gluconeogenesis." *Nat Commun* **6**: 6047.
- [75] Reilly, S. M., S. H. Chiang, S. J. Decker, L. Chang, M. Uhm, M. J. Larsen, J. R. Rubin, J. Mowers, N. M. White, I. Hochberg, M. Downes, R. T. Yu, C. Liddle, R. M. Evans, D. Oh, P. Li, J. M. Olefsky and A. R. Saltiel (2013). "An inhibitor of the protein kinases TBK1 and IKK-varepsilon improves obesity-related metabolic dysfunctions in mice." *Nat Med* **19**(3): 313-321.
- [76] Ritch, R., B. Darbro, G. Menon, C. L. Khanna, F. Solivan-Timpe, B. R. Roos, M. Sarfarzi, K. Kawase, T. Yamamoto, A. L. Robin, A. J. Lotery and J. H. Fingert (2014). "TBK1 gene duplication and normal-tension glaucoma." *JAMA Ophthalmol* **132**(5): 544-548.
- [77] Rosenfeldt, M. T., J. O'Prey, J. P. Morton, C. Nixon, G. MacKay, A. Mrowinska, A. Au, T. S. Rai, L. Zheng, R. Ridgway, P. D. Adams, K. I. Anderson, E. Gottlieb, O. J. Sansom and K. M. Ryan (2013). "p53 status determines the role of autophagy in pancreatic tumour development." *Nature* **504**(7479): 296-300.
- [78] Rotter, V., I. Nagaev and U. Smith (2003). "Interleukin-6 (IL-6) induces insulin resistance in 3T3-L1 adipocytes and is, like IL-8 and tumor necrosis factor-alpha,

- overexpressed in human fat cells from insulin-resistant subjects." J Biol Chem **278**(46): 45777-45784.
- [79] Sabio, G., N. J. Kennedy, J. Cavanagh-Kyros, D. Y. Jung, H. J. Ko, H. Ong, T. Barrett, J. K. Kim and R. J. Davis (2010). "Role of muscle c-Jun NH2-terminal kinase 1 in obesity-induced insulin resistance." Mol Cell Biol **30**(1): 106-115.
- [80] Saltiel, A. R. and J. M. Olefsky (2017). "Inflammatory mechanisms linking obesity and metabolic disease." J Clin Invest **127**(1): 1-4.
- [81] Shen, R. R. and W. C. Hahn (2011). "Emerging roles for the non-canonical IKKs in cancer." Oncogene **30**(6): 631-641.
- [82] Shintani, Y., Y. Fukumoto, N. Chaika, R. Svoboda, M. J. Wheelock and K. R. Johnson (2008). "Collagen I-mediated up-regulation of N-cadherin requires cooperative signals from integrins and discoidin domain receptor 1." J Cell Biol **180**(6): 1277-1289.
- [83] Strack, V., A. M. Hennige, J. Krutzfeldt, B. Bossenmaier, H. H. Klein, M. Kellerer, R. Lammers and H. U. Haring (2000). "Serine residues 994 and 1023/25 are important for insulin receptor kinase inhibition by protein kinase C isoforms beta2 and theta." Diabetologia **43**(4): 443-449.
- [84] Strack, V., B. Stoyanov, B. Bossenmaier, L. Mosthaf, M. Kellerer and H. U. Haring (1997). "Impact of mutations at different serine residues on the tyrosine kinase activity of the insulin receptor." Biochem Biophys Res Commun **239**(1): 235-239.
- [85] Sun, K., C. M. Kusminski and P. E. Scherer (2011). "Adipose tissue remodeling and obesity." J Clin Invest **121**(6): 2094-2101.
- [86] Um, S. H., F. Frigerio, M. Watanabe, F. Picard, M. Joaquin, M. Sticker, S. Fumagalli, P. R. Allegrini, S. C. Kozma, J. Auwerx and G. Thomas (2004). "Absence of S6K1 protects against age- and diet-induced obesity while enhancing insulin sensitivity." Nature **431**(7005): 200-205.
- [87] Um, S. H., M. Sticker-Jantscheff, G. C. Chau, K. Vintersten, M. Mueller, Y. G. Gangloff, R. H. Adams, J. F. Spetz, L. Elghazi, P. T. Pfluger, M. Pende, E. Bernal-Mizrachi, A. Tauler, M. H. Tschop, G. Thomas and S. C. Kozma (2015). "S6K1 controls pancreatic beta cell size independently of intrauterine growth restriction." J Clin Invest **125**(7): 2736-2747.
- [88] Uysal, K. T., S. M. Wiesbrock, M. W. Marino and G. S. Hotamisligil (1997). "Protection from obesity-induced insulin resistance in mice lacking TNF-alpha function." Nature **389**(6651): 610-614.

- [89] Van Mossevelde, S., S. Engelborghs, J. van der Zee and C. Van Broeckhoven (2018). "Genotype-phenotype links in frontotemporal lobar degeneration." Nat Rev Neurol **14**(6): 363-378.
- [90] Vu, H. L. and A. E. Aplin (2014). "Targeting TBK1 inhibits migration and resistance to MEK inhibitors in mutant NRAS melanoma." Mol Cancer Res **12**(10): 1509-1519.
- [91] Wang, M., M. Topalovski, J. E. Toombs, C. M. Wright, Z. R. Moore, D. A. Boothman, H. Yanagisawa, H. Wang, A. Witkiewicz, D. H. Castrillon and R. A. Brekken (2015). "Fibulin-5 Blocks Microenvironmental ROS in Pancreatic Cancer." Cancer Res **75**(23): 5058-5069.
- [92] Wang, S., S. Huang and Y. L. Sun (2017). "Epithelial-Mesenchymal Transition in Pancreatic Cancer: A Review." Biomed Res Int **2017**: 2646148.
- [93] Weigelt, B., J. L. Peterse and L. J. van 't Veer (2005). "Breast cancer metastasis: markers and models." Nat Rev Cancer **5**(8): 591-602.
- [94] Weisberg, S. P., D. Hunter, R. Huber, J. Lemieux, S. Slaymaker, K. Vaddi, I. Charo, R. L. Leibel and A. W. Ferrante, Jr. (2006). "CCR2 modulates inflammatory and metabolic effects of high-fat feeding." J Clin Invest **116**(1): 115-124.
- [95] Westcott, J. M., A. M. Prechtel, E. A. Maine, T. T. Dang, M. A. Esparza, H. Sun, Y. Zhou, Y. Xie and G. W. Pearson (2015). "An epigenetically distinct breast cancer cell subpopulation promotes collective invasion." J Clin Invest **125**(5): 1927-1943.
- [96] Wild, P., H. Farhan, D. G. McEwan, S. Wagner, V. V. Rogov, N. R. Brady, B. Richter, J. Korac, O. Waidmann, C. Choudhary, V. Dotsch, D. Bumann and I. Dikic (2011). "Phosphorylation of the autophagy receptor optineurin restricts Salmonella growth." Science **333**(6039): 228-233.
- [97] Woo, S. R., M. B. Fuertes, L. Corrales, S. Spranger, M. J. Furdyna, M. Y. Leung, R. Duggan, Y. Wang, G. N. Barber, K. A. Fitzgerald, M. L. Alegre and T. F. Gajewski (2014). "STING-dependent cytosolic DNA sensing mediates innate immune recognition of immunogenic tumors." Immunity **41**(5): 830-842.
- [98] Wu, H. and C. M. Ballantyne (2017). "Skeletal muscle inflammation and insulin resistance in obesity." J Clin Invest **127**(1): 43-54.
- [99] Xiao, Y., Q. Zou, X. Xie, T. Liu, H. S. Li, Z. Jie, J. Jin, H. Hu, G. Manyam, L. Zhang, X. Cheng, H. Wang, I. Marie, D. E. Levy, S. S. Watowich and S. C. Sun (2017). "The kinase TBK1 functions in dendritic cells to regulate T cell homeostasis, autoimmunity, and antitumor immunity." J Exp Med **214**(5): 1493-1507.

- [100] Xu, W., Z. Yang and N. Lu (2015). "A new role for the PI3K/Akt signaling pathway in the epithelial-mesenchymal transition." Cell Adh Migr **9**(4): 317-324.
- [101] Yang, K. M., Y. Jung, J. M. Lee, W. Kim, J. K. Cho, J. Jeong and S. J. Kim (2013). "Loss of TBK1 induces epithelial-mesenchymal transition in the breast cancer cells by ERalpha downregulation." Cancer Res **73**(22): 6679-6689.
- [102] Yang, S., Y. Imamura, R. W. Jenkins, I. Canadas, S. Kitajima, A. Aref, A. Brannon, E. Oki, A. Castoreno, Z. Zhu, T. Thai, J. Reibel, Z. Qian, S. Ogino, K. K. Wong, H. Baba, A. C. Kimmelman, M. Pasca Di Magliano and D. A. Barbie (2016). "Autophagy Inhibition Dysregulates TBK1 Signaling and Promotes Pancreatic Inflammation." Cancer Immunol Res **4**(6): 520-530.
- [103] Yang, S., X. Wang, G. Contino, M. Liesa, E. Sahin, H. Ying, A. Bause, Y. Li, J. M. Stommel, G. Dell'antonio, J. Mautner, G. Tonon, M. Haigis, O. S. Shirihai, C. Doglioni, N. Bardeesy and A. C. Kimmelman (2011). "Pancreatic cancers require autophagy for tumor growth." Genes Dev **25**(7): 717-729.
- [104] Ye, J. and O. P. McGuinness (2013). "Inflammation during obesity is not all bad: evidence from animal and human studies." Am J Physiol Endocrinol Metab **304**(5): E466-477.
- [105] Yu, T., Y. S. Yi, Y. Yang, J. Oh, D. Jeong and J. Y. Cho (2012). "The pivotal role of TBK1 in inflammatory responses mediated by macrophages." Mediators Inflamm **2012**: 979105.
- [106] Yuan, M., N. Konstantopoulos, J. Lee, L. Hansen, Z. W. Li, M. Karin and S. E. Shoelson (2001). "Reversal of obesity- and diet-induced insulin resistance with salicylates or targeted disruption of Ikkbeta." Science **293**(5535): 1673-1677.
- [107] Zagorska, A., P. G. Traves, E. D. Lew, I. Dransfield and G. Lemke (2014). "Diversification of TAM receptor tyrosine kinase function." Nat Immunol **15**(10): 920-928.
- [108] Zhao, P., K. I. Wong, X. Sun, S. M. Reilly, M. Uhm, Z. Liao, Y. Skorobogatko and A. R. Saltiel (2018). "TBK1 at the Crossroads of Inflammation and Energy Homeostasis in Adipose Tissue." Cell **172**(4): 731-743.e712.
- [109] Zhu, Z., A. R. Aref, T. J. Cohoon, T. U. Barbie, Y. Imamura, S. Yang, S. E. Moody, R. R. Shen, A. C. Schinzel, T. C. Thai, J. B. Reibel, P. Tamayo, J. T. Godfrey, Z. R. Qian, A. N. Page, K. Maciag, E. M. Chan, W. Silkworth, M. T. Labowsky, L. Rozhansky, J. P. Mesirov, W. E. Gillanders, S. Ogino, N. Hacohen, S. Gaudet, M. J. Eck, J. A. Engelman, R. B. Corcoran, K. K. Wong, W. C. Hahn and D. A. Barbie (2014). "Inhibition of KRAS-driven tumorigenicity by interruption of an autocrine cytokine circuit." Cancer Discov **4**(4): 452-465.

- [110] Zolghadri, Y., S. Pal Choudhuri, O. Ocal, S. Layeghi-Ghalehsoukhteh, F. Berhe, M. A. Hale and T. M. Wilkie (2018). "Malnutrition in Pancreatic Ductal Adenocarcinoma (PDA): Dietary Pancreatic Enzymes Improve Short-Term Health but Stimulate Tumor Growth." Am J Pathol **188**(3): 616-626.

Acknowledgements

I would like to express my deep appreciation for the many people who have guided, helped and encouraged me along the way. First, I would like to thank my wonderful mentor, Dr. Rolf Brekken for giving me the opportunity to train in your lab. From the beginning, you've always been a positive and supportive mentor. I very much appreciate your enthusiasm for science and the way that you shared that with me by allowing me the freedom to pursue what interested me the most. Thank you for encouraging me to present my research often, to attend national meetings and for always promoting my scientific career. I couldn't have asked for a better PhD mentor!

I'm also very appreciative of the Brekken lab members (past and present) for making me feel warm and welcomed during my time in the lab. I've enjoyed being able to discuss ideas, troubleshoot through experiments and just share life with such a supportive and generous group of people. I would like to extend a special thank you to Dr. Mike Dellinger. Thank you for introducing me to TBK1 and for your interest in my science and my development as a trainee. You've been a great friend and mentor to me. I'm going to miss our updates on 'big science' and kids! I would also like to especially thank Emily Arner. I wish we had met sooner in life, as this last year has been the best. I am so grateful to have had your help in wrapping up this project. You are incredibly bright, talented and hard working and I've really enjoyed doing science with you!

I would like to gratefully acknowledge my thesis committee members, Drs. Diego Castrillon, Ray MacDonald and Philipp Scherer for their guidance and constructive advice over the years. You've all helped me grow as a scientist by getting me to think about my project in different ways, yet also making sure that I stayed focused throughout my PhD. I would also like to thank UT Southwestern Simmons Cancer Center and Dr. Jerry Shay for funding from the Cancer Biology training grant (T32 CA124334).

Finally, I would like to express my deep gratitude to my friends and family who have supported me immensely throughout my PhD. My time in graduate school was enriched by the deep friendships that I made with some of my classmates. Thank you Hillary, Alex, Christine, Sarah and Megan for all the camaraderie, encouragement and laughs. I never imagined that I would come out of graduate school with such amazing friends. I also want to extend an enormous thank you to the McCartys who have generously and without reservation taken me, Daniel and Frances into their family and made us feel so welcomed and loved for the past 6 years. Thank you for being there for us; we feel so honored and blessed to have been part of your family. We will miss you all dearly. Thank you to my own family for their sacrificial love and unwavering support throughout my education. Amanda, thank you for always being there for me and for all the trips you made out to Dallas to visit me. Mom and Dad, thank you for being my first cheerleaders in life and for engraining in me from an early age that I could do anything I put my mind to.

Last but not least, I want to express my profound gratitude for my loving husband Daniel. Thank you for taking that risk 6 years ago of quitting your job, following me out here to Texas and joining me on this adventure. You are my number one support and have always believed in me, even at times when I didn't believe in myself. Thank you for actively listening and always being genuinely interested when I talk about science. It's meant so much to have your unfailing support and continuous encouragement throughout graduate school and life in general. And to my sweet girl Frances, thank you for the daily joy that you bring me through your big smile when I walk through the front door and with all your silliness and laughter. The greatest joy in my life is getting to be your mom.